



Cite this: *J. Mater. Chem. A*, 2023, **11**, 15600

## Troger's base polymeric membranes for CO<sub>2</sub> separation: a review

Qingbo Xu,<sup>†a</sup> Bingru Xin,<sup>†b</sup> Jing Wei,<sup>a</sup> Yulei Ma,<sup>Ⓜ<sup>a</sup></sup> Zikang Qing,<sup>a</sup> Chao Feng,<sup>c</sup> Shouliang Yi,<sup>Ⓜ<sup>d</sup></sup> Nanwen Li,<sup>Ⓜ<sup>e</sup></sup> Kai Li,<sup>Ⓜ<sup>f</sup></sup> Fei Wang,<sup>Ⓜ<sup>f</sup></sup> Jie Zhao,<sup>Ⓜ<sup>f</sup></sup> Lin Yang,<sup>ghi</sup> Lu Yao,<sup>Ⓜ<sup>ghi</sup></sup> Wenju Jiang,<sup>Ⓜ<sup>ghi</sup></sup> Yiyang Dai<sup>\*b</sup> and Zhongde Dai<sup>Ⓜ<sup>\*ghi</sup></sup>

Membrane-mediated separation has gained significant attention as a promising strategy for CO<sub>2</sub> separation. The continuous quest for membrane materials with improved CO<sub>2</sub> separation performance remains a priority in advancing membrane gas separation technologies. Troger's base (TB), characterized by its rigid V-shaped bridged bicyclic linking group, presents an excellent building block for enhancing polymer rigidity and hindering chain packing, thereby improving the gas separation performance. Despite considerable progress which has been made on TB polymeric membranes over the past few years, a comprehensive review on this topic is still lacking. Herein, the development of membranes based on TB polymers for CO<sub>2</sub> separation in the past ten years is summarized and discussed. Specifically, pure TB polymeric membranes, functionalized TB polymeric membranes, TB polymer based mixed-matrix membranes (MMMs), and TB polymer based carbon molecular sieve (CMS)/thermal rearranged (TR) membranes are discussed, targeting separation performance. Finally, conclusions are drawn on the progress of CO<sub>2</sub> separation membranes based on TB polymers, with perspectives for future development also presented.

Received 22nd May 2023  
Accepted 4th July 2023

DOI: 10.1039/d3ta03017b

rsc.li/materials-a

<sup>a</sup>College of Architecture and Environment, Sichuan University, Chengdu 610065, China

<sup>b</sup>College of Chemical Engineering, Sichuan University, Chengdu 610065, China. E-mail: daiyy@scu.edu.cn

<sup>c</sup>Chengdu University of Information Technology, School of Resources and Environment, Chengdu, 610225, China

<sup>d</sup>US DOE, Natl Energy Technol Lab, 626 Cochrans Mill Rd, Pittsburgh, PA 15236, USA

<sup>e</sup>State Key Laboratory of Coal Conversion, Institute of Coal Chemistry, Chinese Academy of Sciences, Taiyuan, 030001, China

<sup>f</sup>Faculty of Environmental Science and Engineering, Kunming University of Science and Technology, Kunming, 650500, China

<sup>g</sup>National Engineering Research Centre for Flue Gas Desulfurization, Chengdu 610065, China. E-mail: zhongde.dai@scu.edu.cn

<sup>h</sup>Carbon Neutral Technology Innovation Center of Sichuan, Chengdu 610065, China

<sup>i</sup>College of Carbon Neutrality Future Technology, Sichuan University, Chengdu 610065, China

<sup>†</sup> These two authors contributed equally.



Qingbo Xu is currently a B.E. student under the supervision of Prof. Zhongde Dai at the College of Architecture and Environment at Sichuan University. His research mainly focuses on the separation and capture of carbon dioxide by membranes.



Bingru Xin completed his B.E. degree from the School of Chemical Engineering at Sichuan University in 2022. Currently, he is a M.S. student under the supervision of A. Prof. Yiyang Dai and Prof. Zhongde Dai at the School of Chemical Engineering at Sichuan University. His research mainly focuses on the high-throughput computational screening of porous framework materials for gas separation membranes.

# 1. Introduction

## 1.1 Global warming and CO<sub>2</sub> capture

Human activities, particularly the burning of fossil fuels (coal, oil and gas) and large-scale deforestation, generate a significant amount of carbon dioxide (CO<sub>2</sub>), which contributes to serious global warming.<sup>1,2</sup> The consequences of global warming include changes in precipitation patterns, the melting of glaciers and permafrost, and rising sea levels.<sup>3,4</sup> Given the complexity and uncertainty of these risks, carbon capture, utilization, and storage (CCUS) is widely recognized as an indispensable strategy for mitigating climate change and facilitating a low-carbon and sustainable future.<sup>5</sup> However, the efficiency of the CO<sub>2</sub> capture step, which accounts for approximately 80% of the overall cost, remains a major challenge hindering the widespread adoption of CCUS technologies.<sup>6</sup> Therefore, developing highly efficient means of CO<sub>2</sub> capture is of critical importance to improve the competitiveness of the CCUS strategy.

In recent years, many technologies have been applied for CO<sub>2</sub> capture, including liquid absorption,<sup>7,8</sup> solid adsorption,<sup>9–11</sup> chemical looping<sup>12,13</sup> and membrane separation.<sup>14–17</sup> Among

them, liquid absorption is considered as the most mature technique and has been intensively studied<sup>7,18–21</sup> and used in several pilot tests for CO<sub>2</sub> capture from various sources.<sup>22–24</sup> Many new liquid absorbents, e.g., amino acid salts,<sup>25</sup> ionic liquids (ILs),<sup>26,27</sup> and phase separation amine mixtures<sup>28</sup> have been developed. However, liquid absorption still suffers from problems such as high energy consumption (solvent regeneration step), high tendency of corrosion, and possible secondary pollution due to thermal degradation.<sup>7,29</sup>

On the other hand, although solid adsorption has been widely used in air separation<sup>30,31</sup> and H<sub>2</sub> purification,<sup>32,33</sup> the number of reports focusing on using solid adsorbents for CO<sub>2</sub> capture is relatively small compared to those on liquid absorption. This is primarily because solid adsorption is less effective in removing large quantities of CO<sub>2</sub> from flue gas with low CO<sub>2</sub> concentrations in the feed.<sup>9</sup>

In contrast, membrane gas separation offers several advantages over liquid absorption and solid adsorption, including small footprint, easy operation, no moving parts and liner scale up. Thus, membranes for CO<sub>2</sub> separation have gained significant attention in the past few decades.



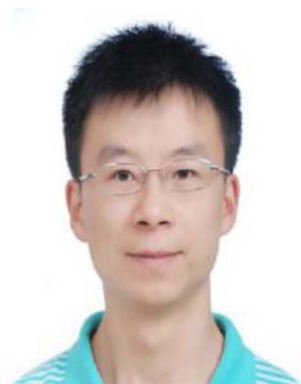
*Dr. Shouliang Yi is a principal research scientist & project lead at the U.S. Department of Energy (DOE) National Energy Technology Laboratory (NETL), dedicated to the design and development of novel high-performance membranes and sorbents with complex morphologies (polymeric membranes, 2D material-based membranes, metal-organic framework based MMMs, and*

*hollow fiber membranes and sorbents) for key energy intensive separations, heavy metal removal, CO<sub>2</sub> capture, utilization, and storage, and negative emission technologies.*



*Dr Zhao Jie received his PhD with Prof. Wang Rong in environmental engineering from Nanyang Technological University, Singapore, in 2019. He is currently a university-appointed associate professor at the Kunming University of Technology, where he focuses on the preparation of separation membranes and their application in the environmental field, including waste gas purification, lithium ion separation membranes, solid-state electrolytes, etc.*

*etc.*



*Dr Nanwen Li completed his PhD in 2009 at the Changchun institute of Applied Chemistry, Chinese Academy of Sciences. He started his independent research work as a researcher at the Institute of Coal Chemistry, Chinese Academy of Sciences, in 2014. His main research areas focus on ion exchange and gas separation membranes, including fuel cells, hydrogen production from electrolytic*

*water, liquid flow energy storage, hydrogen purification, air separation, CO<sub>2</sub> capture technologies, etc.*



*Dr Zhongde Dai completed his PhD in 2016 with Prof. Liyuan Deng at the Norwegian University of Science and Technology, followed by postdoctoral research at the same institute until 2020. He is currently a full professor at Sichuan University, China. Dr Dai's research interests are in developing new membrane materials and membrane processes for different gas separation appli-*

*cations, including natural gas sweetening, CO<sub>2</sub> capture as well as H<sub>2</sub> purification.*

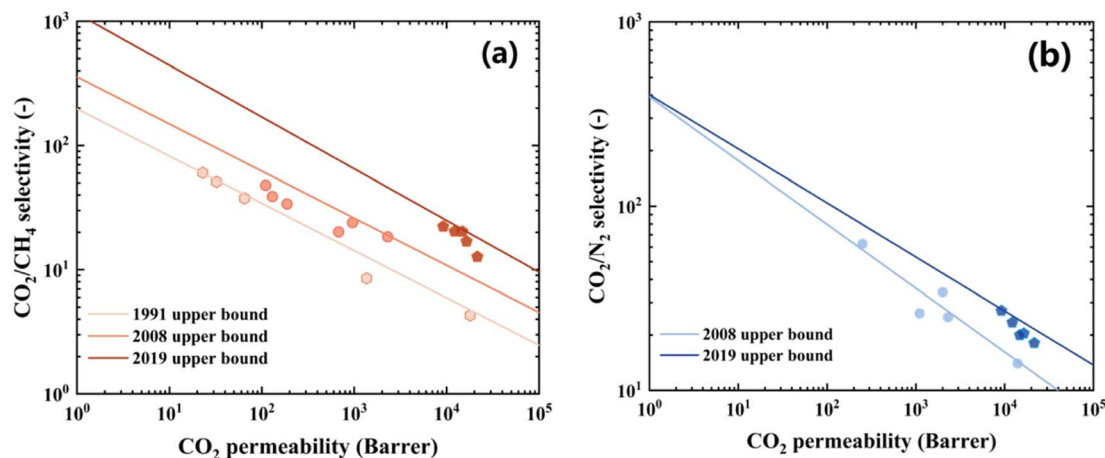


Fig. 1 Robeson upper bound for CO<sub>2</sub>/CH<sub>4</sub> (a) and CO<sub>2</sub>/N<sub>2</sub> (b) separation, reproduced from ref. 48–50.

## 1.2 Membrane CO<sub>2</sub> separation

The application of membranes for CO<sub>2</sub> separation was started in the late 1970s.<sup>34–36</sup> Over the past few decades, various types of membranes have been developed, including polymeric membranes,<sup>37–39</sup> mixed-matrix membranes (MMMs),<sup>40–42</sup> carbon molecular sieve (CMS) membranes,<sup>43,44</sup> and inorganic membranes.<sup>45,46</sup> Among these materials, polymeric membranes have been intensively studied due to their good processibility, relatively low price and moderate CO<sub>2</sub> separation performances.<sup>37,38</sup>

However, it is well-known that there is a trade-off between gas permeability and selectivity in polymeric membranes. In simple terms, membranes with high gas selectivity usually tend to have low permeability, and *vice versa*.<sup>47</sup> The trade-off is well illustrated by the Robeson upper bound, which was introduced in 1991,<sup>48</sup> updated in 2008,<sup>49</sup> and more recently in 2019 (ref. 50) (shown in Fig. 1).

As shown in Fig. 1, permeability and selectivity are indicators of gas separation performance. The permeability can be interpreted as the ability of a gas component to permeate across a membrane.<sup>51</sup> The permeability can be determined using the following eqn (1):

$$P_A = D_A \times S_A = \frac{N_A l}{(p_0 - p_l)} \quad (1)$$

in which  $P$  (Barrer, 1 Barrer =  $10^{-10}$  cm<sup>3</sup> (STP) cm cm<sup>-2</sup> s<sup>-1</sup> cmHg<sup>-1</sup>) is the gas permeability of component A,  $D_A$  (cm<sup>2</sup> s<sup>-1</sup>) is the diffusion coefficient of component A,  $S_A$  (cm<sup>3</sup> (STP) cm<sup>-3</sup> cmHg<sup>-1</sup>) is the solubility coefficient of component A,  $N_A$  (cm<sup>3</sup> (STP) cm<sup>-2</sup> s<sup>-1</sup>) is the flux of component A,  $l$  (cm) is the effective membrane thickness,  $p_0$  (cmHg) is the pressure at the upstream side, and  $p_l$  (cmHg) is the pressure at the downstream side.<sup>52</sup>

For asymmetric or composite membranes for which it is difficult to determine the actual membrane thickness, permeance is widely used to evaluate gas transport performance. The correlation between permeance and permeability can be expressed as eqn (2):

$$\text{Permeance}_A = \frac{P_A}{l} = \frac{N_A}{(p_0 - p_l)} \quad (2)$$

The ideal gas selectivity ( $\alpha_{A/B}^*$ ) is defined as the permeability ratio between the more permeable gas (A) and less permeable one (B). The ideal gas selectivity (the product of the diffusivity and solubility selectivity) can be expressed using the following eqn (3):

$$\alpha_{A/B}^* = \frac{P_A}{P_B} = \left(\frac{D_A}{D_B}\right) \left(\frac{S_A}{S_B}\right) \quad (3)$$

in which  $P_A$  and  $P_B$  are certain gas permeabilities of A and B, respectively.<sup>52</sup>

In the actual membrane separation process, preferentially permeating component will be consumed and retained species will accumulate in the boundary layer, which causes concentration polarization and thus, a deviation between the ideal selectivity ( $\alpha_{A/B}^*$ ) and separation factor ( $\alpha_{A/B}$ ). The separation factor can be determined by using eqn (4):

$$\alpha_{A/B} = \frac{y_A/x_A}{y_B/x_B} \quad (4)$$

The deviation between the ideal selectivity ( $\alpha_{A/B}^*$ ) and separation factor ( $\alpha_{A/B}$ ) can be ignored when the partial pressure at the upstream side is much higher than that at the downstream side.<sup>53</sup>

It is worth mentioning that even though the gas permeability and selectivity were considered as ‘intrinsic’ properties of a membrane material, they may gradually change over time, especially for glassy polymeric membranes, which is known as ‘physical aging’.<sup>54,55</sup> Due to physical aging, gas permeability reduction of up to 40% can be observed for glassy polymeric membranes in an operation period of 6 months;<sup>56</sup> in the past few years, numerous efforts have been made for mitigating physical aging.<sup>57</sup>

In recent years, a significant number of polymeric membranes have been developed with the goal of improving CO<sub>2</sub> permeability and gas selectivity, pushing the data towards the upper right side of the upper bound plot. Meanwhile, tremendous attention has also been paid to controlling physical aging. These membranes include polymers of intrinsic microporosity (PIMs), polyimides (PIs),<sup>58,59</sup> polybenzimidazole (PBI)<sup>60</sup>

and Troger's base based (TB) polymers,<sup>61,62</sup> block copolymers<sup>63,64</sup> and many other polymers.<sup>65</sup> Among them, polymers with the TB group (TB polymer), a nitrogen-containing kinked heterocycle with a V-shaped bridged bicyclic linking group, have emerged as versatile building blocks for gas separation membranes. The incorporation of the TB group enhances polymer chain rigidity and improves the microporosity within the matrix. In the past few years, great progress has been made in the field of TB polymers, including conventional TB polymers, TB-PI polymers, and TB-PIMs, which have been developed and applied for gas separations.<sup>66–69</sup> However, there is no review specifically focused on TB polymers for gas separation. Therefore, this work aims to provide a comprehensive review of the recent advancements in TB polymer-based membranes for CO<sub>2</sub> separation. The review begins by discussing the fundamentals of TB polymer synthesis, followed by the collection and summarization of gas permeation data for TB polymer-based CO<sub>2</sub> separation membranes. Additionally, the third part of this review addressed MMMs based on TB polymers. Furthermore, the review touches upon the relatively lesser-explored area of TR polymeric membranes or CMS membranes derived from TB polymers, although research in this domain is not as extensive as the development of new monomers for TB polymers. Finally, the review concludes by summarizing the findings and providing insights into the future development of TB polymers.

## 2. TB based polymeric membranes for CO<sub>2</sub> separation

In 1887, TB was originally isolated by an accident in a study on the reaction of *p*-toluidine and dimethoxymethane (DMM).<sup>70</sup> Later, because of its attractive stereochemistry<sup>71</sup> and organocatalysis properties,<sup>72</sup> various TB analogs have been

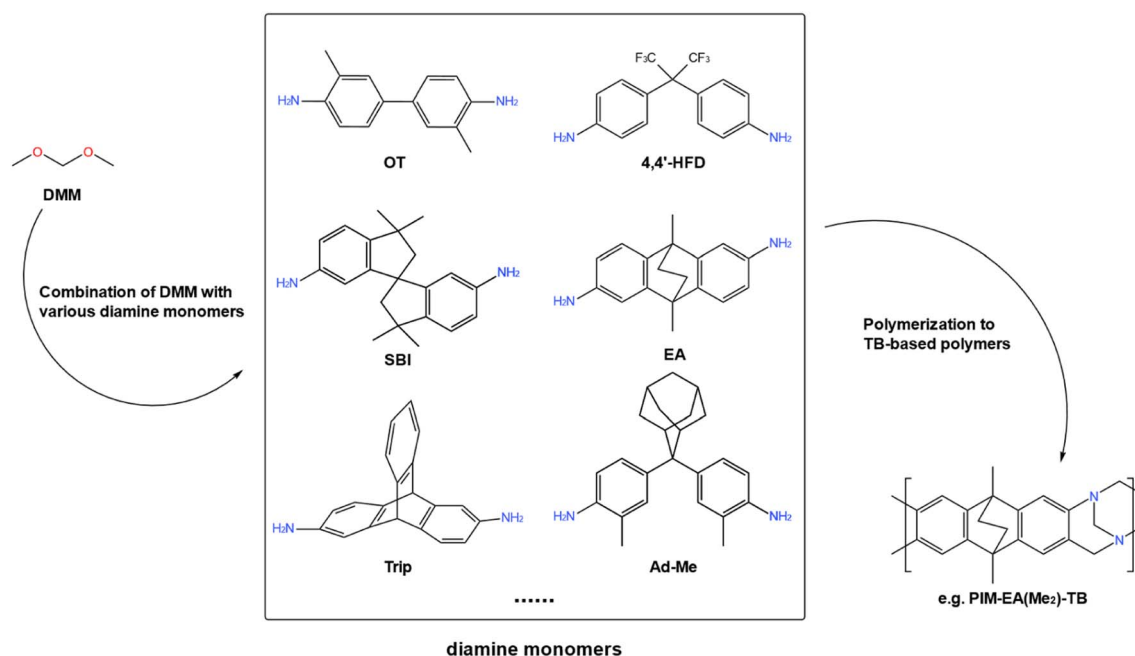
synthesized.<sup>73–75</sup> In the field of polymer synthesis, researchers have developed multiple polymers based on different TB monomers.<sup>76,77</sup> Attempts had not been made to apply TB polymers as gas separation membrane materials until 2013.<sup>70,78</sup> Since then, many efforts have been dedicated to develop new TB polymers with the purpose of improving the CO<sub>2</sub> separation performances.<sup>79–81</sup>

### 2.1 TB polymer based CO<sub>2</sub> separation membranes

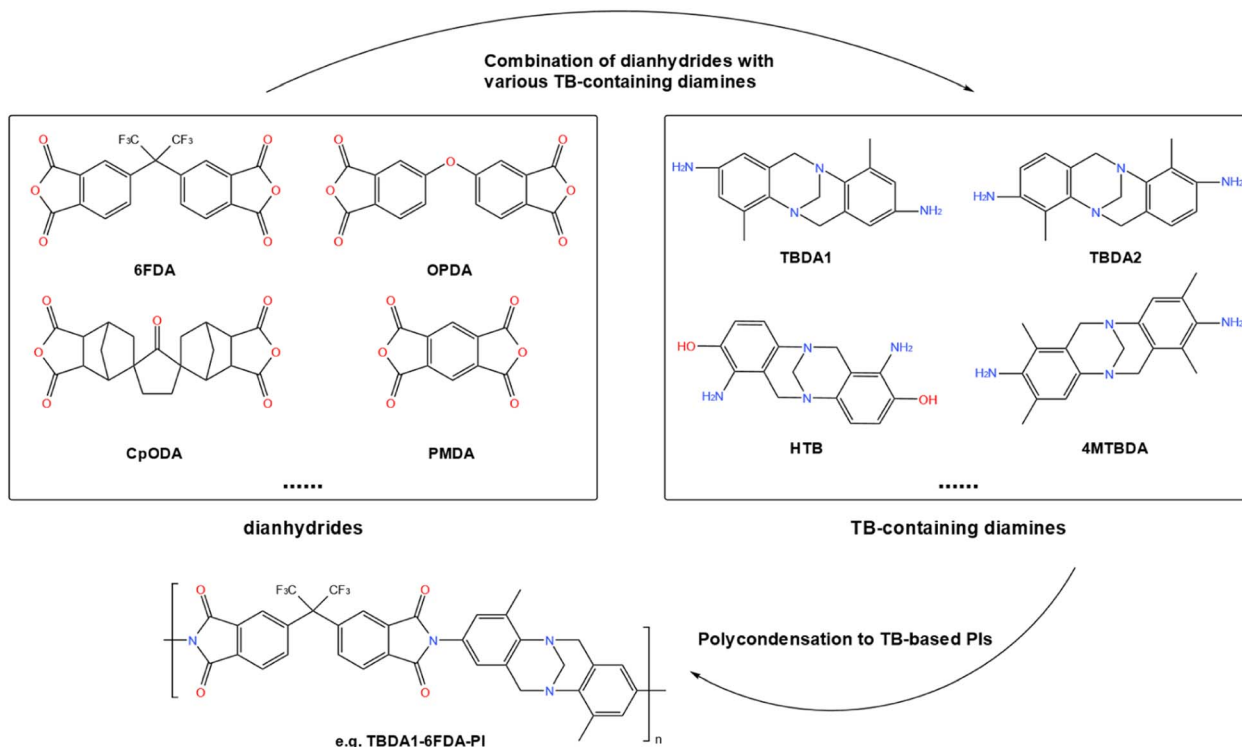
After years of development, there are mainly two methods for TB polymer synthesis for gas separation membranes. The first one is the straightforward method similar to the one developed in 1887,<sup>70</sup> in which the TB polymer was obtained by polymerization of diamine monomer and DMM, as shown in Scheme 1.

Another way of synthesizing TB polymer is a two-step process; the TB unit was first formed in diamine or dianhydride, and then diamine and/or dianhydride was employed to form PI with a TB unit. The reaction scheme is presented in Scheme 2.

**2.1.1 Conventional TB polymers.** Conventional TB polymers are characterized by their low BET surface area and fractional free volume (FFV). In early explorations, TB polymers were derived from commercially available aromatic diamine monomers with repeated units composed of TB and coplanar benzene rings, resulting in low BET surface area and poor CO<sub>2</sub> permeability. For example, TB polymers derived from 2-methyl-1,3-benzenediamine (DAT) and 2,5-dimethyl-1,4-phenylenediamine (DPD) had low surface area and gas permeation data were not tested (shown in Fig. 2).<sup>78</sup> In another study, methyl lateral groups were introduced onto the TB polymer chain, which increase chain spacing. These polymers were found to exhibit a CO<sub>2</sub> permeability of 45.0 and 6.8 Barrer, a CO<sub>2</sub>/CH<sub>4</sub> selectivity of 30.0 and 28.0, and CO<sub>2</sub>/N<sub>2</sub> selectivity



Scheme 1 The conventional route of TB polymer synthesis.



Scheme 2 TB polycondensation between dianhydride and TB-containing diamine.

values of 26.0 and 19.0. However, the overall CO<sub>2</sub> separation performances are still located in the low region.<sup>82</sup>

Later, a more rigid bridging structure such as naphthalene, was chosen as the moiety to yield 1,5-diaminonaphthalene

(1,5-DAN) TB based polymer (1,5-DTBP).<sup>83</sup> Afterwards, two copolymers, (referred to as 90D10HTBP and 50D50HTBP) were prepared by copolymerization with 4,4'-(hexafluoroisopropylidene)dianiline (4,4'-HFD), as depicted in Fig. 2.

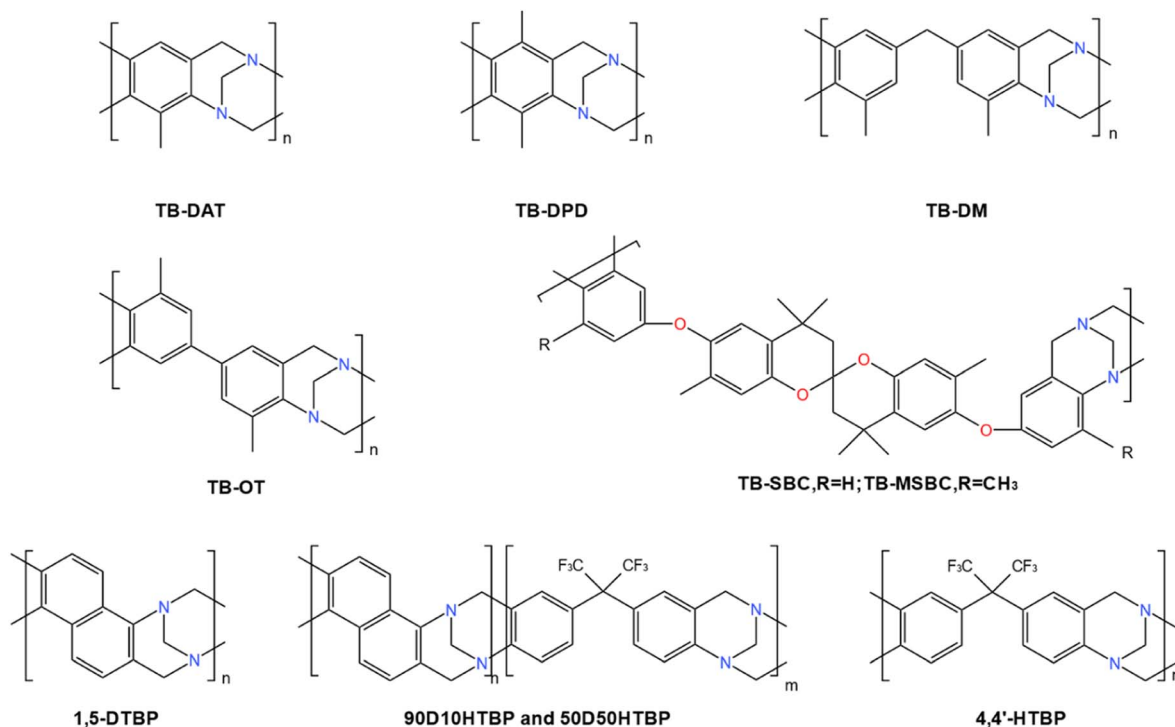


Fig. 2 Examples of conventional TB polymers.

Table 1 CO<sub>2</sub> separation performances of conventional TB polymers

Polymer	$P_{\text{CO}_2}$ (Barrer)	$\alpha_{\text{CO}_2/\text{CH}_4}$ (—)	$\alpha_{\text{CO}_2/\text{N}_2}$ (—)	Ref.
TB-OT	45.0	30.0	26.0	82
TB-DM	6.8	28.0	19.0	82
TB-MSBC	161.7	16.6	—	84
TB-SBC	59.8	16.5	—	84
1,5-DTBP	170.0	24.0	17.4	83
90D10HTBP	292.0	24.4	18.1	83
50D50HTBP	97.0	29.8	20.1	83
4,4'-HTBP	57.0	41.3	23.9	83
1.25 wt%-BTB	129.0	—	33.5	85
2.5 wt%-BTB	137.0	—	32.4	85
5 wt%-BTB	145.0	—	31.6	85

It was discovered that as the 4,4'-HFD content increased, CO<sub>2</sub> permeabilities increased first and then decreased. The 90D10HTBP sample, which contained 10% 4,4'-HFD had the highest CO<sub>2</sub> permeability of 292.0 Barrer, coupled with a CO<sub>2</sub>/N<sub>2</sub> and CO<sub>2</sub>/CH<sub>4</sub> selectivity of 24.4 and 18.1, respectively.<sup>83</sup>

Similarly, it was found that fused rings can enhance chain rigidity in comparison with the relatively flexible C–N single bond. Zhang *et al.*<sup>84</sup> replaced the 4,4'-(hexafluoroisopropylidene)-diphthalic anhydride (6FDA) moiety with a TB group, and two new polymers, namely TB-MSBC and TB-SBC were synthesized from the two spirobichroman-containing diamine monomers, 6,6'-bis(4-amino-3-methylphenoxy)-4,4,4',7,7'-hexamethyl-2,2'-spirobichroman (MSBC) and 6,6'-bis(4-aminophenoxy)-4,4,4',7,7'-hexamethyl-2,2'-spirobichroman (SBC), respectively (shown in Fig. 2). The resulting membranes showed better permeability and selectivity

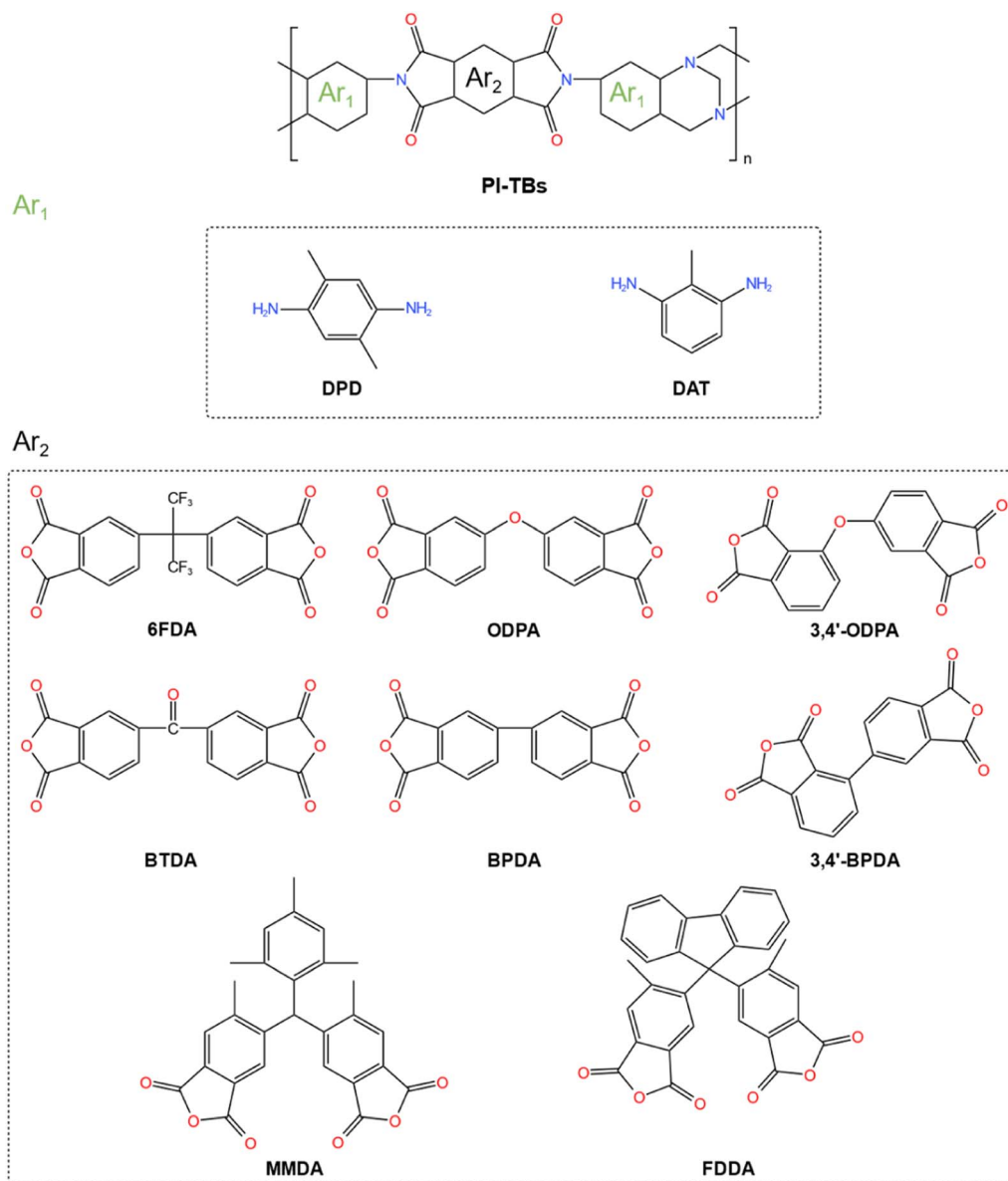


Fig. 3 PI-TBs derived from imide-containing diamine monomers.

Table 2 Gas separation performances of TB-PI polymeric membranes

Polymer	$P_{CO_2}$ (Barrer)	$\alpha_{CO_2/CH_4}$ (—)	$\alpha_{CO_2/N_2}$ (—)	$\alpha_{CO_2/H_2}$ (—)	Ref.
Ac-CoPI-TB-1	1366.0	16.0	17.0	1.3	92
Ac-CoPI-TB-2	555.0	17.0	17.0	2.0	92
Ac-CoPI-TB-3	377.0	17.0	16.0	1.5	92
Ac-CoPI-TB-4	203.0	19.0	20.0	1.2	92
PI-TB-N	731.0	19.0	19.0	1.6	92
PI-TB-1	457.0	17.0	15.0	1.3 <sup>a</sup>	87
PI-TB-2	55.0	26.0	22.0	2.5 <sup>a</sup>	87
PI-TB-3	218.0	32.7	22.9	1.4 <sup>a</sup>	88
PI-TB-4	13.5	13.5	10.8	3.0 <sup>a</sup>	88
PI-TB-5	19.5	11.5	10.5	2.7 <sup>a</sup>	88
PI-TB-6	104.5	18.1	21.3	1.5 <sup>a</sup>	89
PI-TB-7	112.0	20.4	17.5	1.9 <sup>a</sup>	89
PI-TB-8	53.7	26.4	21.3	2.3 <sup>a</sup>	89
PI-TB-9	110.1	22.6	19.4	1.7 <sup>a</sup>	89
PI-TB-12	57.3	34.1	25.8	1.9 <sup>a</sup>	89
CoPI-TB-1	158.0	23.0	23.0	1.6 <sup>a</sup>	90
CoPI-TB-2	209.0	21.0	20.0	1.9 <sup>a</sup>	90
CoPI-TB-3	196.0	22.0	21.0	1.9 <sup>a</sup>	90
CoPI-TB-4	241.0	14.0	12.0	2.8 <sup>a</sup>	90
CoPI-TB-5	228.0	20.0	22.0	1.5 <sup>a</sup>	90
CoPI-TB-6	330.0	17.0	20.0	1.4 <sup>a</sup>	90
TBDA1-6FDA-PI	155.0	46.9	23.8	—	67
TBDA1-ODPA-PI	13.4	36.2	26.8	—	67
TBDA2-6FDA-PI	285.0	35.6	23.8	—	67
TBDA2-ODPA-PI	106.0	48.2	27.9	—	67
TBDA1-SBI-PI	895.0	19.7	25.6	—	68
TBDA2-SBI-PI	1213.0	18.7	24.8	—	68
TB-PIMPI-33	180.0	36.4	26.4	—	100
TB-PIMPI-50	184.0	35.4	24.7	—	100
TB-PIMPI-66	312.0	32.8	21.4	—	100
TB-PIMPI-75	335.0	31.3	20.6	—	100
TB-PIMPI-83	295.0	33.1	24.0	—	100
PIM-PI-TB-1	662.0	15.0	—	—	103
Aged PIM-PI-TB-1	361.0	23.0	—	—	103
PIM-PI-TB-2	595.0	19.0	—	—	103
Aged PIM-PI-TB-2	376.0	21.0	—	—	103
4MTBDA-6FDA	1672.0(1008.0) <sup>b</sup>	14.4(16.8) <sup>b</sup>	—	—	102
4MTBDA-PMDA	4460.0(1689.0) <sup>b</sup>	11.4(14.8) <sup>b</sup>	—	—	102
4MTBDA-SBIDA	5140.0(2476.0) <sup>b</sup>	8.7(—) <sup>b</sup>	—	—	102
4MTBDA-SBFDA	4476.0(1621.0) <sup>b</sup>	12.1(13.0) <sup>b</sup>	—	—	102
Bio-TBPI-1	575.0	—	—	—	94
Bio-TBPI-2	702.0	—	—	—	94
Bio-PITB-1-Vac	1123.0(1008.0) <sup>c</sup>	23.0(25.0) <sup>c</sup>	22.0(22.0) <sup>c</sup>	—	95
Bio-PITB-1-air	1352.0(1076.0) <sup>c</sup>	23.0(25.0) <sup>c</sup>	21.0(22.0) <sup>c</sup>	—	95
Bio-PITB-2-Vac	1201.0(1087.0) <sup>c</sup>	24.0(27.0) <sup>c</sup>	22.0(22.0) <sup>c</sup>	—	95
Bio-PITB-2-air	1384.0(1161.0) <sup>c</sup>	23.0(26.0) <sup>c</sup>	22.0(23.0) <sup>c</sup>	—	95
6FDA-HB	286.0(254.0) <sup>d</sup>	26.0(27.0) <sup>d</sup>	—	—	96
TDAi3-HB	998.0(788.0) <sup>e</sup>	20.0(21.0) <sup>e</sup>	—	—	96
POLY-H	130.1	32.9	19.5	—	101
POLY-F	136.8	31.8	18.7	—	101
POLY-CF <sub>3</sub>	187.1	30.7	12.5	—	101
POLY-COOH	120.5	38.8	19.8	—	101
TB-PI	190.0	30.2	—	1.7 <sup>a</sup>	104
TB-PI-COOH-10	138.0	36.3	—	2.0 <sup>a</sup>	104
TB-PI-COOH-20	112.0	56.0	—	2.2 <sup>a</sup>	104
TB-PI-COOH-30	76.0	76.0	—	2.4 <sup>a</sup>	104
TB-PI-COOH-40	58.0	83.0	—	2.6 <sup>a</sup>	104
TB-PI-COOH-50	37.0	62.0	—	3.7 <sup>a</sup>	104
6FDA-HTB	67.0(55.0) <sup>f</sup>	73.0(76.0) <sup>f</sup>	—	—	66
SBI-HTB	466.0	29.0	—	—	66
TBDA-HTB	71.0(61.0) <sup>g</sup>	38.0(54.0) <sup>g</sup>	—	—	105
TBDA-TMPD	1457.0(744.0) <sup>h</sup>	17.0(20.0) <sup>h</sup>	—	—	105
PA "I"	109.1	50.3	—	—	106

Table 2 (Contd.)

Polymer	$P_{\text{CO}_2}$ (Barrer)	$\alpha_{\text{CO}_2/\text{CH}_4}$ (—)	$\alpha_{\text{CO}_2/\text{N}_2}$ (—)	$\alpha_{\text{CO}_2/\text{H}_2}$ (—)	Ref.
PA “II”	92.2	46.8	—	—	106
PA “III”	84.7	48.4	—	—	106
PA “IV”	86.4	53.7	—	—	106
TNTDA-TBDA1	397.0	31.7	25.7	—	99
CpODA-TBDA1	240.0(203.0) <sup>i</sup>	25.4(29.6) <sup>i</sup>	18.2(18.4) <sup>i</sup>	—	93
CpODA-TBDA2	498.0(343.0) <sup>i</sup>	18.6(21.7) <sup>i</sup>	18.9(20.1) <sup>i</sup>	—	93

<sup>a</sup>  $\text{H}_2/\text{CO}_2$ . <sup>b</sup> The numbers in parentheses refer to the aged data (4MTBDA-6FDA = 524 days; 4MTBDA-PMDA = 333 days; 4MTBDA-SBIDA = 509 days; 4MTBA-SBFDA = 405 days). <sup>c</sup> The numbers in parentheses refer to the data obtained for the membranes aged for 100 days. <sup>d</sup> The numbers in parentheses refer to the data obtained for the membranes aged for 200 days. <sup>e</sup> The numbers in parentheses refer to the data obtained for the membranes aged for 330 days. <sup>f</sup> The numbers in parentheses refer to the data obtained for the membranes aged for one month. <sup>g</sup> The numbers in parentheses refer to the data obtained for the membranes aged for 50 days. <sup>h</sup> The numbers in parentheses refer to the data obtained for the membranes aged for 90 days. <sup>i</sup> The numbers in parentheses refer to the data obtained for the membranes aged for 100 days.

compared to those 6FDA-based PI prepared from the same diamines. Meanwhile, TB-MSBC exhibited higher permeability (161.7 Barrer vs. 59.8 Barrer) and similar selectivity in comparison with the “methyl-less” TB-SBC polymer.

Instead of developing highly rigid linear polymers, Yue *et al.*<sup>85</sup> designed a series of branched TB polymers (*x*-BTB) with mixed diamines, namely tetrakis(4-aminophenyl) methane (TAPM) and *o*-tolidine (OT). Compared to the linear OT-based

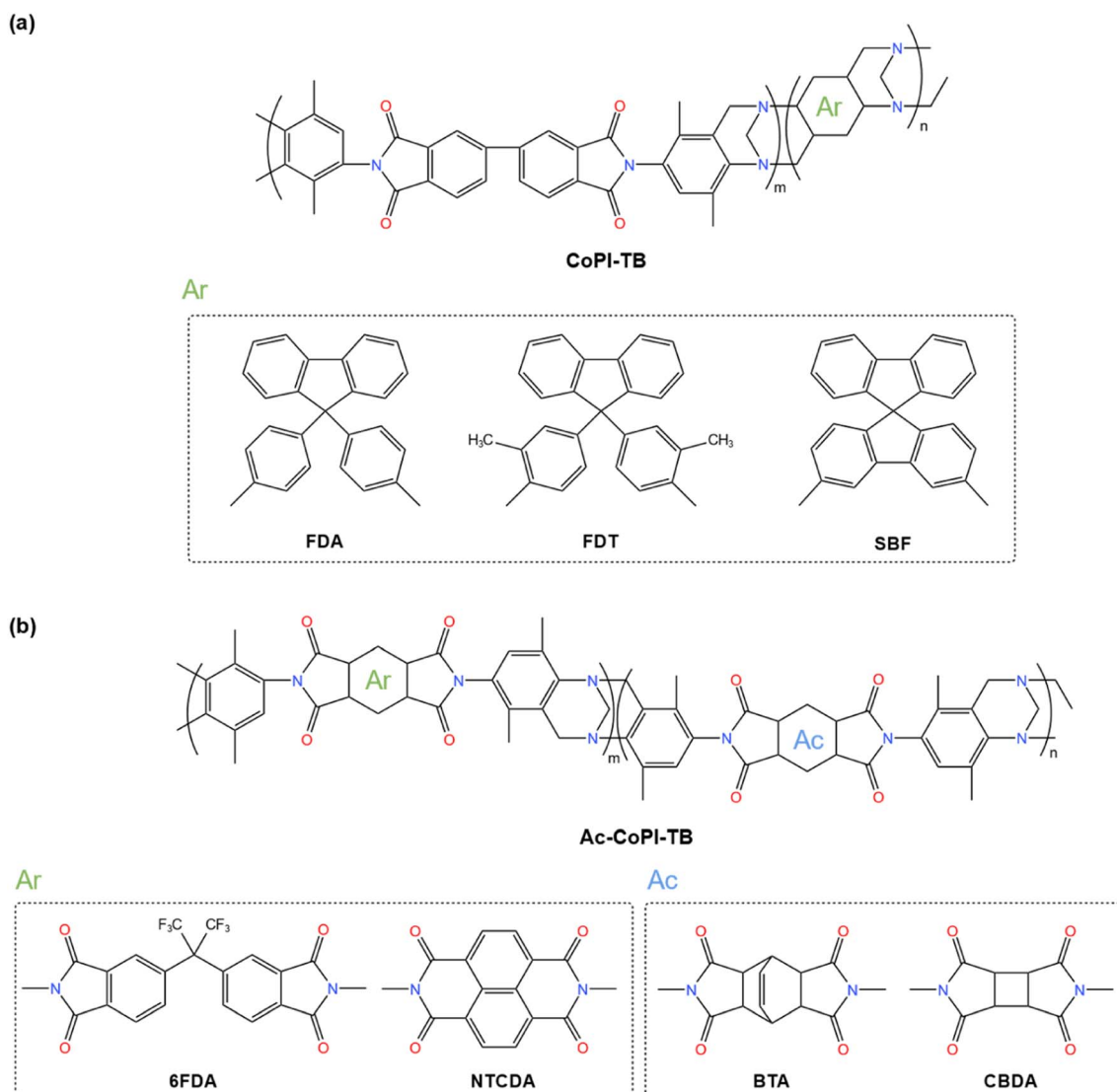


Fig. 4 Co-PI-TBs derived from imide-containing diamine monomers, (a) CoPI-TB, (b) Ac-CoPI-TB.

TB polymer (TB-OT), the *x*-BTBs exhibited much higher CO<sub>2</sub> permeability (129.0–145.0 Barrer) and comparable CO<sub>2</sub>/N<sub>2</sub> selectivity (31.6–33.5), which revealed the advantage of introducing a tetraphenylmethane branch structure into the backbone. Moreover, the *x*-BTBs also exhibited much better physical aging resistance compared to the neat TB-OT polymer. The CO<sub>2</sub> separation performances of conventional TB polymers were collected and are presented in Table 1.

**2.1.2 TB-based PIs.** PIs, known for their good thermal and chemical stabilities, as well as excellent mechanical properties, are highly promising candidates for CO<sub>2</sub> gas separation membranes.<sup>86</sup> In order to improve the CO<sub>2</sub> separation

performances, researchers have explored the incorporation of TB units into the PI polymeric chain to improve the stiffness of the polymer backbone and enhance chain packing. In general, there are two typical methods for preparing TB-based PIs: TB polymerization using imide-containing diamine monomers (PI-TB) and imidization using TB-containing monomers (TB-PI).

**2.1.2.1 PI-TBs.** PI-TB polymers were synthesized by polymerization of imide-containing diamine monomers with DMM, while the imide-containing diamines were normally obtained by 'grafting' two diamines onto both sides of commonly used dianhydrides. By combining 2 different diamines and 8 dianhydrides, a series of TB-based PIs named PI-TB-*x* (*x* = 1, 2...11,

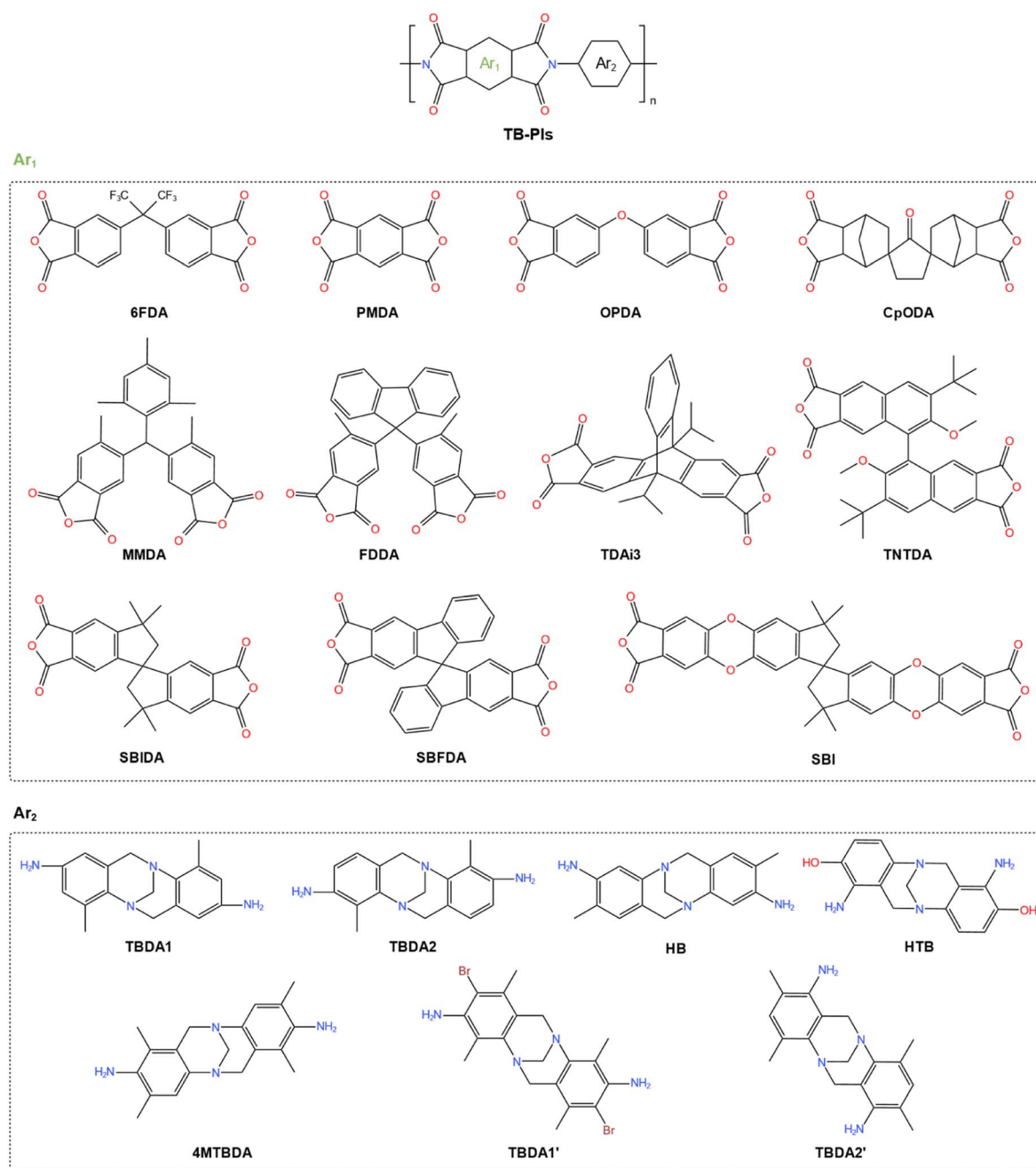


Fig. 5 Representative examples of TB-PIs, reproduce from ref. 68.

12) was developed by Zhuang *et al.*<sup>87–89</sup> (shown in Fig. 3). Gas permeation was also carried out and the results showed that the introduction of a TB unit into the PI polymeric chain greatly improved the CO<sub>2</sub> separation performances (shown in Table 2). For example, the CO<sub>2</sub> permeability of PI-TB-1 was 457.0 Barrer, which was about 11 times higher than that of the PI derived from the same precursors, PI-6FDA-DPD (43.0 Barrer). The obtained PI-TB also presented great tensile strength. It is worth mentioning that the PI-TB developed with different anhydrides also perfectly follow the permeability-selectivity trade-off, a higher CO<sub>2</sub> permeability normally coupled with relatively lower selectivity.

In addition, co-PI-TB can be also obtained by combining different diamines and/or dianhydrides in the PI-TB synthesis process.<sup>90</sup> Depending on the ratio between An-BPDA and the diamine co-monomer, a series of co-PIs abbreviated as CoPI-TB-*x* (*x* = 1–6) were successfully obtained (shown in Fig. 4(a)). The resulting copolymers showed better gas permeability compared with conventional BPDA-based PIs. Due to the additional FFV imparted by the TB units in the backbone, the CO<sub>2</sub> permeability of CoPI-TB-1 and CoPI-TB-2 was about 7-fold and 9-fold higher than that of the neat PI-BAFL-BPDA ( $P_{\text{CO}_2}$  = 23.0 Barrer (ref. 91)). Moreover, it is found out that more rigid monomers normally lead to higher CO<sub>2</sub> permeability.

To further investigate the effects of alicyclic segments on gas transport properties, Zhang *et al.*<sup>92</sup> incorporated the chosen alicyclic segments into TB-PI backbones *via* copolymerization (shown in Fig. 4(b)). The results showed that the introduction of alicyclic segments significantly enhanced H<sub>2</sub>/CO<sub>2</sub> separation performance, while the separation performance for CO<sub>2</sub>/CH<sub>4</sub> and CO<sub>2</sub>/N<sub>2</sub> gas pairs was almost unchanged. In addition, when the testing temperature increased from 35 to 200 °C, the membrane changed from CO<sub>2</sub> selective to H<sub>2</sub> selective, in which the H<sub>2</sub>/CO<sub>2</sub> selectivity of Ac-CoPI-TB-2 increased from 0.59 to 3.70.

**2.1.2.2 TB-PIs.** Except these studies of PI-TBs derived from imide-containing diamine monomers, many efforts also have been put into the research work on synthesizing TB-PIs by polycondensation of diamines with a TB unit and dianhydrides. In this process, the TB unit was first introduced into the diamines, and then the TB-PI polymer can be obtained by a conventional PI synthesis procedure. In 2014, four TB-PIs named TBDA1-6FDA-PI, TBDA2-6FDA-PI, TBDA1-ODPA-PI, and TBDA2-ODPA-PI were synthesized between two TB-containing diamine monomers (TBDA1 and TBDA2) and two anhydride monomers, 6FDA and ODPA<sup>67</sup> (shown in Fig. 5). Compared to traditional PI membranes, the four TB-PIs exhibited greatly improved CO<sub>2</sub> separation performances (shown in Table 2). The TB unit with a rigid and in-built amine structure increased the gas permeability while the high selectivity was maintained nicely. Later on, two new microporous PIs (TBDA1-SBI-PI and TBDA2-SBI-PI) were developed by replacing dianhydrides with spirobisindane based dianhydride<sup>68</sup> (shown in Fig. 5). The obtained two polymers exhibited high CO<sub>2</sub> permeability (895.0 and 1213.0 Barrer), as well as excellent CO<sub>2</sub>/N<sub>2</sub> selectivity (25.6 and 24.8) and CO<sub>2</sub>/CH<sub>4</sub> selectivity (19.7 and 18.7), respectively.

(1) *Bulky and rigid bridging structures in the backbone.* Other than the relatively conventional dihydrates, *e.g.*, 6FDA, PMDA and OPDA, lots of research has also been focusing on integrating rigid and contorted bridging moieties to construct a shape-tolerant TB-PI backbone to enhance overall gas separation performances.

Many dihydrates with PIM like structure were developed and used in PI as well. For example, SBIDA, SBI and SBFDA. As expected, TB-PI synthesized *via* these monomers normally exhibited a relatively high free volume and consequently high CO<sub>2</sub> permeability, and thus, they were also considered as polymers with intrinsic porosity. Other than them, other bulky dihydrates have also been developed and used to synthesize TB-PI as well. Lu *et al.*<sup>93</sup> chose the contorted dianhydride, norbornane-2-spiro- $\alpha$ -cyclopentanone- $\alpha'$ -spiro-2''-norbornane-5,5'',6,6'-tetracarboxylic dianhydride (CpODA) as a building block to yield TB-PIs (shown in Fig. 5). The CpODA-TBDA2 possessed a moderate CO<sub>2</sub> permeability of 498.0 Barrer, which was 2 fold greater than that of CpODA-TBDA1. Moreover, compared to those of the counterparts derived from 6FDA, the CO<sub>2</sub>/CH<sub>4</sub> and CO<sub>2</sub>/N<sub>2</sub> separation performance of the two CpODA-derived TB-PIs was slightly lower. In addition, the two obtained CpODA-derived TB-PIs showed excellent resistance to physical aging. The membranes aged for 100 days showed comparable or greater performance relative to those of the fresh ones.

Similarly, two novel contorted dianhydrides, 5,5'-(mesitylmethylene)bis(4-methylphthalic anhydride) (MMDA) and 5,5'-(9H-fluorene-9,9-diyl)bis(4-methylphthalic anhydride) (FDPA) were developed from guaiacol<sup>94</sup> (shown in Fig. 5). The results showed that the Bio-TBPIs exhibited improved gas permeability relative to that of other reported 6FDA-based TB-PIs. For example, the CO<sub>2</sub> permeability of Bio-TBPI-2 was 702.0 Barrer, which was higher than that of PIM-PI-TB-1 (662.0 Barrer). Moreover, combined with a CO<sub>2</sub> permeability over 500.0 Barrer and CO<sub>2</sub>/CH<sub>4</sub> selectivity over 24.0, the Bio-TBPIs demonstrated exceptional performance for CO<sub>2</sub>/CH<sub>4</sub> separation in comparison with many PIs, which was between 1991 and 2008 upper bounds. In terms of physical aging, the Bio-TBPIs are less affected by physical aging than 6FDA-based TBPIs.

In the following experiment, the same group<sup>95</sup> changed the synthesis method to one-step TB polymerization to get Bio-PITBs. Compared to Bio-TBPIs, the Bio-PITBs presented improved gas permeability with good selectivity. For example, the CO<sub>2</sub> permeability of Bio-PITB-2 is 1352.0 Barrer coupled with a CO<sub>2</sub>/CH<sub>4</sub> selectivity of 23.0. Moreover, Bio-PITBs displayed reverse selective characteristics towards the CO<sub>2</sub>/H<sub>2</sub> gas pair, which was ascribed to the dipole–quadrupole interactions between CO<sub>2</sub> and carbonyl groups in the imide ring, enhancing CO<sub>2</sub> solubility selectivity.

More recently, a Hünlich base (HB), a unique TB-derived unit, was also employed as a building block to form two HB-based polymers, 6FDA-HB and TDAi3-HB<sup>96</sup> (shown in Fig. 5). The results showed that TDAi3-HB exhibited much higher permeability for all the tested gases (H<sub>2</sub>, N<sub>2</sub>, O<sub>2</sub>, CH<sub>4</sub>, CO<sub>2</sub>, and He) but relatively reduced the gas selectivity, which followed the permeability/selectivity trade-off relationship when compared

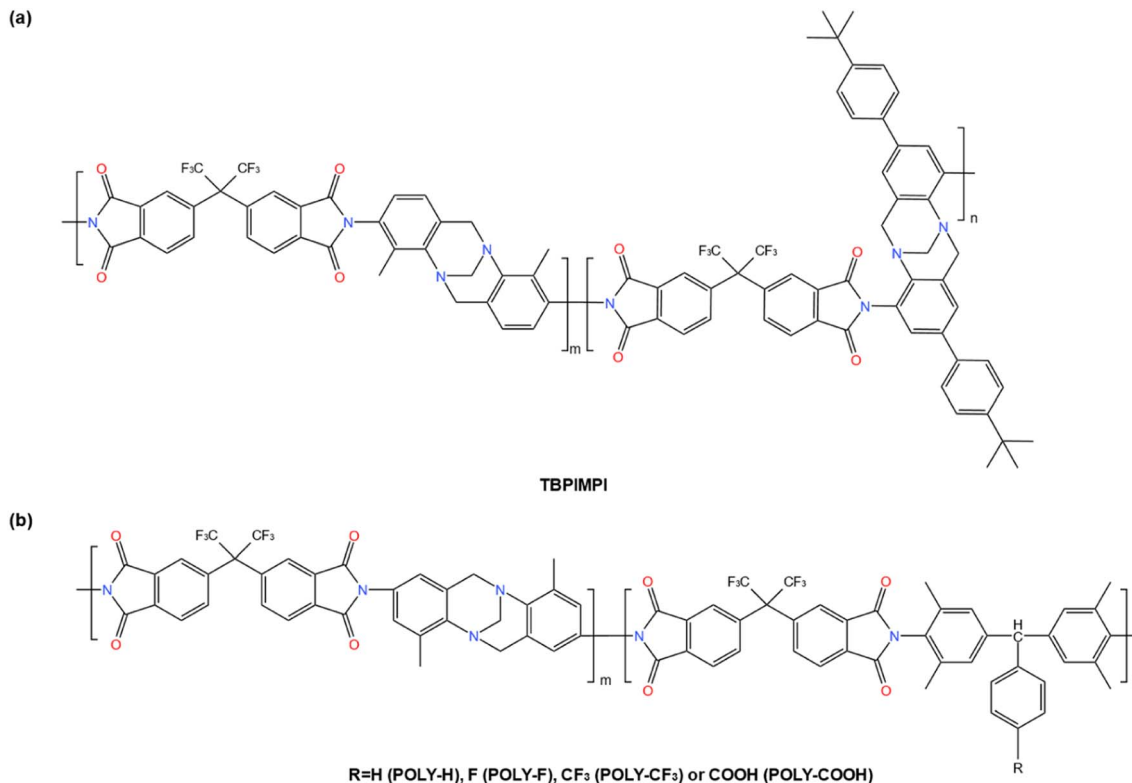


Fig. 6 Co-TB-PIs with a bulky pendant group in ref. 100 and 101. (a) TBPIMPI, (b) CoTB-PI with 4 different side groups.

to 6FDA-HB. A CO<sub>2</sub> permeability of up to 998.0 Barrer coupled with a CO<sub>2</sub>/CH<sub>4</sub> selectivity of 20.0 was documented for TDAi3-HB. Moreover, the obtained TB-PI exhibited better physical aging resistance compared to other PIs derived from the same prototype. After aging for 330 days, the CO<sub>2</sub> permeability of TDAi3-HB dropped only 21% (from 998.0 to 788.0 Barrer). Meanwhile, the two HB-based PIs show good plasticization resistance even at a pressure of 15 bar.

(2) *Pendant moiety and substituent group.* Other than developing a bulky, contorted and rigid structure in the monomer, it is well accepted that tuning the pendant moiety can be a promising strategy to enhance the CO<sub>2</sub> separation performance of polymeric membranes.<sup>97,98</sup> Abundant efforts have been also dedicated to graft various functional groups onto TB polymeric chains with the aim of improving CO<sub>2</sub> separation performances.

By introducing a bulky *tert*-butyl substituent to disturb the chain packing and thus increasing the gas permeability, Hu

*et al.*<sup>99</sup> designed a novel dianhydride, 3,3'-di-*tert*-butyl-2,2'-dimethoxy-[1,1'-binaphthalene]-6,6',7,7'-tetracarboxylic dianhydride (TNTDA) and subsequently yielded a new PIM-PI (TNTDA-TBDA1) through the polycondensation between TNTDA and TBDA1 (shown in Fig. 5). The resulting TNTDA-TBDA1 displayed a 2.5 fold higher CO<sub>2</sub> permeability (397.0 Barrer) with comparable CO<sub>2</sub>/N<sub>2</sub> (25.7) and CO<sub>2</sub>/CH<sub>4</sub> selectivity (31.7) compared to 6FDA-TBDA1.

Later, an *ortho*-substituted TB diamine with pendant *tert*-butyl-phenyl (*t*-BuPh) groups, 2,8-bis(4-*tert*-butylphenyl)-4,10-diamino-6,12-dihydro-5,11-methanodibenzo[*b,f*][1,5]diazocine (TTBDA) was designed by the same group, and a series of TB-PIs was synthesized accordingly (shown in Fig. 6(a)).<sup>100</sup> Compared to 6FDA/TBDA2, the resulting co-TB-PIs with more than 50% TTBDA exhibited superior CO<sub>2</sub> permeability with comparable or better selectivity. Among them, TB-PIMPI-75 presented the greatest gas permeability (335.0 Barrer) with a moderate CO<sub>2</sub>/CH<sub>4</sub> selectivity (31.3).

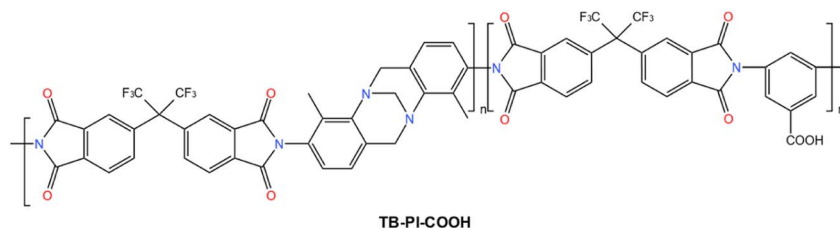


Fig. 7 Structure of the three-block co-TB-PI (TB-PI-COOH) synthesized in ref. 104.

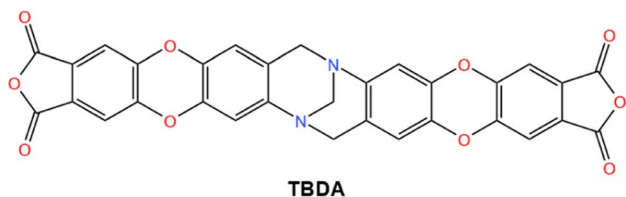


Fig. 8 Novel TB-based dianhydride (TBDA) in ref. 105.

To further investigate the influence of size and polarity of the pendant group on separation performance, Xu *et al.*<sup>101</sup> introduced a series of tetramethyl-substituted TPM-based diamines with different substituted groups ( $-H$ ,  $-F$ ,  $-CF_3$ , and  $-COOH$ ) into the backbone of TB-PI by a simple one-step copolymerization (shown in Fig. 6(b)). The  $CO_2$  permeability of the resulting membranes ranged from 120.5 to 187.1 Barrer with an increase in the order of  $-COOH < -H < -F < -CF_3$ , which were consistent with the resultant polymer FFV values. Moreover,  $-COOH$  created unique affinity to  $CO_2$ , causing the highest ideal selectivities of 19.8 and 38.8 for  $CO_2/N_2$  and  $CO_2/CH_4$ .

TB-containing diamines modified with *ortho*-methyl or bromine substituents can increase steric hindrance and thus obtain highly permeable TB-PIs. Lee *et al.*<sup>102</sup> introduced a second methyl substituent near the two amino groups on the TB monomer and synthesized a series of TB-PIs derived from the TB diamine monomer (4MTBDA). All the 4MTBDA-derived PIs demonstrated an outstanding combination of high gas permeability and good selectivity, which were close to the 2008  $CO_2/CH_4$  upper bound.

Similarly, Ghanem *et al.*<sup>103</sup> designed two di-*ortho*-substituted TB-containing diamines named TBDA1' and TBDA2', and subsequently synthesized 6FDA-based PIs (PIM-PI-TB-1 and PIM-PI-TB-2) *via* the high temperature one-step cyclimidization reaction. Compared to the single-*ortho*-substituted TB-PIs such as TBDA-6FDA-PI and TBDA-ODPA-PI, the two obtained di-*ortho*-substituted TB-PIs showed higher  $CO_2$  permeability (662.0 and 595.0 Barrer) and lower  $CO_2/CH_4$  selectivity (15.0 and 19.0). In addition, after aging for 180 days, the prepared membranes exhibited a 18–60% reduction of permeability with a moderate increase in selectivity.

In terms of the functional group, TB polymers containing OH or COOH groups were commonly studied due to the fascinating interchain hydrogen bond. Ma *et al.*<sup>66</sup> synthesized two *o*-hydroxyl-functionalized TB-based PIs (6FDA-HTB and SBI-HTB). With a higher surface area, SBI-HTB showed better  $CO_2$  permeability (466.0 Barrer) than 6FDA-HTB (67.0 Barrer) but a significantly lower selectivity for  $CO_2/CH_4$  (29.0 vs. 73.0). Compared to the results reported for other 6FDA-based hydroxyl-functionalized PIs without kinked contortion sites, 6FDA-HTB displayed significantly higher gas permeability and selectivity. Moreover, a 10–20% reduction of permeability was documented after only one month of storage.

Considering that the tertiary amine TB units can react with acid groups by the formation of a hydrogen-bonding network, Wang *et al.*<sup>104</sup> synthesized a series of three-block copolymers (TB-PI-COOH) by mixing different proportions of amines with  $-COOH$  groups (shown in Fig. 7). The  $CO_2$  permeability of TB-PI-COOHs decreased from 190.0 Barrer to 37.0 Barrer with the increasing proportion of non-contorted 3,5-diaminobenzoic acid (DABA). Correspondingly, the  $CO_2/CH_4$  and  $H_2/CO_2$  selectivity of TB-PI-COOHs increased from 30.2 to 83.0 and from 1.7 to 3.7. In addition, it is worth mentioning that a hydrogen-bonding network is beneficial for increasing the plasticization resistance.

More recently, Abdulhamid *et al.*<sup>105</sup> designed a novel TB-based dianhydride (TBDA) (shown in Fig. 8) and then yielded two TBDA-based PIs by reacting TBDA with 1,7-diamino-6*H*,12*H*-5,11-methanodibenzo[1,5] diazocine-2,8-diol (HTB) and 2,3,5,6-tetramethyl-*p*-phenylenediamine (TMPD), named TBDA-HTB and TBDA-TMPD. Compared to 6FDA-TMPD, TBDA-TMPD showed better  $CO_2$  permeability (1457.0 Barrer) and  $CO_2/CH_4$  selectivity (17.0). Moreover, attributed to hydrogen-bonding, TBDA-HTB exhibited a great  $CO_2/CH_4$  selectivity of 38.0. In terms of physical aging, TBDA-HTB was less affected than TBDA-TMPD. In particular, the separation performance of TBDA-HTB became closer to the 2008 upper bound after aging.

Besides TB-PIs, Bisoi *et al.*<sup>106</sup> prepared a series of TB-bridged polyamides (PAs) (shown in Fig. 9) through a polycondensation of TBDA1 with four different diacids. The four resulting TB-based PAs exhibited outstanding  $CO_2/CH_4$  selectivity (46.8–53.7) coupled with a  $CO_2$  permeability over 84.0 Barrer. By

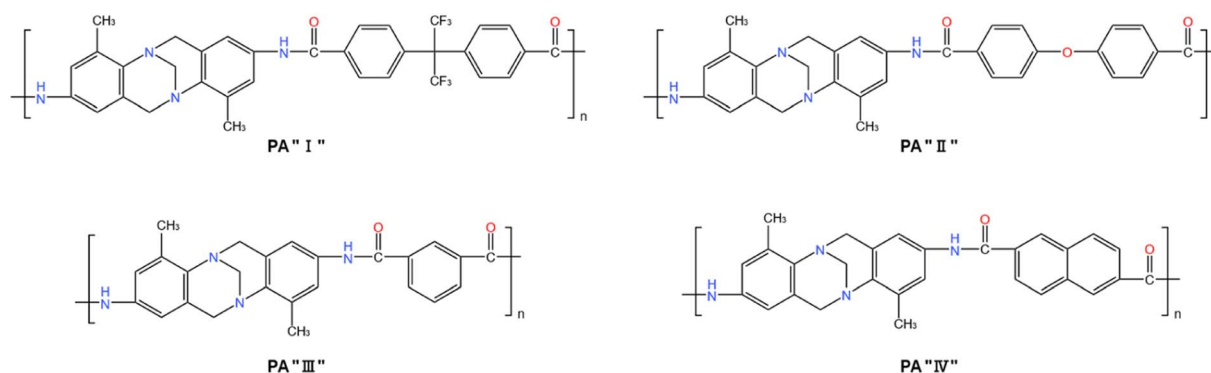


Fig. 9 TB-based PAs developed in ref. 106.

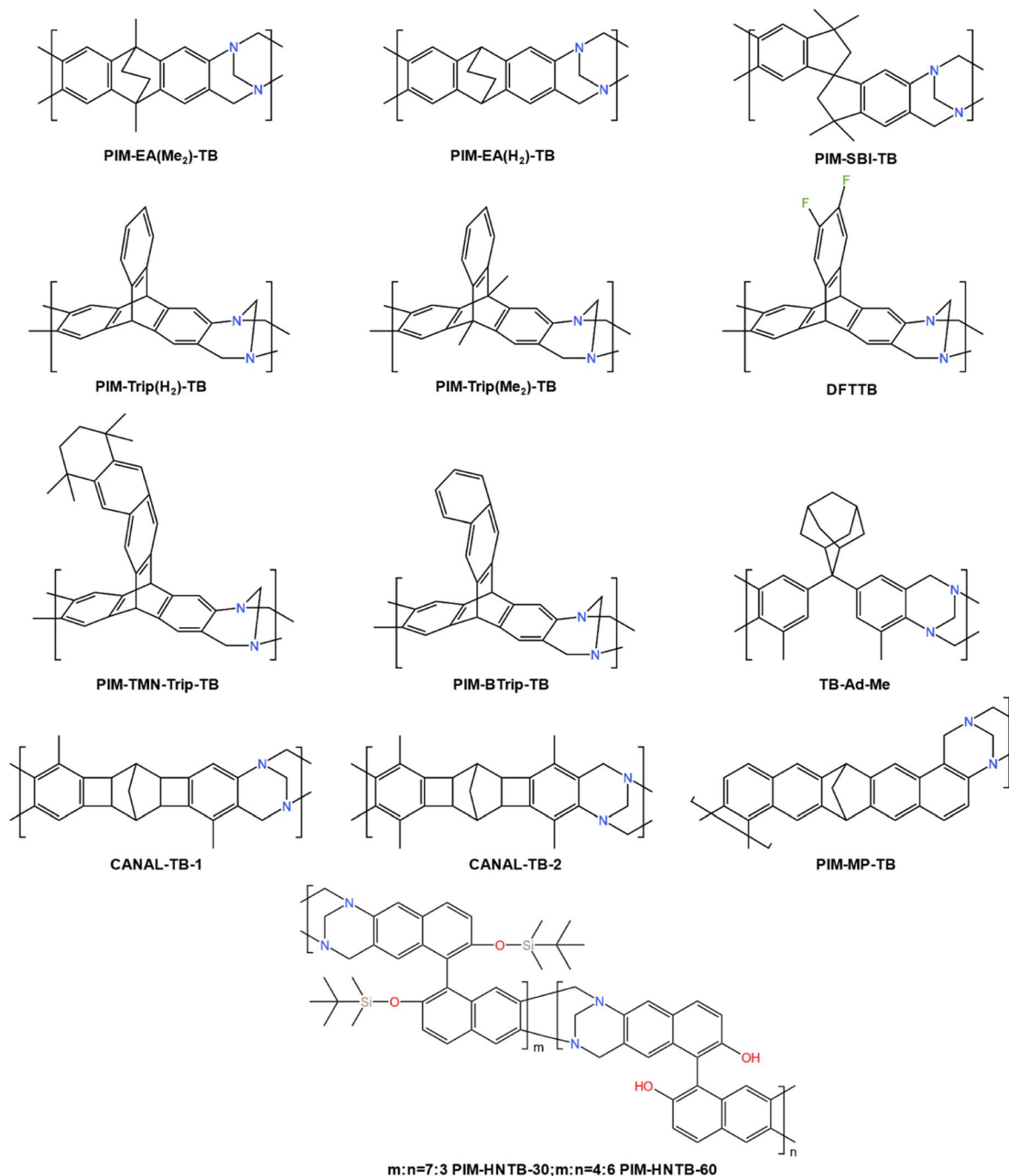


Fig. 10 Examples of high free volume TB polymers.

visualizing these data in the Robeson upper bound plot, it was clear that the  $\text{CO}_2/\text{CH}_4$  separation performance of TB-based PAs was on the 2008 upper bound.<sup>49</sup>

**2.1.3 Other high free volume TB polymers.** According to Freeman's theory, improving the rigidity of polymer chains and preventing chain stacking are effective approaches to improve the FFV and, consequently, gas permeabilities.<sup>107</sup> Consistent with this approach various TB polymers with a high FFV have been developed in recent years.

In 2013, Carta *et al.*<sup>70</sup> first introduced the rigid and contorted TB unit as a building block for PIM synthesis. In their work, they designed two TB-based ladder polymers (PIM-EA( $\text{Me}_2$ )-TB and PIM-SBI-TB), as shown in Fig. 10, derived from 2,6(7)-diamino-9,10-dimethylethanoanthracene and 5,5',6,(6')-diamino-3,3,3',3'-tetramethyl-1,1'-spirobisindane, respectively. The PIM-EA( $\text{Me}_2$ )-TB possessed higher  $\text{CO}_2$  permeability (7140 Barrer *vs.* 2900 Barrer) and  $\text{CO}_2/\text{N}_2$  selectivity (13.6 *vs.* 12.5) over PIM-SBI-TB due to the combined rigidity of the bridged bicyclic TB and ethanoanthracene (EA) units.

Table 3 CO<sub>2</sub> separation performances of high free volume TB polymers

Polymer	$P_{\text{CO}_2}$ (Barrer)	$\alpha_{\text{CO}_2/\text{CH}_4}$ (—)	$\alpha_{\text{CO}_2/\text{N}_2}$ (—)	$\alpha_{\text{CO}_2/\text{H}_2}$ (—)	Ref.
TB-Ad-Me	1820.0	—	15.1	—	108
PIM-HNTB-30	967.0(481.0) <sup>a</sup>	7.0(8.3) <sup>a</sup>	—	—	119
PIM-HNTB-60	833.0(341.0) <sup>b</sup>	11.8(10.4) <sup>b</sup>	—	—	119
CANAL-TB-1	1678.0(749.0) <sup>c</sup>	13.9(14.1) <sup>c</sup>	—	—	117
CANAL-TB-2	2520.0(1751.0) <sup>c</sup>	12.3(13.6) <sup>c</sup>	—	—	117
anti-CANAL-TB-2	2470.0	9.6	—	—	118
syn-CANAL-TB-2	2111.0	9.4	—	—	118
anti-CANAL-TB-4	2232.0	10.6	—	—	118
syn-CANAL-TB-4	2402.0	10.8	—	—	118
PIM-EA(Me <sub>2</sub> )-TB	7140.0(2644.0) <sup>d</sup>	10.0(12.1) <sup>d</sup>	13.6(14.1) <sup>d</sup>	0.9 <sup>k</sup>	70
PIM-SBI-TB	2900.0	—	12.5	—	70
PIM-EA(H <sub>2</sub> )-TB	5990.0	16.0	25.0	1.0 <sup>k</sup>	113
PIM-Trip(H <sub>2</sub> )-TB	9709.0(3951.0) <sup>e</sup>	10.7(18.1) <sup>e</sup>	15.9(20.9) <sup>e</sup>	0.8 <sup>k</sup>	80
PIM-Trip(Me <sub>2</sub> )-TB	3718.0(1880.0) <sup>f</sup>	10.7(12.1) <sup>f</sup>	14.6(19.6) <sup>f</sup>	1.5 <sup>k</sup>	111
PIM-BTrip-TB <sup>h</sup>	13 200.0	9.2	—	—	54
PIM-BTrip-TB <sup>i</sup>	4150.0	14.7	—	—	54
PIM-TMN-Trip-TB	6060.0	—	15.3	—	115
TBPIM33	4353.0	12.3	18.1	—	120
TBPIM25	4441.0	11.8	17.0	—	120
CoPIM-TB-1	7835.0(4977.0) <sup>g</sup>	13.6(16.1) <sup>g</sup>	21.3(21.2) <sup>g</sup>	—	81
CoPIM-TB-2	6767.0(4967.0) <sup>g</sup>	15.1(16.7) <sup>g</sup>	19.5(21.8) <sup>g</sup>	—	81
C-CoPIM-TB-1	5437.0(4937.0) <sup>g</sup>	23.3(23.0) <sup>g</sup>	26.5(31.4) <sup>g</sup>	—	81
C-CoPIM-TB-2	4251.0(4019.0) <sup>g</sup>	25.2(25.6) <sup>g</sup>	29.5(36.6) <sup>g</sup>	—	81
CA-PIM-1	6831.0	16.7	18.7	—	92
CA-PIM-1-300	7672.0	15.6	18.1	—	92
CA-PIM-1-325	8753.0	13.8	15.1	—	92
CA-PIM-1-350	8602.0	14.2	17.3	—	92
CA-PIM-1-375	9671.0	11.7	14.1	—	92
CA-PIM-1-400	12 563.0	4.9	6.2	—	92
CA-PIM-2	5946.0	18.2	18.7	—	92
CA-PIM-2-300	6709.0	15.8	18.0	—	92
CA-PIM-2-325	8051.0	13.7	15.5	—	92
CA-PIM-2-350	7668.0	14.4	16.2	—	92
CA-PIM-2-375	8512.0	12.9	14.3	—	92
CA-PIM-2-400	9854.0	5.2	5.7	—	92
CTTB	7136.0 <sup>l</sup>	22.5 <sup>m</sup>	33.2 <sup>n</sup>	—	112
MTTB	6273.0 <sup>l</sup>	19.7 <sup>m</sup>	29.3 <sup>n</sup>	—	112
ITTB	6880.0 <sup>l</sup>	18.4 <sup>m</sup>	27.6 <sup>n</sup>	—	112
DFTTB	3146.0(1005.0) <sup>j</sup>	21.8(20.5) <sup>j</sup>	—	—	79
PIM-MP-TB <sup>o</sup>	3500.0	13.3	17.5	—	62
PIM-MP-TB <sup>p</sup>	2340.0	14.8	18.7	—	62
PIM-MP-TB <sup>q</sup>	633.0	24.4	29.6	—	62
PIM-MP-TB <sup>r</sup>	378.0	25.7	28.4	—	62

<sup>a</sup> The numbers in parentheses refer to the data obtained for the membranes aged for 250 days. <sup>b</sup> The numbers in parentheses refer to the data obtained for the membranes aged for 180 days. <sup>c</sup> The numbers in parentheses refer to the data obtained for the membranes aged for 300 days. <sup>d</sup> The numbers in parentheses refer to the data obtained for the membranes aged for 106 days. <sup>e</sup> The numbers in parentheses refer to the data obtained for the membranes aged for 102 days. <sup>f</sup> The numbers in parentheses refer to the data obtained for the membranes aged for 407 days. <sup>g</sup> The numbers in parentheses refer to the data obtained for the membranes aged for 40 days. <sup>h</sup> Methanol treated. <sup>i</sup> After aging for 166 days. <sup>j</sup> The numbers in parentheses refer to the data obtained for the membranes aged for 180 days. <sup>k</sup> H<sub>2</sub>/CO<sub>2</sub>. <sup>l</sup> H<sub>2</sub> permeability (Barrer). <sup>m</sup>  $\alpha$  (H<sub>2</sub>/CH<sub>4</sub>). <sup>n</sup>  $\alpha$  (H<sub>2</sub>/N<sub>2</sub>). <sup>o</sup> Methanol treated. <sup>p</sup> Day 1 after thermal conditioning under vacuum at 140 °C. <sup>q</sup> After aging for 118 days and intermediate mixed gas permeation. <sup>r</sup> After 370 days of aging and intermediate mixed gas permeation.

Later, considering that the turnstile-like rotary thermal motion of methyl substituents at the bridgehead of the EA unit may reduce the selectivity of PIM-EA(Me<sub>2</sub>)-TB, EA was replaced with a 3D paddle-like triptycene (Trip) moiety and a new ladder-type PIM-Trip(H<sub>2</sub>)-TB was obtained<sup>80</sup> (shown in Fig. 10). As expected, higher CO<sub>2</sub> permeability (9709.0 Barrer) and better CO<sub>2</sub>/N<sub>2</sub> selectivity (15.9) were obtained for PIM-Trip(H<sub>2</sub>)-TB over PIM-EA(Me<sub>2</sub>)-TB (gas permeation data shown in Table 3). After

aging for 100 days, a 60% reduction of the CO<sub>2</sub> permeability was documented for PIM-Trip(H<sub>2</sub>)-TB membranes with a thickness of 132  $\mu\text{m}$ , showing that a faster physical aging may happen for thinner membranes. The same group<sup>108</sup> also designed a cardo-polymer (TB-Ad-Me) through one-step TB polymerization between DMM and 2,2-bis(3-methyl-4-aminophenyl) adamantane. The resulting product showed a moderately high CO<sub>2</sub> permeability of 1820.0 Barrer and unremarkable selectivity for

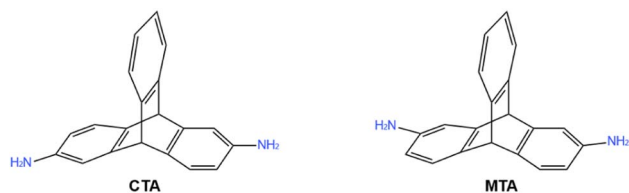


Fig. 11 Trip-2,6-diamine (CTA) and Trip-2,7-diamine (MTA) regioisomer monomers.

the CO<sub>2</sub>/CH<sub>4</sub> gas pair, which was only close to the 1991 upper bound.

More recently, a huge number of studies have been carried out on PIM-Trip-TB.<sup>109–112</sup> Malpass-Evans *et al.*<sup>111,113</sup> prepared two TB based polymers, PIM-EA(H<sub>2</sub>)-TB and PIM-Trip (Me<sub>2</sub>)-TB (shown in Fig. 10), and comparably evaluated their CO<sub>2</sub> performance. It is found that the “methyl-less” TB-PIMs displayed superior separation performance than their counterparts with a bridgehead methyl substituent. For instance, CO<sub>2</sub>/CH<sub>4</sub> separation results of PIM-Trip(H<sub>2</sub>)-TB lay above the 2008 upper bound while those of PIM-Trip (Me<sub>2</sub>)-TB were only close to the 1991 upper bound. Notably, despite a higher total pore volume of PIM-Trip(Me<sub>2</sub>)-TB caused by a bridgehead methyl substituent, its permeability for CO<sub>2</sub> was 3718.0 Barrer, only about 38% that of PIM-Trip(H<sub>2</sub>)-TB. In addition, physical aging enhanced the overall performance of H<sub>2</sub>-bridgehead polymers, which was opposite to that of methyl-bridgehead polymers.

In another study, Trip-2,6-diamine (CTA) and Trip-2,7-diamine (MTA) regioisomer monomers<sup>112</sup> (shown in Fig. 11) were synthesized to investigate the regioisomer effect in TB-based gas separation membranes. The resulting TB polymers were named CTTB and MTTB, respectively. It is found that the CO<sub>2</sub> separation performance of ITTB was lower because of the looser polymer main-chain packing, which indicated that a pure-regioisomer normally resulted in a more uniform chain packing.

Later, to amplify the role of chain spacing in enhancing permeability, Rose *et al.*<sup>54</sup> created benzotriptycene by fusing

a benzene ring to the Trip unit and subsequently synthesized a new PIM-TB (PIM-BTrip-TB, shown in Fig. 10). Ascribed to benzotriptycene's greater “internal molecular free volume”<sup>114</sup> relative to that of Trip, PIM-BTrip-TB demonstrated an enhanced CO<sub>2</sub> permeability of 13 200.0 Barrer. However, the high CO<sub>2</sub> permeability was quickly reduced due to serious physical aging, and after 116 days, the CO<sub>2</sub> permeability fell from 13 200.0 to 4150.0 Barrer with a usual increase in CO<sub>2</sub>/CH<sub>4</sub> selectivity from 9.2 to the value of 14.7. A subsequent study conducted by the same group<sup>115</sup> indicated that a CO<sub>2</sub> permeability of 6060.0 Barrer and CO<sub>2</sub>/N<sub>2</sub> selectivity of 15.3 can be documented for PIM-TMN-Trip-TB, which was close to the 2008 upper bound.

In another study, Rose *et al.*<sup>62</sup> designed a rigid TB-based PIM (PIM-MP-TB) by employing methanopentacene (MP) and DMM as monomers (shown in Fig. 10). Compared to many of conventional PIMs, PIM-MP-TB exhibited great selectivity for CO<sub>2</sub>/CH<sub>4</sub> and CO<sub>2</sub>/N<sub>2</sub> gas pairs combined with moderate CO<sub>2</sub> permeability (3500.0 Barrer) due to the shorter methylene bridge and greater proportion of aromatic rings within the polymer chain. In addition, the membrane demonstrated almost unchanged CO<sub>2</sub> separation performances even after one year of aging.

Inspired by the method to yield rigid and contorted ladder backbones reported by Liu *et al.*,<sup>116</sup> Ma *et al.*<sup>117</sup> synthesized norbornyl bis-(aminobenzocyclobutene) ladder aryl diamines from two commercially available *p*-bromoanilines and norbornadiene, and the CANAL ladder polymers (CANAL-TB-1 and CANAL-TB-2) were obtained (shown in Fig. 10). Both CANAL-TBs exhibited a moderate CO<sub>2</sub>/CH<sub>4</sub> selectivity ranging from 12.3 to 13.9, while CANAL-TB-2 exhibited higher CO<sub>2</sub> permeability (2520.0 Barrer) than CANAL-TB-1 (1678.0 Barrer), which was ascribed to the more open internal structure of CANAL-TB-2.

Later, Hu *et al.*<sup>118</sup> prepared a series of CANAL-TB polymers derived from pure regioisomers of CANAL diamines (shown in Fig. 12). The results manifested that *syn*-CANAL-TB-4 exhibited concomitant greater gas permeability and selectivity compared to *anti*-CANAL-TB-4 (gas permeation data shown in Table 3). Meanwhile, *anti*-CANAL-TB-2 with a CO<sub>2</sub> permeability of 2470.0

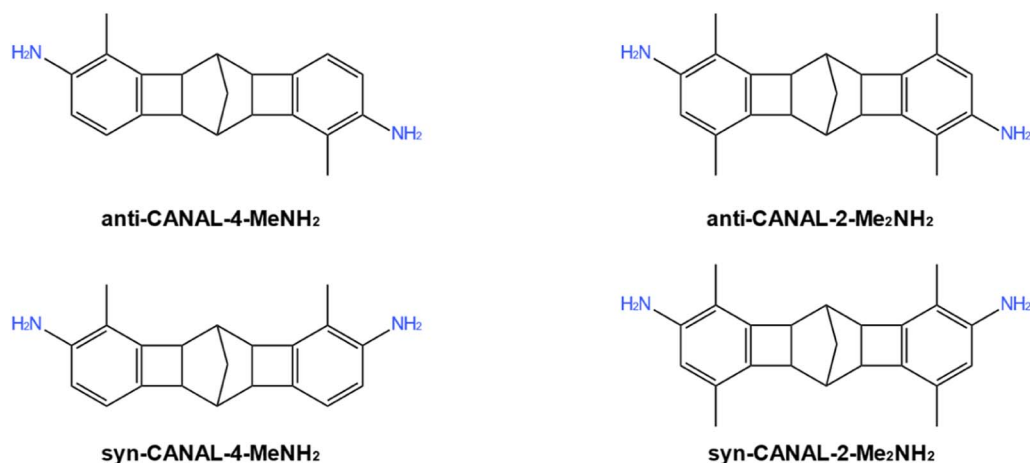


Fig. 12 Regioisomers of norbornyl bis-benzocyclobutene-containing (N<sub>2</sub>BC) diamines.

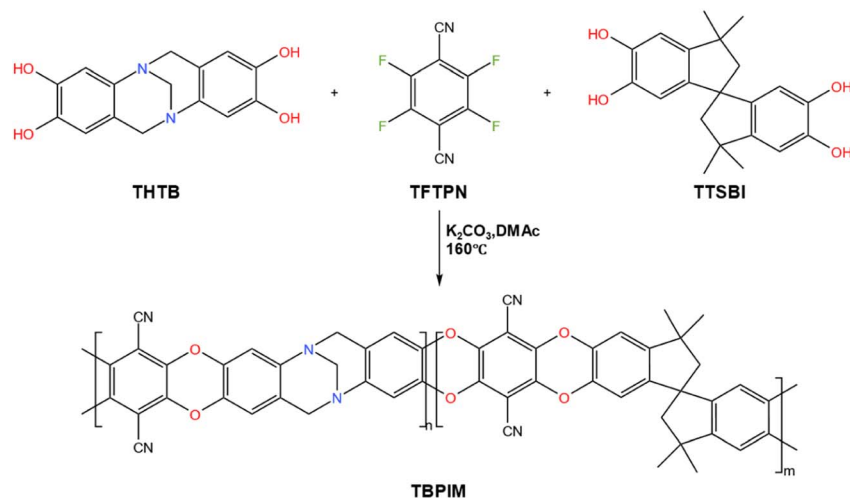


Fig. 13 Synthetic route of TB-PIM copolymers in ref. 120.

Barrer and  $\text{CO}_2/\text{CH}_4$  selectivity of 9.6 outperformed *syn*-CANAL-TB-2 in separation performance. All these results demonstrated the advantages of isomeric effects in the development of excellent performance gas separation membranes.

In addition to focusing on synthesizing new rigid polymer backbone structures, functional molecular design to finely tune gas separation performance has also been investigated. Ma *et al.*<sup>79</sup> designed a 2,3-difluoro-functionalized triptycene (DFTrip) building block and eventually synthesized an intrinsically microporous TB-derived ladder polymer (DFTTB, shown

in Fig. 10). The fresh DFTTB membrane exhibited outstanding combination of a high  $\text{CO}_2$  permeability of 3146.0 Barrer and  $\text{CO}_2/\text{CH}_4$  selectivity of 21.8. Surprisingly, after 180 days of aging, there was a 68% reduction of  $\text{CO}_2$  permeability (from 3146.0 Barrer to 1005.0 Barrer) with an unexpected decrease in  $\text{CO}_2/\text{CH}_4$  selectivity from 21.8 to 20.5 as well. The significant reduction of  $\text{CO}_2$  permeability and the abnormal decrease in  $\text{CO}_2/\text{CH}_4$  selectivity with aging diminished the value of DFTTB in industrial application of  $\text{CO}_2$  separation.

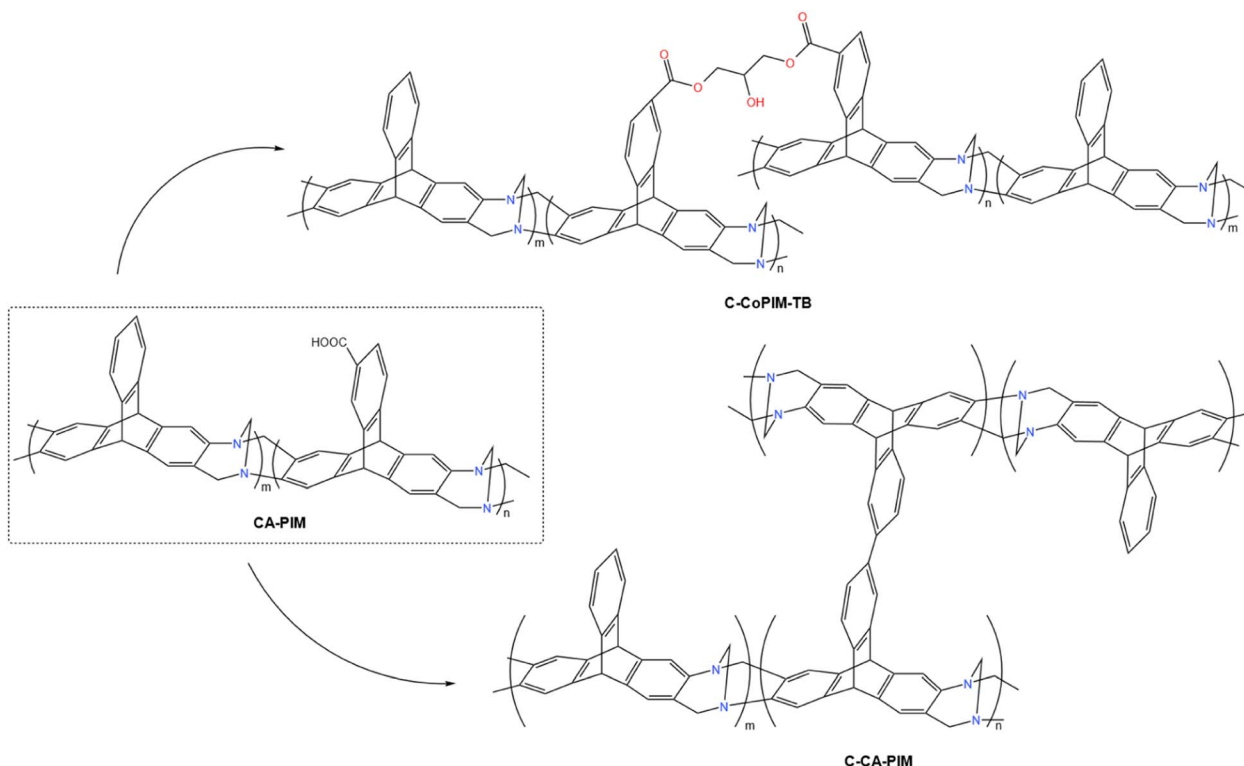


Fig. 14 Cross-linked high free volume TB-PIM polymers in ref. 81 and 121.

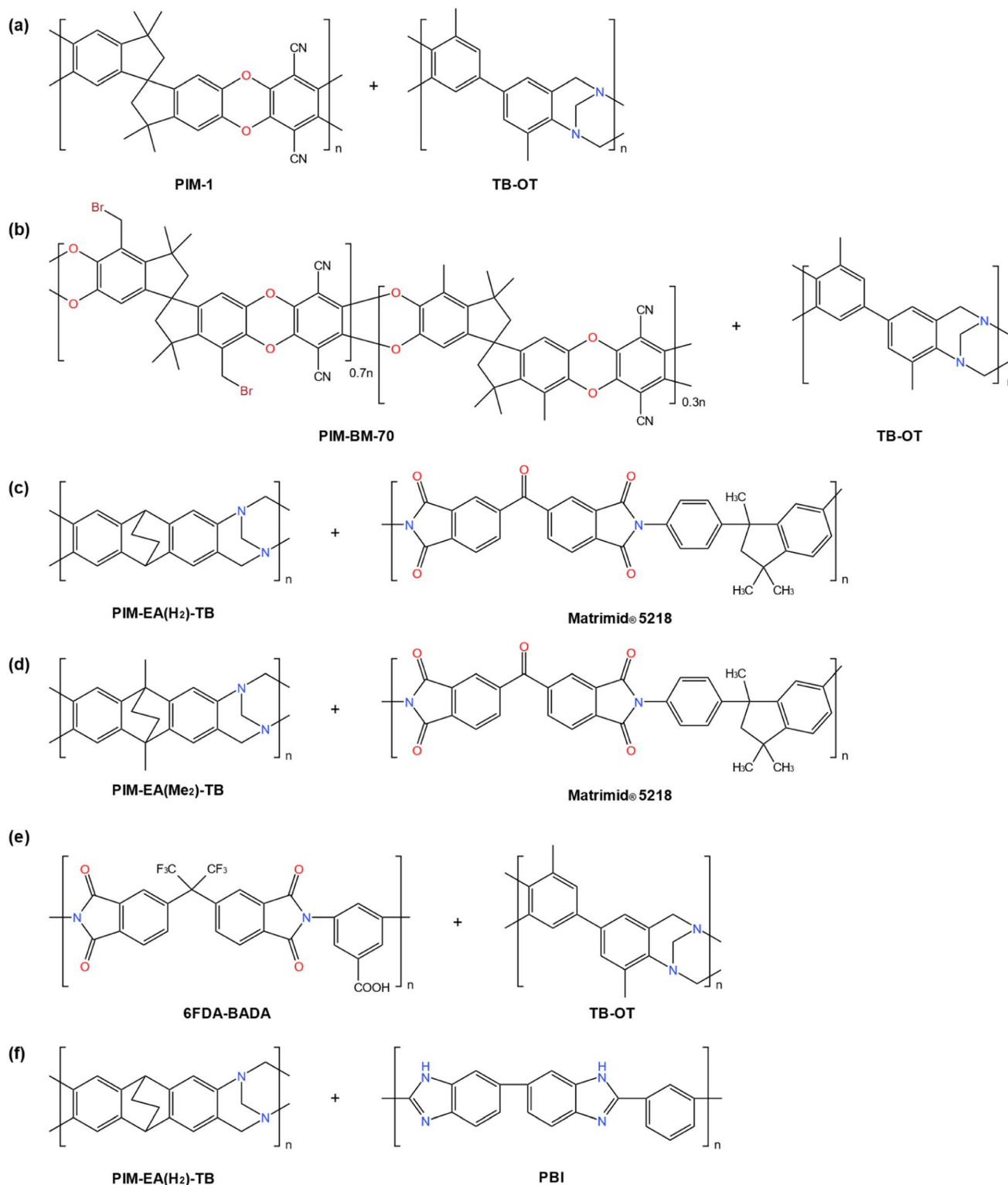


Fig. 15 TB polymer based polymeric blends used for CO<sub>2</sub> separation. (a) PIM1/TB-OT, (b) PIM-BM-70/TB-OT, (c) PIM-EA(H<sub>2</sub>)-TB/Matrimid® 5218, (d) PIM-EA(Me<sub>2</sub>)-TB/Matrimid® 521, (e) 6FDA-BADA/TB-OT, (f) PIM-EA(H<sub>2</sub>)-TB/PBI.

Van *et al.*<sup>119</sup> designed a 1,1'-binaphthalene-diamine monomer (NH<sub>2</sub>-BINOL-TBS) to form OH-functionalized TB-based PIMs (PIM-HNTB, shown in Fig. 10). Compared to the DFTTB membrane reported in ref. 79, the obtained PIM-HNTBs showed

moderate CO<sub>2</sub> permeability (833.0–967.0 Barrer) and relatively low CO<sub>2</sub>/CH<sub>4</sub> selectivity (7.0–11.8). It is worth mentioning that higher content of –OH groups in the polymer led to better

overall performance for fresh membranes but a faster physical aging rate.

Compared to grafting various functional groups onto the polymeric chain, a TB unit was also introduced into the PIM-1 polymer chain and a TB-PIM copolymer was obtained (TB-PIMs, shown in Fig. 13).<sup>120</sup> Compared with PIM-1, the presence of a TB unit in the copolymers resulted in lower *d*-spacing and FFV, and thus less gas permeability and better selectivity of TB-PIMs. For example, the CO<sub>2</sub> permeability of TB-PIM-25 was 4353.0 Barrer while the CO<sub>2</sub> permeability of PIM-1 was 6538.0 Barrer. Correspondingly, a TB-PIM copolymer, such as TB-PIM-33, had improved selectivity for the gas pair CO<sub>2</sub>/N<sub>2</sub> (18.1) and CO<sub>2</sub>/CH<sub>4</sub> (12.3).

In practical separation applications, reducing physical aging is crucial for long-term stability. Chemical crosslinking and thermal crosslinking are considered to be feasible methods to slow down physical aging. Initially, carboxylic acid containing Trip-based TB copolymers (CoPIM-TB-1 and CoPIM-TB-2) were synthesized with 2,6-diaminotriptycene-14-carboxylic acid (DATCA) and 2,6-diaminotriptycene (DAT'),<sup>81</sup> and subsequently, C-CoPIM-TB-1 and C-CoPIM-TB-2 were formed by cross-linking glycidol with copolymers (shown in Fig. 14). Compared with PIM-Trip(H<sub>2</sub>)-TB, the resulting cross-linked membranes showed a significantly improved selectivity with reduced gas permeabilities. For instance, the CO<sub>2</sub>/CH<sub>4</sub> selectivity of C-CoPIM-TB-1 and C-CoPIM-TB-2 was 23.3 and 25.2 while that of PIM-Trip-TB was 13.0. In addition, after aging for 40 days, the permeability of C-CoPIM-TB-1 and C-CoPIM-TB-2 to CO<sub>2</sub> decreased by 9% and 5%, respectively, which was much less than that of PIM-Trip(H<sub>2</sub>)-TB aged for the same length (42%).

Later, thermal decarboxylation crosslinking was introduced to a carboxylate polymer precursor (CA-PIM) to improve anti-plasticization properties of the membranes (shown in Fig. 14).<sup>92</sup> The results showed that the obtained membranes possessed great resistance to plasticization, even at a CO<sub>2</sub> pressure up to 30 bar. Meanwhile, the CO<sub>2</sub> permeability of CA-PIM-1 and CA-PIM-2 increased accompanied with the reduction of selectivity as the heating temperature increases (gas

permeation data shown in Table 3). Except CA-PIM-1-400 and CA-PIM-2-400 which had partial carbonization, the CO<sub>2</sub>/CH<sub>4</sub> separation performance of the rest of the copolymers remained above the 2008 Robson upper bound.

**2.1.4 TB polymer blends.** Compared to the synthesis of new polymers with a novel structure and superior CO<sub>2</sub> separation performances, polymer blending has been considered as a versatile, straightforward and least expensive route for developing membranes with desirable separation performance.<sup>122</sup> However, the compatibility between the blending components is crucial for the development of high-performance gas separation membranes.<sup>122,123</sup> Research has been also carried out on blending a TB polymer into different polymeric matrices to improve CO<sub>2</sub> membrane separation/mechanical properties. The development of membranes based on TB polymer blends is summarized in the following section.

Knowing that the PIM-1 polymer was miscible with the TB-OT polymer in any proportion, Zhao *et al.*<sup>123</sup> synthesized PIM/TB-OT blending membranes with different compositions of PIM-1 and TB-OT (shown in Fig. 15(a)). The CO<sub>2</sub> permeability of the blending membranes decreased while the ideal selectivity increased on increasing the content of the TB-OT polymer. For example, as the TB-OT polymer loading increased from 20 wt% to 80 wt%, CO<sub>2</sub> permeability decreased gradually from 5765.0 to 727.0 Barrer with the increase of CO<sub>2</sub>/CH<sub>4</sub> selectivity from 11.3 to 16.2. Interestingly, at lower temperature, ideal selectivity of these membranes, particularly for CO<sub>2</sub>/N<sub>2</sub> and CO<sub>2</sub>/CH<sub>4</sub> was much higher than that of the value at high temperature. For example, the higher gas selectivity of 54.3 for CO<sub>2</sub>/N<sub>2</sub>, and 44.0 for CO<sub>2</sub>/CH<sub>4</sub> of the PIM/TB-OT(8 : 2) membrane could be achieved at -25 °C.

Attempts have been made for blending functionalized PIM-1 with a TB polymer to form blending membranes. Chen *et al.*<sup>124</sup> took bromomethylated PIMs (PIM-BM) and TB-OT as prototypes to form the polymer blends (PIM-BM/TB-OT) (shown in Fig. 15(b)). Different from the previous reports,<sup>123</sup> the PIM-1 and TB polymers were physically blended, and in Chen's work,<sup>124</sup> the membranes were cross-linked by exposing the blend

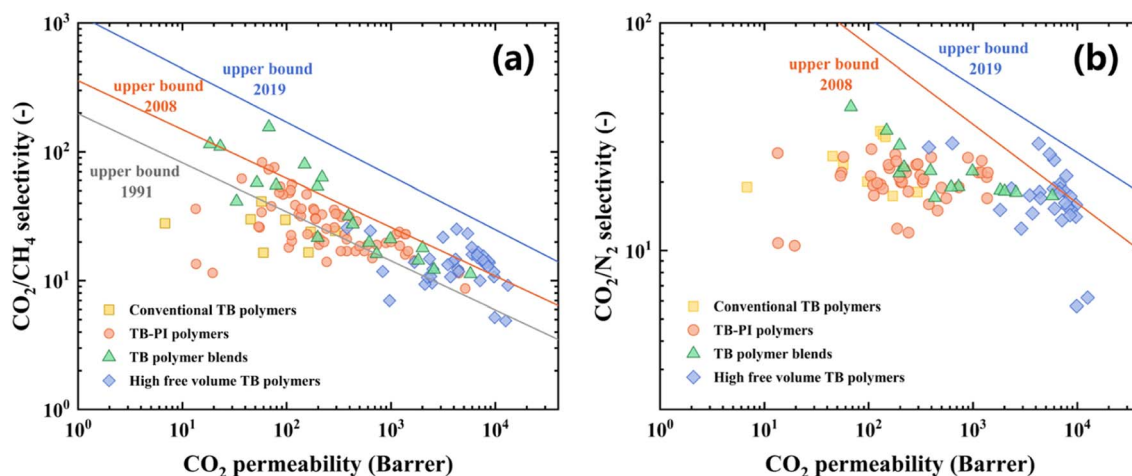


Fig. 16 CO<sub>2</sub>/CH<sub>4</sub> (a) and CO<sub>2</sub>/N<sub>2</sub> (b) separation performance of TB based polymeric membranes.

Table 4 CO<sub>2</sub> separation performances of TB polymer blend membranes

Polymer	$P_{\text{CO}_2}$ (Barrer)	$\alpha_{\text{CO}_2/\text{CH}_4}$ (—)	$\alpha_{\text{CO}_2/\text{N}_2}$ (—)	$\alpha_{\text{CO}_2/\text{H}_2}$ (—)	Ref.
Matrimid/PIM-EA(H <sub>2</sub> )-TB	198.0	21.6	29.0	—	125
PBI/PIM-EA(H <sub>2</sub> )-TB	131.0 <sup>a</sup>	—	—	—	126
PIM/TB-OT (8 : 2)	5765.0	11.3	17.4	—	123
PIM/TB-OT (6 : 4)	2585.0	12.2	18.0	—	123
PIM/TB-OT (4 : 6)	1824.0	14.4	18.4	—	123
PIM/TB-OT (2 : 8)	727.0	16.2	19.1	—	123
PI/TB-OT	79.3	55.1	—	—	127
PI/TB-OT-100 °C-16 h	51.8	57.6	—	—	127
PI/TB-OT-120 °C-16 h	18.4	115.0	—	—	127
PI/TB-OT-150 °C-16 h	23.1	110.0	—	—	127
PI/TB-OT-250 °C-16 h	33.1	41.4	—	—	127
PIM-BM/TB-OT	2007.2	18.0	18.2	—	124
PIM-BM/TB-OT-80 °C-20 h	987.4	21.1	22.3	—	124
PIM-BM/TB-OT-120 °C-20 h	617.5	19.8	19.0	—	124
PIM-BM/TB-OT-200 °C-20 h	391.3	31.7	22.4	—	124
PIM-BM/TB-OT-250 °C-5 h	430.7	27.5	17.1	—	124
PIM-BM/TB-OT-250 °C-10 h	197.0	54.1	21.9	—	124
PIM-BM/TB-OT-250 °C-20 h	148.5	79.9	33.7	—	124
PIM-BM/TB-OT-300 °C-2 h	218.4	63.4	23.2	—	124
PIM-BM/TB-OT-300 °C-5 h	67.6	155.7	42.8	—	124

<sup>a</sup> H<sub>2</sub> permeability.

membranes at a temperature of above 250 °C, with ppm-level O<sub>2</sub>. Pristine PIM-BM/TB-OT possessed high CO<sub>2</sub> permeability (2007.2 Barrer) with moderate CO<sub>2</sub>/CH<sub>4</sub> selectivity (18.0). After thermal crosslinking, the CO<sub>2</sub>/CH<sub>4</sub> selectivity increased significantly from 18.0 to 155.7 due to the formation of narrow pore structures. The CO<sub>2</sub>/CH<sub>4</sub> separation performance of the XPIM-BM/TB-OT membrane treated at 300 °C for 5 h was above the 2019 upper bound. Moreover, after aging for 360 days, XPIM-BM/TB-OT still held outstanding gas separation performance far above the 2008 Robeson upper bound.<sup>49</sup>

In another work, highly permeable PIM-EA(H<sub>2</sub>)-TB was blended with a classic PI (Matrimid® 5218) widely used for CO<sub>2</sub>/CH<sub>4</sub> separation (shown in Fig. 15(c)).<sup>125</sup> The gas permeability of

the Matrimid® 5218/PIM-EA(H<sub>2</sub>)-TB blend membrane improved relative to that of pure Matrimid® 5218. For instance, the CO<sub>2</sub> permeability of the blending membrane increased from 8.6 to 198.0 Barrer coupled with a CO<sub>2</sub>/CH<sub>4</sub> and CO<sub>2</sub>/N<sub>2</sub> selectivity of 21.6 and 29.0, which made its performance closer to the 2008 upper bound. Later, the same group<sup>126</sup> replaced PIM-EA(H<sub>2</sub>)-TB with PIM-EA(Me<sub>2</sub>)-TB and obtained Matrimid® 5218/PIM-EA(Me<sub>2</sub>)-TB blends (shown in Fig. 15(d)). Supported by Sulzer PAN UF, a thin film composite (TFC) membrane was fabricated. The permeability of the resulting material increased by about two orders of magnitude with respect to that of pure Matrimid® 5218, accompanied by an increase in selectivity (from 10.0 to 14.0 for CO<sub>2</sub>/CH<sub>4</sub> and from 20.0 to 26.0 for CO<sub>2</sub>/N<sub>2</sub>).

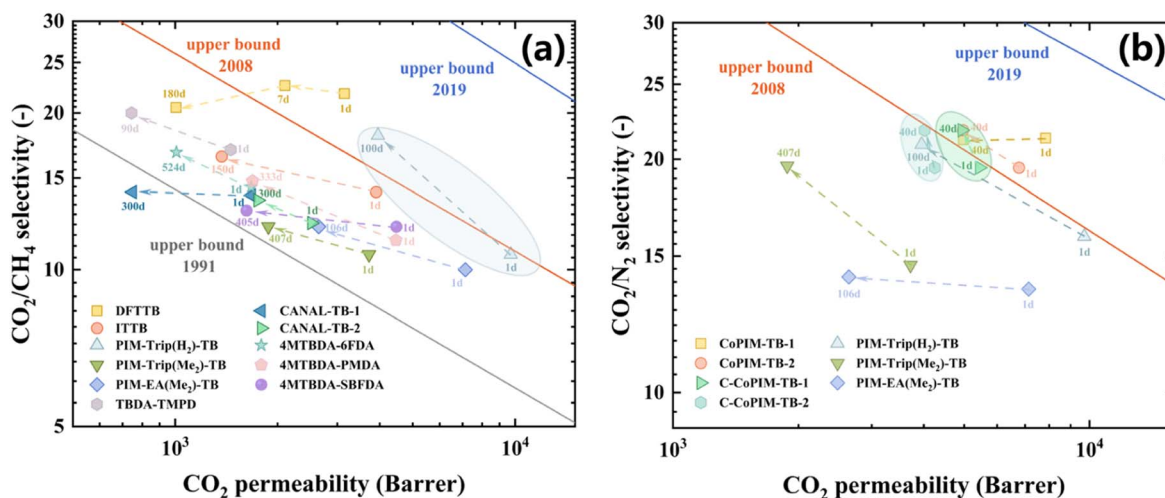


Fig. 17 Physical aging of representative TB based polymeric membranes, (a) CO<sub>2</sub>/CH<sub>4</sub> and (b) CO<sub>2</sub>/N<sub>2</sub> separation performances.

Thermal linking of blend membranes can be also achieved by thermal treatment of PI with  $-\text{COOH}$  groups (6FDA-BADA) (shown in Fig. 15(e)).<sup>127</sup> The obtained PI/TB-OT blending membranes showed higher  $\text{CO}_2$  permeability (18.4–79.3 Barrer) than pristine PI, and excellent  $\text{CO}_2/\text{CH}_4$  selectivity (41.4–115.0) compared to that of a pure TB-OT polymer. In addition, in comparison with pristine 6FDA-BADA and TB-OT membranes, the PI/TB-OT blending membranes possessed better resistance to  $\text{CO}_2$  plasticization and slightly better physical aging resistance as well.

In addition, TB has also been studied as one of the components of blends for the  $\text{H}_2/\text{CO}_2$  separation process at high temperature. It is well-known that polybenzimidazole (PBI) is widely used in membranes for  $\text{H}_2/\text{CO}_2$  separation, but it is limited by its low permeability. Sanchez-Lainez *et al.*<sup>128</sup> tried to add PIM-EA( $\text{H}_2$ )-TB to PBI to improve permeability (shown in Fig. 15(f)). The blends with 10 wt% PIM-EA( $\text{H}_2$ )-TB increased the  $\text{H}_2$  permeability from 31.9 to 131.0 Barrer while the  $\text{H}_2/\text{CO}_2$  selectivity was nicely maintained. Moreover, they added zeolitic imidazolate-8 (ZIF-8) nanoparticles to a blend of PBI and PIM-EA( $\text{H}_2$ )-TB and yielded asymmetric membranes with an optimized  $\text{H}_2$  permeance of 83.5 GPU and  $\text{H}_2/\text{CO}_2$  selectivity of 19.4.

Advances in  $\text{CO}_2/\text{CH}_4$  and  $\text{CO}_2/\text{N}_2$  separation performance of TB based polymeric membranes are summarized in Fig. 16. As can be seen from the figure, though abundant attempts have been made for developing TB based polymeric membranes for  $\text{CO}_2$  separation, and many of them exhibited high  $\text{CO}_2$  permeability (*e.g.*, close to 10 000 Barrer), only a bunch of them overcame the 2008 upper bound. In terms of TB-PI polymers, the incorporation of a TB group did improve the performance of

traditional PI, but it was not as attractive as expected. For TB polymer blends, the proper combination might get amazing  $\text{CO}_2/\text{CH}_4$  separation performance close to the 2019 upper bound, though most of them presented lower  $\text{CO}_2$  permeability and slightly higher selectivity compared to the neat polymers (data shown in Table 4).

Physical aging behavior of the representative TB based polymeric membranes is summarized and presented in Fig. 17. Physical aging, as an inevitable thermal relaxation process of glassy polymers such as TB polymers, will reduce the internal free volume and thus reduce  $\text{CO}_2$  permeability over time. As can be seen from Fig. 17, most of the representative TB polymers underwent a general aging process with decreased permeability and only a moderate increase or even decrease in selectivity. By contrast, PIM-Trip ( $\text{H}_2$ )-TB and C-CoPIM-TB-1 (2) exhibited more outstanding separation performance after aging, which verified the idea of the control effect of chain rigidity on physical aging. In other words, the adjustment of polymer rigidity is a valid approach to tune the aging behavior of TB polymers.<sup>98,129–133</sup>

## 2.2 Functionalized TB polymeric membranes for $\text{CO}_2$ separation

Ionization is an effective method for fine-tuning the porosity and functionalizing microporous polymers to enhance their gas separation performance.<sup>134,135</sup> Common ionization methods include carboxylation, sulfonation, quaternization and other ionization processes.<sup>135–137</sup> For TB polymers, on one hand, the easy protonation of the tertiary nitrogen of TB units enables the TB polymer to form a rigid poly-cationic framework, and thus,

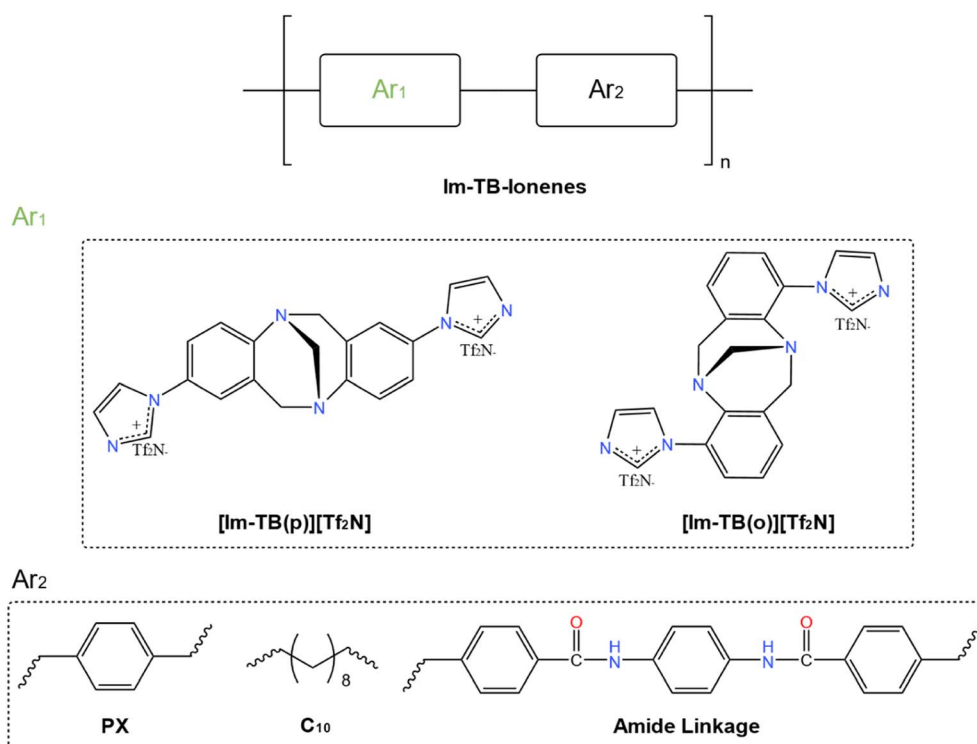


Fig. 18 TB-containing ionene polymers derived from imidazolium-mediated monomers in ref. 69 and 140.

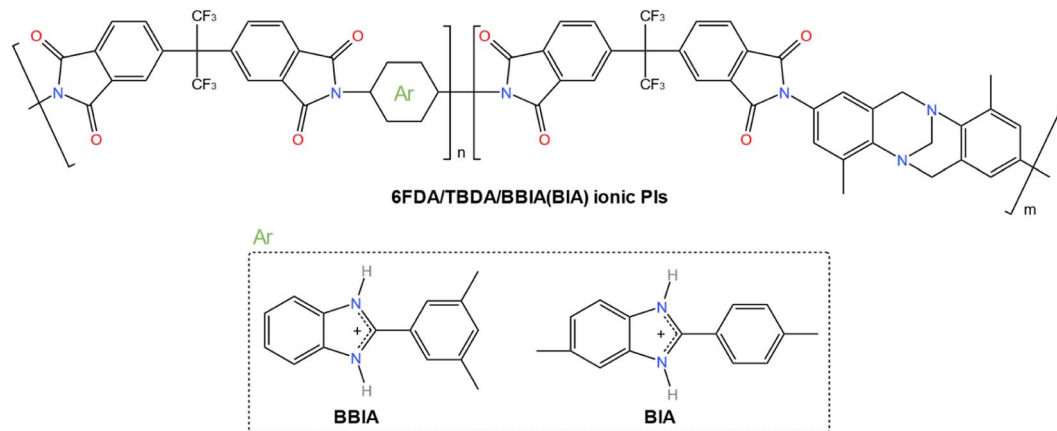


Fig. 19 Ionic PIs containing BIA or BBIA as the third monomer in ref. 141.

quaternization is commonly employed to functionalize a TB polymer.<sup>138,139</sup> On the other hand, the incorporation of an imidazole ring, which is prone to quaternization, in the formation of TB polymers is also feasible. Thus, there can be two methods to prepare functionalized TB polymers: pre-functionalization (monomers) and post-functionalization (polymers).<sup>138</sup>

In terms of the functionalization of monomers, starting from commercially available imidazole, 2-fluoronitrobenzene (2-FNB) or 4-fluoronitrobenzene (4-FNB), Kammakakam *et al.*<sup>69,140</sup> synthesized the TB base monomers having “*ortho*”- and “*para*”-substituted diimidazole (Im-TB(*o*) and Im-TB(*p*)). Then a series of imidazolium-mediated TB-based ionene polymers (Im-TB-ionene) (shown in Fig. 18) were synthesized *via* the two diimidazole-functionalized TB monomers, followed by  $[\text{TF}_2\text{N}]^-$  anion ion exchange. Similar to typical ionomers, the resulting Im-TB-ionene exhibited low  $\text{CO}_2$  permeability ( $\sim 4.9$  Barrer) and moderate  $\text{CO}_2/\text{CH}_4$  selectivity ( $\sim 56.7$ ) and  $\text{CO}_2/\text{N}_2$  selectivity

(45.4). Unfortunately, the overall  $\text{CO}_2$  separation performances of the Im-TB-ionenes fell below the 2008 upper bound which can be ascribed to the obstacle of gas permeability. With the aim of improving  $\text{CO}_2$  permeability, they subsequently mixed  $\text{CO}_2$ -philic IL into Im-TB to form composite membranes. The resultant composite membranes show enhanced  $\text{CO}_2$  permeability (from 5.3 to 47.2 Barrer) without sacrificing selectivity in comparison with Im-TB(*o* & *p*)-PA. However, the overall  $\text{CO}_2$  separation performances are still in the low region.

Later, with a slightly adapted strategy, Xu *et al.*<sup>141</sup> designed two imidazolium-mediated diamine monomers named BIA and BBIA, and then prepared 6FDA/TBDA/BIA (or BBIA) PI, abbreviated as PI-1 (2), by reacting 6FDA with TBDA1, and a BIA (BBIA) monomer (shown in Fig. 19). Later on,  $\text{BF}_4^-$  and  $\text{TFSI}^-$  were used to yield four ionic PIs (PI-1- $\text{BF}_4$ , PI-2- $\text{BF}_4$ , PI-1- $\text{TFSI}$ , and PI-2- $\text{TFSI}$ ) in NMP solution. All the resulting membranes showed better permeability than pristine Im-TB-ionenes; for instance, a  $\text{CO}_2$  permeability of 90.1 Barrer was documented by

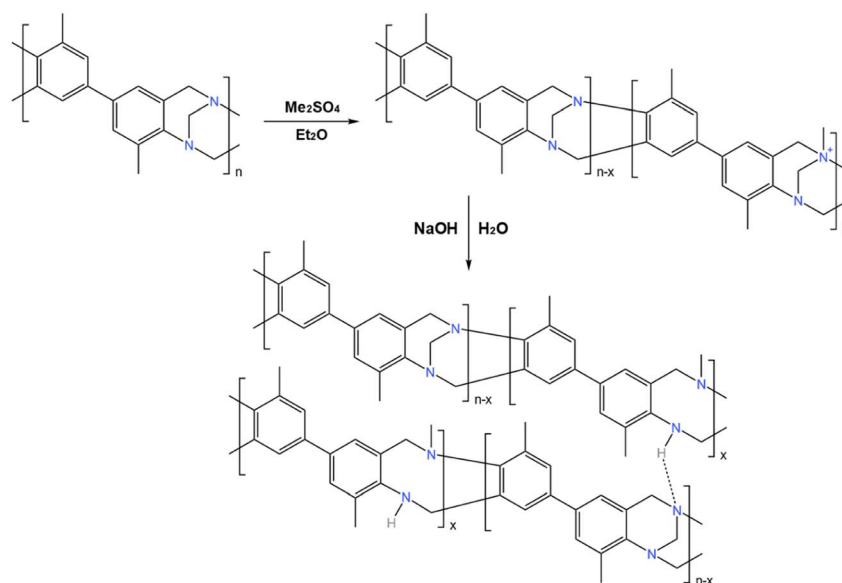


Fig. 20 Synthetic route of TB-OR-x.

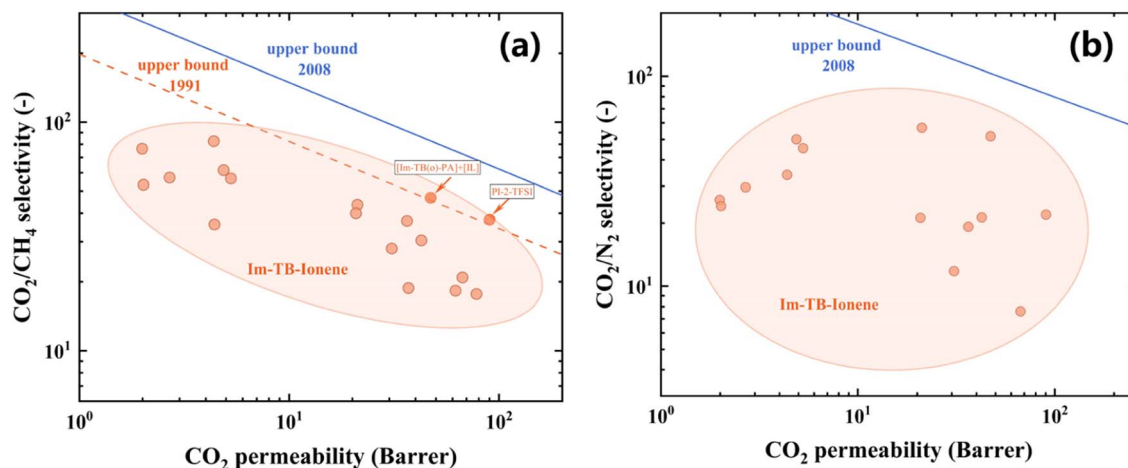


Fig. 21 CO<sub>2</sub>/CH<sub>4</sub> (a) and CO<sub>2</sub>/N<sub>2</sub> (b) separation performance of functionalized TB polymeric membranes.

PI-2-TFSI. In terms of selectivity, PI-1 exhibited the highest CO<sub>2</sub>/CH<sub>4</sub> selectivity of 40.0 while PI-2-TFSI exhibited the highest CO<sub>2</sub>/N<sub>2</sub> selectivity of 22.0. Interestingly, ionic PI membranes with [TFSI]<sup>−</sup> had better gas separation performance than membranes containing [BF<sub>4</sub>]<sup>−</sup>, which indicated that adjusting the type of anion can optimize the CO<sub>2</sub> separation performance.

In terms of post-functionalization of the TB polymers, quaternization occurs on the tertiary nitrogen of TB units.<sup>142,143</sup> Using this strategy, ionic TB polymers such as ITB-DM, ITB-OT, and ITB-Trip, were prepared *via* N-quaternization of the TB structure, and the obtained membranes exhibited excellent performance in helium recovery.<sup>82</sup> Even though post-functionalized TB polymeric membranes were rarely reported for CO<sub>2</sub> separation, it is an interesting topic worth further investigating.

With the aim of improving the durability of plasticization and physical aging, a new method of open-loop TB polymers

which can form hydrogen bonds between polymer chains was developed.<sup>144</sup> In this study, the ring-opened polymers (TB-OR) were synthesized through a ring-opening reaction of TB in a reaction system containing dimethyl sulfate (Me<sub>2</sub>SO<sub>4</sub>) and diethyl ether (Et<sub>2</sub>O) (shown in Fig. 20). The results indicated that as the degree of ring-opening increased, the TB-OR membranes demonstrated higher selectivity while maintaining lower permeability. Moreover, the TB-OR membranes had greater plasticization resistance than TB-OT membranes due to the presence of intermolecular hydrogen bonds.

Advances in CO<sub>2</sub>/CH<sub>4</sub> and CO<sub>2</sub>/N<sub>2</sub> separation performance of functionalized TB polymeric membranes are summarized in Fig. 21. As can be seen from the figure, most functionalized TB polymeric membranes exhibited better CO<sub>2</sub>/CH<sub>4</sub> and CO<sub>2</sub>/N<sub>2</sub> selectivity compared to pristine TB polymer membranes; however, the enhancement in selectivity is normally coupled with reduction in gas permeability. Therefore, many of the

Table 5 CO<sub>2</sub> separation performances of functionalized TB polymeric membranes

Polymer	$P_{\text{CO}_2}$ (Barrer)	$\alpha_{\text{CO}_2/\text{CH}_4}$ (—)	$\alpha_{\text{CO}_2/\text{N}_2}$ (—)	$\alpha_{\text{CO}_2/\text{H}_2}$ (—)	Ref.
[Im-TB(o)-Xy][Tf <sub>2</sub> N]	2.0	76.5	25.8	—	69
[Im-TB(o)-C <sub>10</sub> ][Tf <sub>2</sub> N]	4.4	82.5	33.9	—	69
[Im-TB(p)-Xy][Tf <sub>2</sub> N]	2.0	53.2	24.1	—	69
[Im-TB(p)-C <sub>10</sub> ][Tf <sub>2</sub> N]	2.7	57.2	29.6	—	69
Im-TB(o)-PA	5.3	56.7	45.4	2.7	140
Im-TB(p)-PA	4.9	61.6	50.1	2.7	140
[Im-TB(o)-PA] + [IL]	47.2	46.7	51.7	4.4	140
[Im-TB(p)-PA] + [IL]	21.1	43.6	56.8	3.9	140
PI-1	20.8	40.0	21.2	—	141
PI-1-BF <sub>4</sub>	30.8	28.0	11.8	—	141
PI-1-TFSI	36.4	37.0	19.2	—	141
PI-2	42.6	30.4	21.3	—	141
PI-2-BF <sub>4</sub>	66.9	20.9	7.6	—	141
PI-2-TFSI	90.1	37.5	21.97	—	141
TB-OR-30	78.0	17.7	—	2.3 <sup>a</sup>	144
TB-OR-35	62.0	18.3	—	2.4 <sup>a</sup>	144
TB-OR-50	37.0	18.8	—	2.6 <sup>a</sup>	144
M-TB-OR	4.4	35.7	—	5.1 <sup>a</sup>	144

<sup>a</sup> H<sub>2</sub>/CO<sub>2</sub>.

Table 6 CO<sub>2</sub> separation performances of TB polymer based MMMs

MMMs	$P_{\text{CO}_2}$ (Barrer)	$\alpha_{\text{CO}_2/\text{CH}_4}$ (—)	$\alpha_{\text{CO}_2/\text{N}_2}$ (—)	$\alpha_{\text{CO}_2/\text{H}_2}$ (—)	Ref.
PI-TB	258.0	35.0	24.0	1.4 <sup>a</sup>	159
PI-TB/ZIF-8 (7 wt%)	560.0	27.0	20.0	1.4 <sup>a</sup>	
PI-TB/ZIF-8 (20 wt%)	896.0	21.0	16.0	1.6 <sup>a</sup>	
PI-TB/ZIF-8 (30 wt%)	1437.0	16.0	12.0	1.8 <sup>a</sup>	
PI-TB/ZIF-8@PDA (7 wt%)	380.0	25.0	19.0	1.6 <sup>a</sup>	
PI-TB/ZIF-8@PDA (20 wt%)	702.0	23.0	18.0	1.6 <sup>a</sup>	
PI-TB/ZIF-8@PDA (30 wt%)	1056.0	20.0	14.0	1.8 <sup>a</sup>	
TB	93.5	21.3	—	—	160
TB/ZIF-8 (10 wt%)	107.2	20.1	—	—	
TB/ZIF-8 (20 wt%)	195.3	6.8	—	—	
TB/ZIF-8 (30 wt%)	273.1	1.8	—	—	
TB/ZIF-8@PDA (10 wt%)	109.1	19.6	—	—	
TB/ZIF-8@PDA (20 wt%)	134.4	19.5	—	—	
TB/ZIF-8@PDA (30 wt%)	198.6	18.7	—	—	
TB/ZIF-8@PDA (40 wt%)	209.2	17.4	—	—	
TB/ZIF-8@PDA (50 wt%)	277.3	15.5	—	—	
TB/ZIF-8@PDA (10 wt%)	109.8	18.3	20.9	—	161
TB/ZIF-8@PDA (30 wt%)	195.3	17.8	18.7	—	
TB/ZIF-8@PDA (50 wt%)	275.7	15.2	18.2	—	
TBOR/ZIF-8@PDA (10 wt%)	50.9	23.4	21.6	—	
TBOR/ZIF-8@PDA (30 wt%)	87.5	23.0	21.5	—	
TBOR/ZIF-8@PDA (50 wt%)	165.1	20.6	21.1	—	
TB/ZIF-L-Zn (0 wt%)	148.3	23.7	24.5	2.0 <sup>a</sup>	162
TB/ZIF-L-Zn (5 wt%)	230.6	18.6	17.2	1.7 <sup>a</sup>	
TB/ZIF-L-Zn (10 wt%)	227.5	15.4	14.4	2.0 <sup>a</sup>	
TB/ZIF-L-Zn (20 wt%)	475.4	13.0	12.0	1.9 <sup>a</sup>	
TB/ZIF-L-Co (0 wt%)	148.3	23.9	24.6	2.0 <sup>a</sup>	
TB/ZIF-L-Co (5 wt%)	126.1	18.1	16.6	2.4 <sup>a</sup>	
TB/ZIF-L-Co (10 wt%)	234.3	13.4	13.5	2.6 <sup>a</sup>	
TB/ZIF-L-Co (20 wt%)	551.6	12.0	11.0	2.2 <sup>a</sup>	
PI-TB/UiO-66-NH <sub>2</sub> (0 wt%)	156.0	31.2	20.5	—	163
PI-TB/UiO-66-NH <sub>2</sub> (10 wt%)	224.0	28.3	20.0	—	
PI-TB/UiO-66-NH <sub>2</sub> (20 wt%)	295.0	27.3	19.5	—	
PI-TB/UiO-66-NH <sub>2</sub> (30 wt%)	415.0	25.0	18.9	—	
PI-TB/UiO-66-NH <sub>2</sub> (40 wt%)	317.0	24.4	20.6	—	
TB/NH <sub>2</sub> -MIL-53 (0 wt%)	101.6	18.4	18.8	—	164
TB/NH <sub>2</sub> -MIL-53 (10 wt%)	187.6	20.2	21.0	—	
TB/NH <sub>2</sub> -MIL-53 (20 wt%)	324.5	18.9	19.9	—	
TB/NH <sub>2</sub> -MIL-53 (25 wt%)	138.8	18.9	19.1	—	
TB/NH <sub>2</sub> -MIL-53 (30 wt%)	85.6	19.2	18.9	—	
ITTB	2052.0	15.3	22.6	—	165
ITTB/CNT-0.6%	2064.0	15.3	21.3	—	
ITTB/CNT-1.0%	2620.0	15.9	21.7	—	
ITTB/CNT-1.5%	2504.0	19.0	22.6	—	
ITTB/CNT-2.0%	2181.0	16.2	22.5	—	

<sup>a</sup>  $\alpha$  (H<sub>2</sub>/CO<sub>2</sub>).

obtained functionalized TB polymeric membranes presented lower overall CO<sub>2</sub> separation performances (Table 5).

### 3. TB based MMMs for CO<sub>2</sub> separation

Even though huge progress has been made on TB based polymeric membranes for CO<sub>2</sub> separation, membranes fabricated *via* TB polymers also suffer from the trade-off between the permeability and selectivity.<sup>65</sup> The permeability-selectivity trade-off for conventional polymer membranes is determined

by the Robeson upper bound.<sup>49,145,146</sup> Fabrication of MMMs by adding nanofillers into the polymeric matrix to improve the gas separation performances has been considered as a promising strategy to overcome the trade-off. MMMs are a category of membranes made by blending nanofillers (normally inorganic) into the polymeric matrix to improve the overall gas separation performances.<sup>147–149</sup> The MMMs combined the excellent separation performances of inorganic materials and the good processibility of the polymeric materials, and thus, it has been widely studied.<sup>150,151</sup> To date, a vast number of materials have been used as fillers in MMMs, including traditional

inorganic fillers such as zeolites,<sup>152</sup> CMS,<sup>153</sup> carbon nanotubes (CNTs),<sup>154</sup> graphene,<sup>155</sup> as well as new porous fillers such as metal–organic frameworks (MOFs)<sup>156,157</sup> and covalent–organic frameworks (COFs).<sup>158</sup> Attempts have also been made for developing MMMs based on TB polymers. In this part, the progress on MMMs based on TB polymers has been summarized and discussed. Table 6 summarizes the research progress of TB polymer MMMs for CO<sub>2</sub> separation.

Both ZIF-8 and functionalized ZIF-8 have been intensively studied as nanofillers in MMMs.<sup>166–168</sup> Wang *et al.*<sup>159</sup> conducted a study where they used both ZIF-8 and PDA-functionalized ZIF-8 to fabricate MMMs with an inherently microporous polyimide (TBDA2-6FDA-PI).<sup>169</sup> Similar to other MMMs, the presence of ZIF-8 in the TB polymer matrix greatly improved the CO<sub>2</sub> permeability while reducing the selectivity for all gas pairs. Under optimized conditions, a maximum CO<sub>2</sub> permeability of 1437.0 Barrer was achieved, along with a CO<sub>2</sub>/CH<sub>4</sub> selectivity of 16.0. Conversely, functionalizing the ZIF-8 particles with PDA improved the compatibility between the nanofiller and the polymer matrix, leading to improved selectivity but decreased CO<sub>2</sub> permeability.

In another study, PDA-coated ZIF-8 was utilized as a nanofiller in a polyimide matrix with dimethyl biphenyl linkages to fabricate MMMs.<sup>130,160</sup> The functionalization enhanced the compatibility between the nanofillers and the TB matrix, enabling higher loading of the nanofillers. Gas permeation results show that as the nanofiller content increased from 10 wt% to 50 wt%, a 2.5-fold increment of the CO<sub>2</sub> permeability was found with only a 20% decrease in CO<sub>2</sub>/CH<sub>4</sub> selectivity. In addition, the obtained membrane demonstrated excellent resistance to plasticization and displayed robust mechanical strength.

Researchers have also attempted to incorporate PDA-modified ZIF-8 into a ring-opening TB polymer (TBOR) matrix to form MMMs.<sup>161</sup> The TBOR/ZIF-8@PDA MMMs demonstrated superior H<sub>2</sub> separation capabilities compared to their CO<sub>2</sub> separation performances. The significance of the interfaces between the nanofiller and polymeric matrix is highlighted as

they play a crucial role in enhancing the gas separation performance.

In addition to conventional ZIF-8 particles, ZIFs with 2D shapes (ZIF-L-Zn and ZIF-L-Co) were also developed and used in a TB matrix to form MMMs.<sup>162</sup> The study revealed that ZIF-L-Co was more effective in promoting gas permeability with similar selectivity for all gas pairs compared to ZIF-L-Zn. The MMM with ZIF-L-Co showed excellent CO<sub>2</sub> separation performance, with a CO<sub>2</sub> permeability up to 1131.5 Barrer for TB/ZIF-L-Co (20 wt%) at 60 °C and 2 bar feed pressure conditions, with a CO<sub>2</sub>/N<sub>2</sub> and CO<sub>2</sub>/CH<sub>4</sub> selectivity of 7.0 and 6.0, respectively. This study unequivocally demonstrated the significant influence of the nanofiller morphology on gas separation characteristics.

The CO<sub>2</sub>/CH<sub>4</sub> separation performances of MMMs fabricated *via* ZIFs and TB polymers are presented in Fig. 22. It is clearly shown that almost all MMMs showed a consistent increase in CO<sub>2</sub> permeability with increasing filler loading, but also a corresponding decrease in CO<sub>2</sub>/CH<sub>4</sub> selectivity, especially for TB/ZIF-8, with a sharp decrease in selectivity above 10 wt% ZIF-8 loading (shown in Fig. 22). In addition, functionalization of ZIF-8 can significantly maintain the CO<sub>2</sub>/CH<sub>4</sub> selectivity, but the improvement of the CO<sub>2</sub> permeability was also weakened (shown in Fig. 22(b)).

Apart from the ZIF-8 nanofiller, other nanofillers such as UiO-66 (ref. 163) and MIL-53(Al)<sup>164</sup> have also been used in TB based MMMs. The MMMs containing 30 wt% UiO-66-NH<sub>2</sub> exhibited the best gas separation performance among the investigated samples,<sup>163</sup> with a CO<sub>2</sub> permeability increase of approximately 166% (415.0 Barrer), while maintaining CO<sub>2</sub>/CH<sub>4</sub> and CO<sub>2</sub>/N<sub>2</sub> gas selectivity comparable to that of a neat polymer membrane (25.0 and 18.9, respectively).

In terms of the MMMs based on NH<sub>2</sub>-MIL-53(Al), it was observed that both the CO<sub>2</sub> permeability and selectivity first increased and then decreased with an increase in MOF loading from 10 wt% to 30 wt%. This trend may be attributed to potential MOF pore blockage or non-ideal MOF accumulation. The best performing MMM among the TB/NH<sub>2</sub>-MIL-53(Al) composites had a filler concentration of 20 wt%, exhibiting

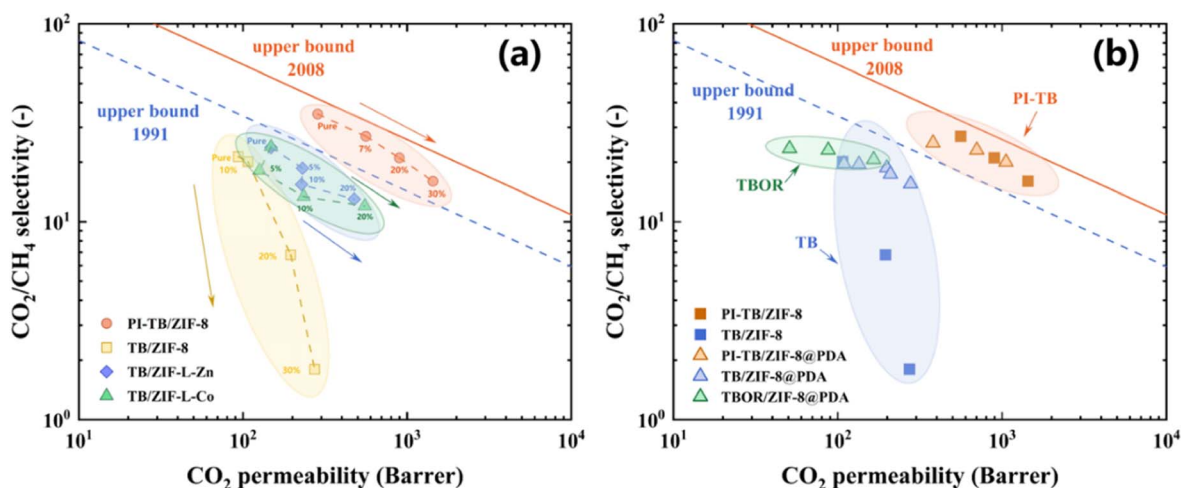


Fig. 22 Effect of ZIF filler loading (a) and PDA modification (b) on CO<sub>2</sub>/CH<sub>4</sub> separation performance.

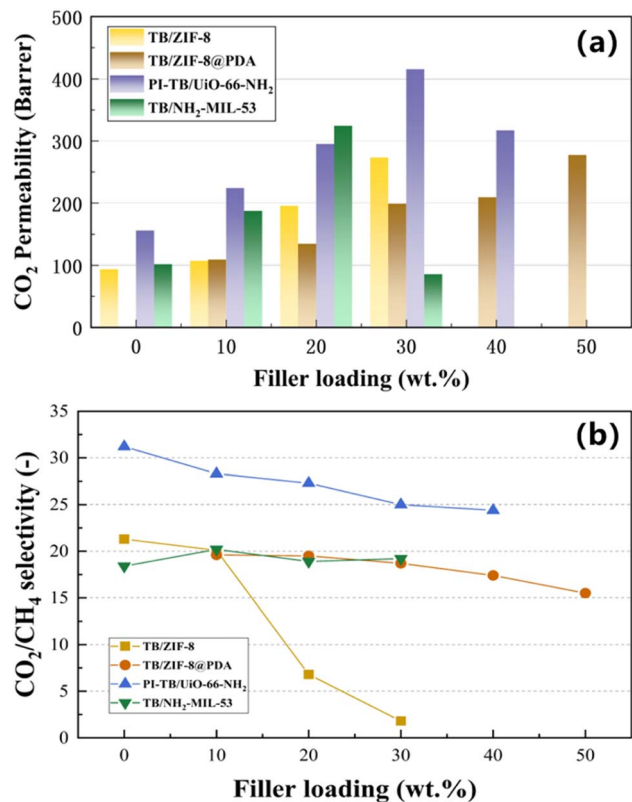


Fig. 23 Effect of porous filler loading on CO<sub>2</sub> permeability (a) and CO<sub>2</sub>/CH<sub>4</sub> selectivity (b) of TB-porous nanofiller MMMs.

a CO<sub>2</sub> permeability of 324.5 Barrer, which is three times that of pure TB membranes, without affecting CO<sub>2</sub>/N<sub>2</sub> and CO<sub>2</sub>/CH<sub>4</sub> selectivity.

Fig. 23 illustrates MMMs based on a TB polymer and commonly used porous nanofillers. Interestingly, it has been observed that ZIF-TB MMMs exhibit a gradual increase in CO<sub>2</sub> permeability as the nanofiller content in the MMMs increases. On the other hand, for Uio-66-NH<sub>2</sub> and NH<sub>2</sub>-MIL-53(Al) based

MMMs, a positive nanofiller loading exists, and further increase of the nanofiller loading will result in a reduction in CO<sub>2</sub> permeability, which may be a negative effect due to filler build-up blocking the polymer pores.<sup>170</sup>

In contrast, non-porous fillers have demonstrated superior performance compared to porous fillers in terms of gas diffusion in certain cases. For instance, Li *et al.*<sup>165</sup> used COOH-functionalized CNT as a filler to form MMMs with triadene trapezoidal polymer TB-PIM as the host matrix, taking into account that the acid-base interaction between COOH and TB improves interfacial compatibility. The permeability of the ITTB/CNT membrane with a loading of 1 wt% was 2504.0 Barrer, which is 22% than that of a neat TB polymer, while CO<sub>2</sub>/N<sub>2</sub> and CO<sub>2</sub>/CH<sub>4</sub> selectivity were nicely maintained (22.6 and 19.0, respectively).

Compared to pure polymer membranes, MMMs based on TB polymers show better CO<sub>2</sub> separation performance, although they do not reach the desired level. Fig. 24 shows the CO<sub>2</sub>/CH<sub>4</sub> and CO<sub>2</sub>/N<sub>2</sub> separation performance of the MMMs, respectively. When examining the filler aspect, only a few MMMs with CNTs as a filler break the Robeson 2008<sup>49</sup> upper bound. This suggests that non-porous fillers could offer new opportunities for TB polymer MMMs. On the other hand, the compatibility between TB polymer substrates and fillers at the interface is also a crucial factor affecting the CO<sub>2</sub> separation performance. Therefore, from this perspective, considering various potential methods of functionalizing traditional TB polymers with other functional groups (PI-TB, TBOR *etc.*) is also a promising approach to enhance CO<sub>2</sub> separation performance.

#### 4. TB based CMS/TR membranes for CO<sub>2</sub> separation

Using appropriate polymers as precursors to form carbon molecule sieve (CMS) membranes is another effective way to improve the gas separation performances. Through high temperature pyrolysis under certain conditions, amorphous carbon structure networks can be formed (CMS

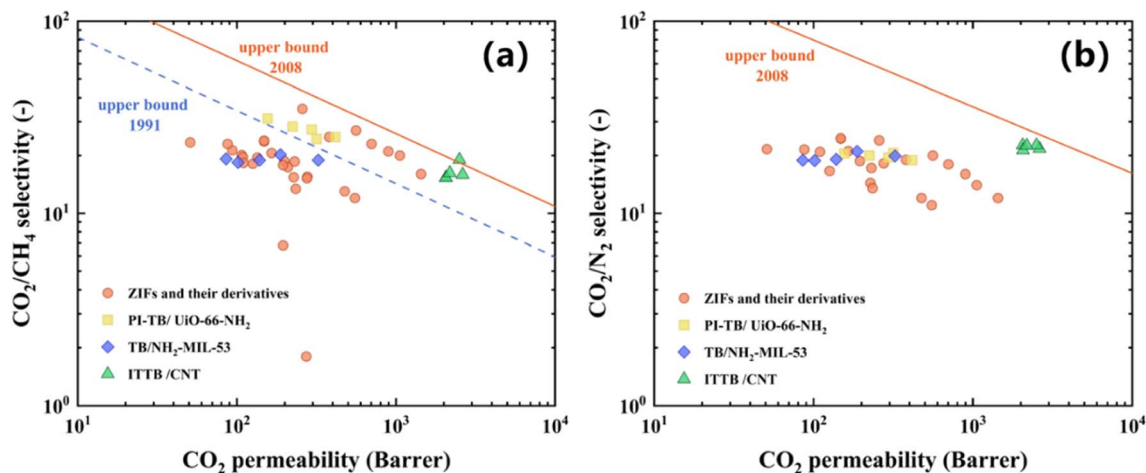


Fig. 24 CO<sub>2</sub>/CH<sub>4</sub> (a) and CO<sub>2</sub>/N<sub>2</sub> (b) separation performance of TB polymer MMMs.

Table 7 CO<sub>2</sub> separation performances of TB polymer based CMS/TR membranes

CMS/TR membranes	$P_{\text{CO}_2}$ (Barrer)	$\alpha_{\text{CO}_2/\text{CH}_4}$ (—)	$\alpha_{\text{CO}_2/\text{N}_2}$ (—)	$\alpha_{\text{CO}_2/\text{H}_2}$ (—)	Ref.
TB-CMS (550 °C)	16 050.0	34.0	21.0	—	176
TB-CMS (650 °C)	4200.0	62.0	36.0	—	
TB-CMS (800 °C)	1406.0	112.0	37.0	—	
CANAL-TB-1 (120 °C)	3435.0	—	—	0.98 <sup>a</sup>	177
CANAL-TB-1-CMS (600 °C)	80.0	—	—	3.80 <sup>a</sup>	
CANAL-TB-1-CMS (700 °C)	6.5	—	—	13.2 <sup>a</sup>	
CANAL-TB-1-CMS (800 °C)	1.05	—	—	39.0 <sup>a</sup>	
CANAL-TB-1-CMS (850 °C) <sup>b</sup>	0.067	—	—	162.0 <sup>a</sup>	
CANAL-TB-1-CMS (900 °C) <sup>b</sup>	0.92	—	—	248.0 <sup>a</sup>	
6FDA-AcTB 1	72.0	21.0	18.0	—	178
6FDA-TR-TB 2	158.0	24.0	13.0	—	
6F6FTB-0.3 (450 °C)	1944.0	23.0	18.0	—	179
6F6FTB-0.4 (300 °C)	41.0	19.0	30.0	—	
6F6FTB-0.4 (400 °C)	241.0	21.0	34.0	—	
6F6FTB-0.4 (450 °C)	2271.0	18.0	22.0	—	
6F6FTB-0.5 (450 °C)	1317.0	18.0	15.0	—	
6FHABTB-0.5 (450 °C)	687.0	25.0	22.0	—	
6FTMTB-0.5 (450 °C)	472.0	31.0	20.0	—	
TB/PSS (400 °C)	34.5 <sup>c</sup>	319.9 <sup>d</sup>	71.9 <sup>e</sup>	—	180
TB/PSS (450 °C)	113.1 <sup>c</sup>	377.0 <sup>d</sup>	205.6 <sup>e</sup>	—	
TB/PSS (500 °C)	473.3 <sup>c</sup>	678.1 <sup>d</sup>	291.7 <sup>e</sup>	—	
TB/PSS (550 °C)	675.0 <sup>c</sup>	552.4 <sup>d</sup>	297.1 <sup>e</sup>	—	
TB/PSS (600 °C)	197.6 <sup>c</sup>	581.6 <sup>d</sup>	278.6 <sup>e</sup>	—	

<sup>a</sup>  $\alpha$  (H<sub>2</sub>/CO<sub>2</sub>). <sup>b</sup> The measurements were carried out at 35 °C and 10 bar. <sup>c</sup> H<sub>2</sub> permeability (Barrer). <sup>d</sup>  $\alpha$  (H<sub>2</sub>/CH<sub>4</sub>). <sup>e</sup>  $\alpha$  (H<sub>2</sub>/N<sub>2</sub>).

membranes).<sup>171,172</sup> Alternatively, by thermally rearranging polymer chains, spatial rearrangement can be achieved, leading to the development of thermally rearranged (TR) membranes.<sup>173–175</sup> This section focuses on CMS membranes and TR membranes based on TB polymers. Table 7 summarizes the research progress of TB polymer-based CMS/TR membranes for CO<sub>2</sub> separation.

Attempts for making CMS based on TB polymers were also made by Wang *et al.*<sup>181</sup> In their work, TB-PI was selected as a precursor for a CMS membrane at different carbonization temperatures. The obtained TB-CMS membranes exhibit much higher gas permeabilities than pristine TB-PI membranes for all gases. For instance, the CO<sub>2</sub> permeability of TB-CMS membranes is up to 1406.0–16050.0 Barrer while it is only 285.0 Barrer for a TB-PI membrane. Meanwhile, the carbonization temperature of the TB-PI membranes plays a role in the distribution of pore size and thus, their permeation properties. As the soaking temperature increases, the gas permeability decreases gradually while the gas selectivity increases. Overall, the TB-CMS membranes possess perfect gas separation performance, especially for CO<sub>2</sub> separation, surpassing the 2015 upper bound.

In addition to the preparation of CMS from TB-PI polymers, Hazi *et al.*<sup>177</sup> developed CMS membranes from aromatic trapezoidal PIM polymers, a polymer precursor synthesized in two steps by combining catalytic arene-norbornene annulation (CANAL) and TB. In the gas separation performance tests, the CO<sub>2</sub> permeability of the CANAL-TB-1-CMS membrane exhibited a gradual decrease (80.0 Barrer to 0.02 Barrer) with increasing

carbonization temperature (600–900 °C), while the H<sub>2</sub>/CO<sub>2</sub> selectivity gradually increased (3.8 to 248.0).

Meckler *et al.*<sup>178</sup> developed thermally rearranged (TR) membranes using a TB polymer, 6FDA-AcTB-1, which was thermally rearranged to obtain 6FDA-TR-TB-2 membranes. Fig. 25(a) and (b) show the membrane performance plotted against the 2008 upper bounds for CO<sub>2</sub>/N<sub>2</sub> and CO<sub>2</sub>/CH<sub>4</sub> separations for 6FDA-AcTB-1 (black) and 6FDA-TR-TB-2 (blue), respectively. The CO<sub>2</sub> permeability of the membranes increased from 72.0 to 158.0 Barrer with almost unchanged CO<sub>2</sub>/N<sub>2</sub> and CO<sub>2</sub>/CH<sub>4</sub> selectivity after TR treatment.

Hu *et al.*<sup>179</sup> also conducted studies on TB-TR membranes by using three different *o*-hydroxy diamine polymers (Fig. 25(c)) to form copolymers with TB polymers. When the TR temperature increases from 300 °C to 450 °C, it results in an increasing CO<sub>2</sub> permeability and a continuous decrease in CO<sub>2</sub>/CH<sub>4</sub> and CO<sub>2</sub>/N<sub>2</sub> selectivity. Conversely, as the TB content increases in the mixture, the CO<sub>2</sub> permeability first goes up and then down, which shows a peak at 40–50% TB content. Overall, membrane performance was best at 50% TB content with 450 °C TR treatment. The three TR membranes 6F6FTB-0.5, 6FHABTB-0.5 and 6FTMTB-0.5 showed a CO<sub>2</sub> permeability of 1314.0, 687.0 and 472.0 Barrer, respectively, without sacrificing too much selectivity. This demonstrates the positive effect of TB chain segment introduction on membrane performance improvement.

The preparation of CMS membranes requires high carbonization temperatures (>800 °C). Recently, Guo *et al.*<sup>180</sup> developed a new low temperature carbonization method. They mixed poly(styrene sulfonic acid) (PSS) with an –SO<sub>3</sub>H group as a novel

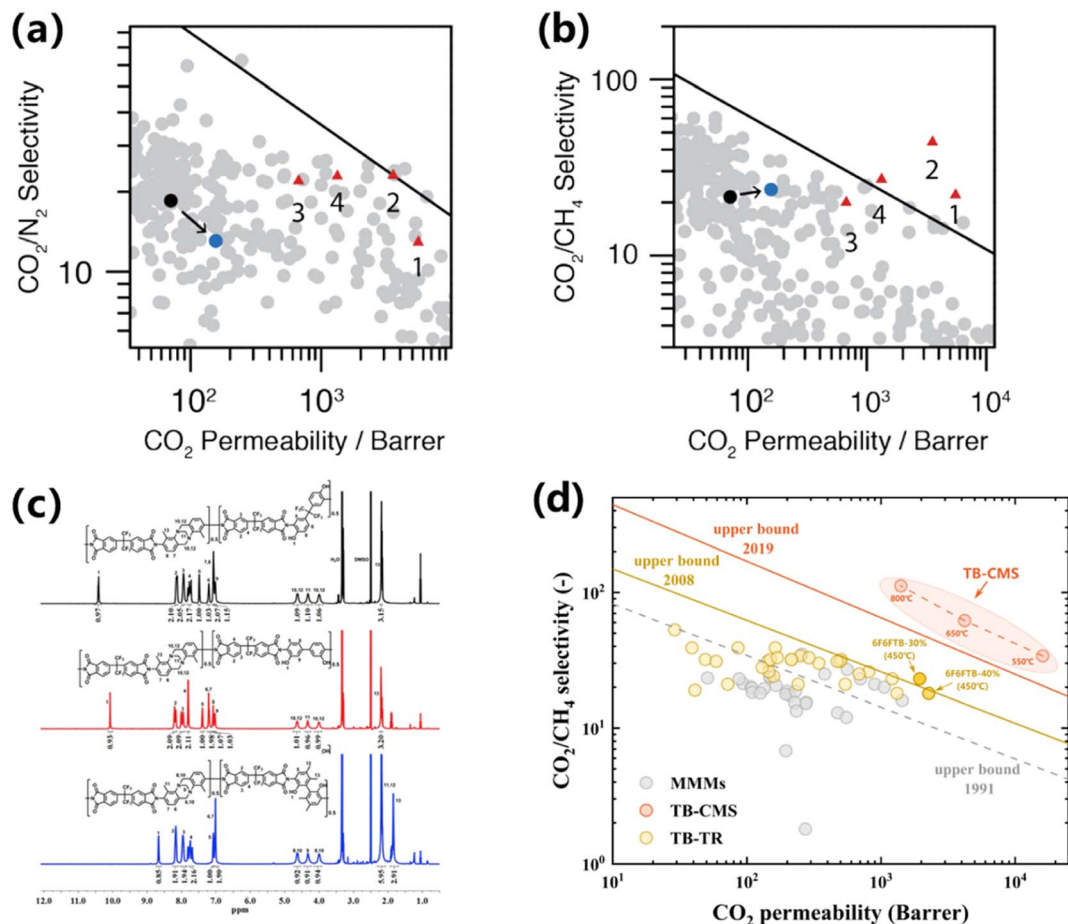


Fig. 25 6FDA-ActB 1 (black) and 6FDA-TR-TB 2 (blue) membrane performance plotted against the 2008 upper bounds for  $\text{CO}_2/\text{N}_2$  (a) and  $\text{CO}_2/\text{CH}_4$  (b) separations. The red triangles mark the performance of several relevant TR polymers from the literature: 1-cTR-450,<sup>182</sup> 2-tTR-450, 3-spiroTR-PBO-6F,<sup>183</sup> and 4-TR TDA1-APAF,<sup>184</sup> while the grey circles represent other polymer membranes reported in the literature, reproduced from ref. 178 Copyright 2018. (c) H NMR spectra of representative Co-TBHPis, 6F6FTB-0.5 (black), 6FHABTB-0.5 (red), and 6FTMTB-0.5 (blue) reproduced from ref. 179 Copyright 2020. (d)  $\text{CO}_2/\text{CH}_4$  separation performance of TB polymer CMS/TR membranes.

pore generator into a precursor membrane made of the TB polymer matrix. While the  $\text{CO}_2$  separation performance was not tested, CMS membranes with good  $\text{H}_2$  separation performance were obtained using a pyrolysis temperature in the range of

400–550 °C. This offers new insights for complex preparation processes of CMS membranes regarding TB polymers.

In summary, CMS membranes based on TB polymers exhibited impressive  $\text{CO}_2$  separation performance compared to

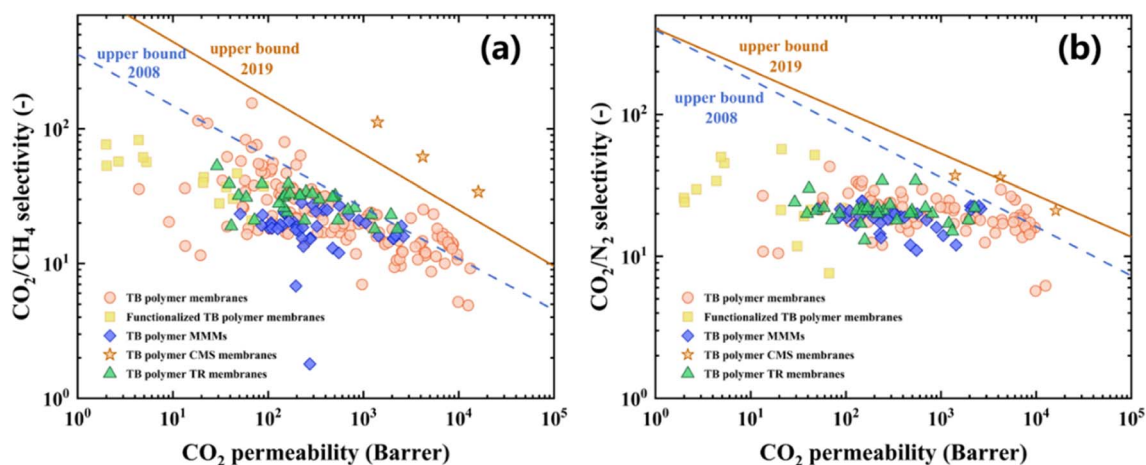


Fig. 26 (a)  $\text{CO}_2/\text{CH}_4$  and (b)  $\text{CO}_2/\text{N}_2$  separation performance of neat TB polymeric membranes, TB based MMMs and TB based CMS membranes.

both TB polymer based MMMs and TB-TR membranes (Fig. 25(d)). Compared to the neat TR polymers, thermal rearrangement significantly improved the CO<sub>2</sub> separation performances, but these were still under the 2008 Robeson<sup>49</sup> upper bound. In the future, developing CMS membranes based on TB polymers requires more attention.

Overall, the CO<sub>2</sub>/N<sub>2</sub> and CO<sub>2</sub>/CH<sub>4</sub> separation performances of neat TB polymeric membranes, MMMs, and CMS/TR membranes are presented in Fig. 26. Among them, even though the reports about CMS membranes based on TB polymers are rather limited, the TB based CMS membranes exhibit the most attractive CO<sub>2</sub> separation performances for both CO<sub>2</sub>/N<sub>2</sub> and CO<sub>2</sub>/CH<sub>4</sub> separation. On the other hand, functionalization of the TB polymer appears to slightly improve the selectivity, but at the cost of a significant reduction in CO<sub>2</sub> permeability. Introducing nanofillers into the polymeric matrix is known to be an effective strategy to improve CO<sub>2</sub> separation performances for many polymers,<sup>185</sup> but it is not that effective in promoting CO<sub>2</sub> separation performances for TB based polymeric membranes. Developing new TB polymers with higher excess free volume generally leads to higher CO<sub>2</sub> permeability, but often comes at the cost of relatively lower selectivity and faster physical aging.

## 5. Conclusions and perspectives

This review summarizes the recent advancements in TB polymers for CO<sub>2</sub> separation membranes, including pure TB polymers, functionalized membranes, MMMs, and CMS and TR membranes. Based on the findings, several conclusions can be drawn:

TB polymer membranes, particularly those with high free volume, demonstrate high CO<sub>2</sub> permeability and moderate CO<sub>2</sub>/CH<sub>4</sub> and CO<sub>2</sub>/N<sub>2</sub> selectivity. The copolymer membrane obtained by cross-linking with PIM shows promising potential for CO<sub>2</sub> separation. Similar to other high free volume polymer membranes, TB polymer membranes face challenges related to physical aging and plasticization. Overcoming these obstacles is crucial for practical application of TB polymer membranes.

TB polymer based MMMs are also widely studied for CO<sub>2</sub> separation. So far, only a few fillers, such as MOFs and zeolites, have been used as nanofillers in TB polymer based MMMs. Nonporous fillers such as CNTs were also reported. Regrettably, based on literature data, most MMMs did not exceed the 2008 upper bound.

Moreover, studies have been conducted to enhance the gas separation performance of TB polymeric membranes through thermal treatment. CMS membranes derived from the TB polymer exhibit exceptionally high CO<sub>2</sub> permeability and CO<sub>2</sub>/CH<sub>4</sub> and CO<sub>2</sub>/N<sub>2</sub> selectivity. While the performance of TR membranes is relatively lower compared to that of CMS membranes, a high-performance TR membrane can still be achieved by carefully selecting suitable thermal treatment conditions, including temperature and soaking time. This indicates the potential of TR membranes as promising candidates for CO<sub>2</sub> separation applications.

Based on the above results, several perspectives can be identified:

(1) In the context of pure TB polymeric membranes, it is desirable to focus on developing TB polymers with increased rigidity and higher free volume. In addition, exploring new methods to effectively improve physical aging and plasticization resistance in TB polymeric membranes is also important.

(2) For TB polymer based MMMs, mathematical models can be developed to simulate and optimize the selection of suitable polymer/filler combinations. Moreover, attempts should be directed towards improving the interfacial compatibility between the polymer and nanofillers.

(3) In the case of CMS and TR membranes based on TB polymers, as there are limited reports on the development of CMS membranes using TB polymers as precursors, further research efforts can be dedicated to this topic.

In addition to the abovementioned perspectives, new techniques and methods can be also powerful tools in promoting the CO<sub>2</sub> separation performance. For instance, machine learning can be also applied to discover and predict TB polymers with better CO<sub>2</sub> separation capabilities.<sup>186–188</sup> Overall, TB polymers and their derivatives hold great promise as membrane materials for CO<sub>2</sub> separation and warrant further in-depth research.

## Abbreviations

PIMs	Polymers of intrinsic microporosity
TB	Troger's base
PIs	Polyimides
PAs	Polyamides
PBI	Polybenzimidazole
TR polymer	Thermally rearranged polymer
TB polymer	Tröger's base polymer
CMS	Carbon molecular sieve
MMMs	Mixed-matrix membranes
CO <sub>2</sub>	Carbon dioxide
CCUS	Carbon capture, utilization and storage
FFV	Fractional free volume
<i>T<sub>g</sub></i>	Glass transition temperature
DMM	Dimethoxymethane
ILs	Ionic liquids
TAPM	Tetrakis(4-aminophenyl)methane
Trip	Triptycene
OT	<i>o</i> -Tolidine
TB-OT	OT-based TB polymer
Me <sub>2</sub> SO <sub>4</sub>	Dimethyl sulfate
Et <sub>2</sub> O	Diethyl ether
DPD	2,5-Dimethyl-1,4-phenylenediamine
DAT	2-Methyl-1,3-benzenediamine
1,5-DAN	1,5-Diaminonaphthalene
4,4'-HFD	4,4'-(Hexafluoroisopropylidene)dianiline
MSBC	6,6'-Bis(4-amino-3-methylphenoxy)-4,4,4',4',7,7'-hexamethyl-2,2'-spirobichroman
SBC	6,6'-Bis(4-aminophenoxy)-4,4,4',4',7,7'-hexamethyl-2,2'-spirobichroman
CA-PIM	Carboxylate polymer precursor
PIM-BM	Bromomethylated PIMs
TFC	Thin film composite

CNT	Carbon nanotube
MOFs	Metal-organic frameworks
COFs	Covalent-organic frameworks
PDA	Polydopamine
FDA	4,4'-(9-Fluorenylidene)dianiline
FDT	4,4'-(9-Fluorenylidene)di- <i>o</i> -toluidine
SBF	9,9-Spirobifluorene-2,2'-diamine
6FDA	4,4'-(Hexafluoroisopropylidene) diphthalic anhydride
CpODA	Norbornane-2-spiro- $\alpha$ -cyclopentanone- $\alpha'$ -spiro-2'-norbornane-5,5'',6,6''-tetracarboxylic dianhydride
MMDA	5,5'-(Mesitylmethylene)bis(4-methylphthalic anhydride)
FDDA	5,5'-(9 <i>H</i> -Fluorene-9,9-diyl)bis(4-methylphthalic anhydride)
TNTDA	3,3'-di- <i>tert</i> -Butyl-2,2'-dimethoxy-[1,1'-binaphthalene]-6,6',7,7'-tetracarboxylic dianhydride
<i>t</i> -BuPh	Pendant <i>tert</i> -butyl-phenyl
TTBDA	2,8-Bis(4-( <i>tert</i> -butyl)phenyl)-4,10-diamino-6,12-dihydro-5,11-methanodibenzo[ <i>b,f</i> ][1,5] diazocine
DABA	3,5-Diaminobenzoic acid
HTB	1,7-Diamino-6 <i>H</i> ,12 <i>H</i> -5,11-methanodibenzo[1,5] diazocine-2,8-diol
TMPD	2,3,5,6-Tetramethyl- <i>p</i> -phenylenediamine
EA	Ethanoanthracene
SBI	Spirobisindane
CTA	Trip-2,6-diamine
MTA	Trip-2,7-diamine
MP	Methanopentacene
DFTrip	2,3-Difluoro-functionalized triptycene
TBS	<i>tert</i> -Butyldimethylsilyl
THTB	Tetrahydroxy-TB
TTSBI	5,5',6,6'-Tetrahydroxy-3,3,3',3'-tetramethylspirobisindane
DATCA	2,6-Diaminotriptycene-14-carboxylic acid
DAT'	2,6-Diaminotriptycene
2FNB	2-Fluoronitrobenzene
4FNB	4-Fluoronitrobenzene
Im-TB-ionene	Imidazolium-mediated TB-based ionene polymer
TBDA2-6FDA-PI	Intrinsically microporous polyimide with a Tröger's base functional group
TBOR	Ring-opened Tröger's base polymer
ITTB	Microporous triptycene based ladder TB-PIMs
ZIF-8	Zeolitic imidazolate-8
ZIF-L-Zn	Two-dimensional (2D) leaf ZIFs synthesized from Zn(NO <sub>3</sub> ) <sub>2</sub> · 6H <sub>2</sub> O
ZIF-L-Co	Two-dimensional (2D) leaf ZIFs synthesized from Co(NO <sub>3</sub> ) <sub>2</sub> · 6H <sub>2</sub> O
CANAL	Catalytic arene-norbornene annulation
6FDA-AcTB	<i>ortho</i> -Acetate functionalized Tröger's base polyimide precursors
6FDA-TR-TB	Thermal rearrangement of 6FDA-AcTB
Co-TBHPIs	A series of TB-based copolyimide precursors which are synthesized from 6FDA with TBDA2(11-methanodibenzo[1,5]-diazocine)

6F6FTB	Co-TBHPIs synthesized from <i>o</i> -hydroxy diamine 2,2'-bis(3-amino-4-hydroxyphenyl) hexafluoropropane (APAF) as the raw material
6FHABTB	Co-TBHPIs synthesized from <i>o</i> -hydroxy diamine 3,3'-dihydroxy-4,4'-diamino-biphenyl (HAB) as the raw material
6FTMTB	Co-TBHPIs synthesized from <i>o</i> -hydroxy diamine 3,3'-diamino-5,5',6,6'-tetramethyl-[1,1'-biphenyl]-2,2'-diol (TMBDA) as the raw material
PSS	Polystyrene sulfonic acid

## Conflicts of interest

There are no conflicts to declare.

## Acknowledgements

This work acknowledges the financial support from the Sichuan Science and Technology Program (2021YFH0116) and National Natural Science Foundation of China (No. 52170112).

## References

- M. J. Ring, *et al.*, Causes of the global warming observed since the 19th century, *Atmos. Clim. Sci.*, 2012, **2**(04), 401.
- H. Jian-Bin, *et al.*, Debates on the causes of global warming, *Adv. Clim. Chang. Res.*, 2012, **3**(1), 38–44.
- J. Houghton, Global warming, *Rep. Prog. Phys.*, 2005, **68**(6), 1343.
- R. A. Kerr, Global warming is changing the world, *Science*, 2007, **316**(5822), 188–190.
- K. Jiang, *et al.*, China's carbon capture, utilization and storage (CCUS) policy: A critical review, *Renewable Sustainable Energy Rev.*, 2020, **119**, 109601.
- H. Liu, *et al.*, Worldwide status of CCUS technologies and their development and challenges in China, *Geofluids*, 2017, **2017**, 6126505.
- F. O. Ochedi, *et al.*, Carbon dioxide capture using liquid absorption methods: a review, *Environ. Chem. Lett.*, 2021, **19**, 77–109.
- X. Wang, *et al.*, Immobilization of amino acid ionic liquids into nanoporous microspheres as robust sorbents for CO<sub>2</sub> capture, *J. Mater. Chem. A*, 2013, **1**(9), 2978–2982.
- Q. Wang, *et al.*, CO<sub>2</sub> capture by solid adsorbents and their applications: current status and new trends, *Energy Environ. Sci.*, 2011, **4**(1), 42–55.
- R. Chang, *et al.*, Synthetic solid oxide sorbents for CO<sub>2</sub> capture: state-of-the art and future perspectives, *J. Mater. Chem. A*, 2022, **10**(4), 1682–1705.
- G. Sneddon, *et al.*, Aminated poly(vinyl chloride) solid state adsorbents with hydrophobic function for post-combustion CO<sub>2</sub> capture, *J. Mater. Chem. A*, 2017, **5**(23), 11864–11872.
- S. Abuelgasim, W. Wang and A. Abdalazeez, A brief review for chemical looping combustion as a promising CO<sub>2</sub> capture technology: Fundamentals and progress, *Sci. Total Environ.*, 2021, **764**, 142892.

- 13 Z. Sun, *et al.*, Synergistic enhancement of chemical looping-based CO<sub>2</sub> splitting with biomass cascade utilization using cyclic stabilized Ca<sub>2</sub>Fe<sub>2</sub>O<sub>5</sub> aerogel, *J. Mater. Chem. A*, 2019, 7(3), 1216–1226.
- 14 U. W. Siagian, *et al.*, Membrane-based carbon capture technologies: Membrane gas separation vs. membrane contactor, *J. Nat. Gas Sci. Eng.*, 2019, 67, 172–195.
- 15 B. Zhu, *et al.*, Rational design of poly(ethylene oxide) based membranes for sustainable CO<sub>2</sub> capture, *J. Mater. Chem. A*, 2020, 8(46), 24233–24252.
- 16 N. Kosinov, *et al.*, High flux high-silica SSZ-13 membrane for CO<sub>2</sub> separation, *J. Mater. Chem. A*, 2014, 2(32), 13083–13092.
- 17 Z. Wang, *et al.*, Polymers of intrinsic microporosity/metal-organic framework hybrid membranes with improved interfacial interaction for high-performance CO<sub>2</sub> separation, *J. Mater. Chem. A*, 2017, 5(22), 10968–10977.
- 18 W. Budzianowski, Explorative analysis of advanced solvent processes for energy efficient carbon dioxide capture by gas-liquid absorption, *Int. J. Greenhouse Gas Control*, 2016, 49, 108–120.
- 19 C.-H. Yu, C.-H. Huang and C.-S. Tan, A review of CO<sub>2</sub> capture by absorption and adsorption, *Aerosol Air Qual. Res.*, 2012, 12(5), 745–769.
- 20 W. Jiang, *et al.*, Advances in applications of ionic liquids for phase change CO<sub>2</sub> capture, *Chem. Eng. J.*, 2022, 136767.
- 21 M. Wang, *et al.*, Post-combustion CO<sub>2</sub> capture with chemical absorption: A state-of-the-art review, *Chem. Eng. Res. Des.*, 2011, 89(9), 1609–1624.
- 22 A. Kiani, K. Jiang and P. Feron, Techno-economic assessment for CO<sub>2</sub> capture from air using a conventional liquid-based absorption process, *Front. Energy Res.*, 2020, 8, 92.
- 23 C.-C. Cormos, Assessment of chemical absorption/adsorption for post-combustion CO<sub>2</sub> capture from Natural Gas Combined Cycle (NGCC) power plants, *Appl. Therm. Eng.*, 2015, 82, 120–128.
- 24 C.-C. Cormos, Evaluation of reactive absorption and adsorption systems for post-combustion CO<sub>2</sub> capture applied to iron and steel industry, *Appl. Therm. Eng.*, 2016, 105, 56–64.
- 25 R. Ramezani, S. Mazinani and R. Di Felice, State-of-the-art of CO<sub>2</sub> capture with amino acid salt solutions, *Rev. Chem. Eng.*, 2022, 38(3), 273–299.
- 26 S. Seo, *et al.*, Phase-change ionic liquids for postcombustion CO<sub>2</sub> capture, *Energy Fuels*, 2014, 28(9), 5968–5977.
- 27 Q. Huang, *et al.*, Hybrid ionic liquid capsules for rapid CO<sub>2</sub> capture, *Ind. Eng. Chem. Res.*, 2019, 58(24), 10503–10509.
- 28 Q. Zhuang, *et al.*, Ten years of research on phase separation absorbents for carbon capture: Achievements and next steps, *Int. J. Greenhouse Gas Control*, 2016, 52, 449–460.
- 29 K. P. Resnik, J. T. Yeh and H. W. Pennline, Aqua ammonia process for simultaneous removal of CO<sub>2</sub>, SO<sub>2</sub> and NO<sub>x</sub>, *Int. J. Environ. Technol. Manage.*, 2004, 4(1–2), 89–104.
- 30 G. Arora and S. I. Sandler, Air separation by single wall carbon nanotubes: Thermodynamics and adsorptive selectivity, *J. Chem. Phys.*, 2005, 123(4), 044705.
- 31 M. Hassan, D. Ruthven and N. Raghavan, Air separation by pressure swing adsorption on a carbon molecular sieve, *Chem. Eng. Sci.*, 1986, 41(5), 1333–1343.
- 32 B. Silva, *et al.*, H<sub>2</sub> purification by pressure swing adsorption using CuBTC, *Sep. Purif. Technol.*, 2013, 118, 744–756.
- 33 S. Iyuke, *et al.*, Application of Sn-activated carbon in pressure swing adsorption for purification of H<sub>2</sub>, *Chem. Eng. Sci.*, 2000, 55(20), 4745–4755.
- 34 R. W. Baker and K. Lokhandwala, Natural gas processing with membranes: an overview, *Ind. Eng. Chem. Res.*, 2008, 47(7), 2109–2121.
- 35 Y. Gu, E. L. Cussler and T. P. Lodge, ABA-triblock copolymer ion gels for CO<sub>2</sub> separation applications, *J. Membr. Sci.*, 2012, 423, 20–26.
- 36 R. W. Baker and B. T. Low, Gas separation membrane materials: a perspective, *Macromolecules*, 2014, 47(20), 6999–7013.
- 37 L. M. Robeson, Polymer membranes for gas separation, *Curr. Opin. Solid State Mater. Sci.*, 1999, 4(6), 549–552.
- 38 R. S. K. Valappil, N. Ghasem and M. Al-Marzouqi, Current and future trends in polymer membrane-based gas separation technology: A comprehensive review, *J. Ind. Eng. Chem.*, 2021, 98, 103–129.
- 39 A. K. Sekizkardes, *et al.*, Microporous polymeric composite membranes with advanced film properties: pore intercalation yields excellent CO<sub>2</sub> separation performance, *J. Mater. Chem. A*, 2018, 6(45), 22472–22477.
- 40 H. B. T. Jeazet, C. Staudt and C. Janiak, Metal-organic frameworks in mixed-matrix membranes for gas separation, *Dalton Trans.*, 2012, 41(46), 14003–14027.
- 41 M. Aroon, *et al.*, Performance studies of mixed matrix membranes for gas separation: A review, *Sep. Purif. Technol.*, 2010, 75(3), 229–242.
- 42 X. Guo, *et al.*, Mixed-matrix membranes for CO<sub>2</sub> separation: Role of the third component, *J. Mater. Chem. A*, 2019, 7(43), 24738–24759.
- 43 M.-B. Hägg and X. He, Carbon molecular sieve membranes for gas separation, *Membr. Eng. Treat. Gases*, 2011, 2, 162–191.
- 44 T. Araújo, G. Bernardo and A. Mendes, Cellulose-based carbon molecular sieve membranes for gas separation: a review, *Molecules*, 2020, 25(15), 3532.
- 45 S. Morooka and K. Kusakabe, Microporous inorganic membranes for gas separation, *MRS Bull.*, 1999, 24(3), 25–29.
- 46 D. De Meis, M. Richetta and E. Serra, Microporous inorganic membranes for gas separation and purification, *InterCeram: Int. Ceram.*, 2018, 67, 16–21.
- 47 P. Goh, *et al.*, Recent advances of inorganic fillers in mixed matrix membrane for gas separation, *Sep. Purif. Technol.*, 2011, 81(3), 243–264.
- 48 L. M. Robeson, Correlation of separation factor versus permeability for polymeric membranes, *J. Membr. Sci.*, 1991, 62(2), 165–185.

- 49 L. M. Robeson, The upper bound revisited, *J. Membr. Sci.*, 2008, **320**(1–2), 390–400.
- 50 A. X. Wu, J. A. Drayton and Z. P. Smith, The perfluoropolymer upper bound, *AIChE J.*, 2019, **65**(12), e16700.
- 51 S. Wang, *et al.*, Advances in high permeability polymer-based membrane materials for CO<sub>2</sub> separations, *Energy Environ. Sci.*, 2016, **9**(6), 1863–1890.
- 52 Y. Wang, *et al.*, Polymers of intrinsic microporosity for energy-intensive membrane-based gas separations, *Mater. Today Nano*, 2018, **3**, 69–95.
- 53 S. Bhattacharya and S.-T. Hwang, Concentration polarization, separation factor, and Peclet number in membrane processes, *J. Membr. Sci.*, 1997, **132**(1), 73–90.
- 54 I. Rose, *et al.*, Highly Permeable Benzotriptycene-Based Polymer of Intrinsic Microporosity, *ACS Macro Lett.*, 2015, **4**(9), 912–915.
- 55 S. J. D. Smith, *et al.*, Control of Physical Aging in Super-Glassy Polymer Mixed Matrix Membranes, *Acc. Chem. Res.*, 2020, **53**(7), 1381–1388.
- 56 M. Galizia, *et al.*, 50th Anniversary Perspective: Polymers and Mixed Matrix Membranes for Gas and Vapor Separation: A Review and Prospective Opportunities, *Macromolecules*, 2017, **50**(20), 7809–7843.
- 57 D. S. Bakhtin, *et al.*, Mitigation of Physical Aging of Polymeric Membrane Materials for Gas Separation: A Review, *Membranes*, 2023, **13**(5), 519.
- 58 N. B. McKeown, Polymers of Intrinsic Microporosity (PIMs), *Polymer*, 2020, **202**, 122736.
- 59 Y. Rogan, *et al.*, A highly permeable polyimide with enhanced selectivity for membrane gas separations, *J. Mater. Chem. A*, 2014, **2**(14), 4874–4877.
- 60 K. Y. Wang, M. Weber and T.-S. Chung, Polybenzimidazoles (PBIs) and state-of-the-art PBI hollow fiber membranes for water, organic solvent and gas separations: A review, *J. Mater. Chem. A*, 2022, **10**(16), 8687–8718.
- 61 Z.-X. Low, *et al.*, Gas Permeation Properties, Physical Aging, and Its Mitigation in High Free Volume Glassy Polymers, *Chem. Rev.*, 2018, **118**(12), 5871–5911.
- 62 R. Williams, *et al.*, A highly rigid and gas selective methanopentacene-based polymer of intrinsic microporosity derived from Tröger's base polymerization, *J. Mater. Chem. A*, 2018, **6**(14), 5661–5667.
- 63 A. S. Embaye, *et al.*, Poly(ether-block-amide) Copolymer Membranes in CO<sub>2</sub> Separation Applications, *Energy Fuels*, 2021, **35**(21), 17085–17102.
- 64 B. J. Adzima, *et al.*, Modular polymerized ionic liquid block copolymer membranes for CO<sub>2</sub>/N<sub>2</sub> separation, *J. Mater. Chem. A*, 2014, **2**(21), 7967–7972.
- 65 Y. Han and W. S. W. Ho, Polymeric membranes for CO<sub>2</sub> separation and capture, *J. Membr. Sci.*, 2021, **628**, 119244.
- 66 X. Ma, *et al.*, Facile synthesis of a hydroxyl-functionalized troger's base diamine: a new building block for high-performance polyimide gas separation membranes, *Macromolecules*, 2017, **50**(24), 9569–9576.
- 67 Z. Wang, *et al.*, Troger's base-based microporous polyimide membranes for high-performance gas separation, *ACS Macro Lett.*, 2014, **3**(7), 597–601.
- 68 Z. Wang, D. Wang and J. Jin, Microporous polyimides with rationally designed chain structure achieving high performance for gas separation, *Macromolecules*, 2014, **47**(21), 7477–7483.
- 69 I. Kammakakam, *et al.*, Design and Synthesis of Imidazolium-Mediated Troger's Base-Containing Ionene Polymers for Advanced CO<sub>2</sub> Separation Membranes, *ACS Omega*, 2019, **4**(2), 3439–3448.
- 70 M. Carta, *et al.*, An efficient polymer molecular sieve for membrane gas separations, *Science*, 2013, **339**(6117), 303–307.
- 71 B. Wepster, Steric effects on mesomerism: XI, The ultra-violet absorption spectrum of Tröger's base and the stereochemistry of aromatic amines, *Recl. Trav. Chim. Pays-Bas*, 1953, **72**(8), 661–672.
- 72 Y. Goldberg and H. Alper, Transition metal complexes of Tröger's base and their catalytic activity for the hydrosilylation of alkynes, *Tetrahedron Lett.*, 1995, **36**(3), 369–372.
- 73 S. Larson and C. Wilcox, Structure of 5, 11-methano-2, 8-dimethyl-5, 6, 11, 12-tetrahydrodibenzo [b, f][1, 5] diazocine (Tröger's base) at 163 K, *Acta Crystallogr., Sect. C: Cryst. Struct. Commun.*, 1986, **42**(2), 224–227.
- 74 C. S. Wilcox and M. D. Cowart, New approaches to synthetic receptors. Synthesis and host properties of a water soluble macrocyclic analog of Tröger's base, *Tetrahedron Lett.*, 1986, **27**(46), 5563–5566.
- 75 F. Cooper and M. Partridge, Cyclic amidines. Part IV. 5: 6: 11: 12-Tetrahydro-5: 11-endomethylenephnomazine and Tröger's base, *J. Chem. Soc.*, 1955, 991–994.
- 76 A. Abdolmaleki, S. Heshmat-Azad and M. Kheradmand-fard, Noncoplanar rigid-rod aromatic polyhydrazides containing Tröger's base, *J. Appl. Polym. Sci.*, 2011, **122**(1), 282–288.
- 77 X. Du, *et al.*, Tröger's base-functionalised organic nanoporous polymer for heterogeneous catalysis, *Chem. Commun.*, 2010, **46**(6), 970–972.
- 78 M. Carta, *et al.*, The synthesis of microporous polymers using Tröger's base formation, *Polym. Chem.*, 2014, **5**(18), 5267–5272.
- 79 X. Ma, *et al.*, Unprecedented gas separation performance of a difluoro-functionalized triptycene-based ladder PIM membrane at low temperature, *J. Mater. Chem. A*, 2021, **9**(9), 5404–5414.
- 80 M. Carta, *et al.*, Triptycene induced enhancement of membrane gas selectivity for microporous Tröger's base polymers, *Adv. Mater.*, 2014, **26**(21), 3526–3531.
- 81 C. Zhang, *et al.*, Post-crosslinking of triptycene-based Tröger's base polymers with enhanced natural gas separation performance, *J. Membr. Sci.*, 2018, **556**, 277–284.
- 82 P. Zheng, *et al.*, Ionization of Tröger's base polymer of intrinsic microporosity for high-performance membrane-mediated helium recovery, *J. Membr. Sci.*, 2023, **672**, 121425.

- 83 Y. Xiao, *et al.*, Molecular design of Tröger's base-based polymers with intrinsic microporosity for gas separation, *J. Membr. Sci.*, 2017, **521**, 65–72.
- 84 C. Zhang, *et al.*, Molecular design of Troger's base-based polymers containing spirobichroman structure for gas separation, *Ind. Eng. Chem. Res.*, 2017, **56**(44), 12783–12788.
- 85 J. Yue, *et al.*, Branched Tröger's base polymer membranes for gas separation, *Polymer*, 2022, **262**, 125437.
- 86 H. Sanaeepur, *et al.*, Polyimides in membrane gas separation: Monomer's molecular design and structural engineering, *Prog. Polym. Sci.*, 2019, **91**, 80–125.
- 87 Y. Zhuang, *et al.*, Intrinsically microporous soluble polyimides incorporating Tröger's base for membrane gas separation, *Macromolecules*, 2014, **47**(10), 3254–3262.
- 88 Y. Zhuang, *et al.*, High-strength, soluble polyimide membranes incorporating Tröger's Base for gas separation, *J. Membr. Sci.*, 2016, **504**, 55–65.
- 89 Y. Zhang, *et al.*, Effect of structural isomerism on physical and gas transport properties of Tröger's Base-based polyimides, *Polymer*, 2022, **239**, 124412.
- 90 Y. Zhuang, *et al.*, Soluble, microporous, Tröger's Base copolyimides with tunable membrane performance for gas separation, *Chem. Commun.*, 2016, **52**(19), 3817–3820.
- 91 S. Kazama, T. Teramoto and K. Haraya, Carbon dioxide and nitrogen transport properties of bis (phenyl) fluorene-based cardo polymer membranes, *J. Membr. Sci.*, 2002, **207**(1), 91–104.
- 92 Y. Zhang, *et al.*, Alicyclic segments upgrade hydrogen separation performance of intrinsically microporous polyimide membranes, *J. Membr. Sci.*, 2020, **611**, 118363.
- 93 Y. Lu, *et al.*, Intrinsically microporous polyimides derived from norbornane-2-spiro- $\alpha$ -cyclopentanone- $\alpha'$ -spiro-2'-norbornane-5, 5'', 6, 6''-tetracarboxylic dianhydride, *Polymer*, 2021, **228**, 123955.
- 94 X. Hu, *et al.*, Tröger's Base (TB)-containing polyimide membranes derived from bio-based dianhydrides for gas separations, *J. Membr. Sci.*, 2020, **610**, 118255.
- 95 X. Hu, *et al.*, Highly permeable polyimides incorporating Tröger's base (TB) units for gas separation membranes, *J. Membr. Sci.*, 2020, **615**, 118533.
- 96 Y. Wang, *et al.*, Facile synthesis and gas transport properties of Hünlich's base-derived intrinsically microporous polyimides, *Polymer*, 2020, **201**, 122619.
- 97 T. Corrado and R. Guo, Macromolecular design strategies toward tailoring free volume in glassy polymers for high performance gas separation membranes, *Mol. Syst. Des. Eng.*, 2020, **5**(1), 22–48.
- 98 R. Swaidan, *et al.*, Rational design of intrinsically ultramicroporous polyimides containing bridgehead-substituted triptycene for highly selective and permeable gas separation membranes, *Macromolecules*, 2014, **47**(15), 5104–5114.
- 99 X. Hu, *et al.*, Synthesis and gas separation performance of intrinsically microporous polyimides derived from sterically hindered binaphthalenetetracarboxylic dianhydride, *Polym. Chem.*, 2020, **11**(25), 4172–4179.
- 100 X. Hu, *et al.*, Intrinsically microporous co-polyimides derived from *ortho*-substituted Tröger's Base diamine with a pendant tert-butyl-phenyl group and their gas separation performance, *Polymer*, 2018, **153**, 173–182.
- 101 X. Xu, *et al.*, Synthesis of polyimides containing Tröger's base and triphenylmethane moieties with a tunable fractional free volume for CO<sub>2</sub> separation, *Polym. Chem.*, 2022, **13**(39), 5545–5556.
- 102 M. Lee, *et al.*, Enhancing the gas permeability of Troger's base derived polyimides of intrinsic microporosity, *Macromolecules*, 2016, **49**(11), 4147–4154.
- 103 B. Ghanem, *et al.*, Novel 6FDA-based polyimides derived from sterically hindered Tröger's base diamines: Synthesis and gas permeation properties, *Polymer*, 2016, **96**, 13–19.
- 104 Z. Wang, *et al.*, Tuning the gas selectivity of Tröger's base polyimide membranes by using carboxylic acid and tertiary base interactions, *ChemSusChem*, 2018, **11**(16), 2744–2751.
- 105 M. A. Abdulhamid, Tröger's base-derived dianhydride as a promising contorted building block for polyimide-based membranes for gas separation, *Sep. Purif. Technol.*, 2023, **123208**.
- 106 S. Bisoi, *et al.*, Gas separation properties of Troeger's base-bridged polyamides, *e-Polym.*, 2017, **17**(4), 283–293.
- 107 B. D. Freeman, Basis of permeability/selectivity tradeoff relations in polymeric gas separation membranes, *Macromolecules*, 1999, **32**(2), 375–380.
- 108 M. Carta, *et al.*, Synthesis of cardo-polymers using Tröger's base formation, *Polym. Chem.*, 2014, **5**(18), 5255–5261.
- 109 M. Balcik, Y. Wang and I. Pinnau, Exploring the effect of intra-chain rigidity on mixed-gas separation performance of a Triptycene-Tröger's base ladder polymer (PIM-Trip-TB) by atomistic simulations, *J. Membr. Sci.*, 2023, **677**, 121614.
- 110 G. Genduso, *et al.*, Permeation, sorption, and diffusion of CO<sub>2</sub>-CH<sub>4</sub> mixtures in polymers of intrinsic microporosity: The effect of intrachain rigidity on plasticization resistance, *J. Membr. Sci.*, 2019, **584**, 100–109.
- 111 R. Malpass-Evans, *et al.*, Effect of bridgehead methyl substituents on the gas permeability of Tröger's-base derived polymers of intrinsic microporosity, *Membranes*, 2020, **10**(4), 62.
- 112 Z. Zhu, *et al.*, Enhanced Gas Separation Properties of Tröger's Base Polymer Membranes Derived from Pure Triptycene Diamine Regioisomers, *Macromolecules*, 2020, **53**(5), 1573–1584.
- 113 E. Lasseguette, *et al.*, Temperature and pressure dependence of gas permeation in a microporous Tröger's base polymer, *Membranes*, 2018, **8**(4), 132.
- 114 T. M. Long and T. M. Swager, Using “internal free volume” to increase chromophore alignment, *J. Am. Chem. Soc.*, 2002, **124**(15), 3826–3827.
- 115 I. Rose, *et al.*, Polymer ultrapermeability from the inefficient packing of 2D chains, *Nat. Mater.*, 2017, **16**(9), 932–937.

- 116 S. Liu, *et al.*, Efficient Synthesis of Rigid Ladder Polymers via Palladium Catalyzed Annulation, *J. Am. Chem. Soc.*, 2014, **136**(50), 17434–17437.
- 117 X. Ma, *et al.*, Facile Synthesis and Study of Microporous Catalytic Arene-Norbornene Annulation-Tröger's Base Ladder Polymers for Membrane Air Separation, *ACS Macro Lett.*, 2020, **9**(5), 680–685.
- 118 X. Hu, *et al.*, Synthesis, microstructures, and gas separation performance of norbornyl bis-benzocyclobutene-Tröger's base polymers derived from pure regioisomers, *Polym. Chem.*, 2022, **13**(19), 2842–2849.
- 119 J. Van Yken, *et al.*, Potential of metals leaching from printed circuit boards with biological and chemical lixiviants, *Hydrometallurgy*, 2020, **196**, 105433.
- 120 Z. G. Wang, *et al.*, Tröger's base-based copolymers with intrinsic microporosity for CO<sub>2</sub> separation and effect of Tröger's base on separation performance, *Polym. Chem.*, 2014, **5**(8), 2793–2800.
- 121 T. Zhang, L. Deng and P. Li, Decarboxylation Cross-Linking of Triptycene-Based Tröger's Base Polymers for Gas Separation, *Ind. Eng. Chem. Res.*, 2020, **59**(41), 18640–18648.
- 122 W. F. Yong and H. Zhang, Recent advances in polymer blend membranes for gas separation and pervaporation, *Prog. Mater. Sci.*, 2021, **116**, 100713.
- 123 S. Zhao, *et al.*, Blending of compatible polymer of intrinsic microporosity (PIM-1) with Tröger's Base polymer for gas separation membranes, *J. Membr. Sci.*, 2018, **566**, 77–86.
- 124 X. Chen, *et al.*, Ultra-selective molecular-sieving gas separation membranes enabled by multi-covalent-crosslinking of microporous polymer blends, *Nat. Commun.*, 2021, **12**(1), 6140.
- 125 E. Esposito, *et al.*, Highly permeable Matrimid®/PIM-EA (H<sub>2</sub>)-TB blend membrane for gas separation, *Polymers*, 2018, **11**(1), 46.
- 126 M. Longo, *et al.*, Thin Film Composite Membranes Based on the Polymer of Intrinsic Microporosity PIM-EA(Me-2)-TB Blended with Matrimid (R) 5218, *Membranes*, 2022, **12**(9), 881.
- 127 X. Chen, *et al.*, Hydrogen bonding-induced 6FDA-DABA/TB polymer blends for high performance gas separation membranes, *J. Membr. Sci.*, 2022, **655**, 120575.
- 128 J. Sanchez-Lainez, *et al.*, Hydrogen Separation at High Temperature with Dense and Asymmetric Membranes Based on PIM-EA(H-2)-TB/PBI Blends, *Ind. Eng. Chem. Res.*, 2018, **57**(49), 16909–16916.
- 129 S. J. Smith, *et al.*, Control of physical aging in super-glassy polymer mixed matrix membranes, *Acc. Chem. Res.*, 2020, **53**(7), 1381–1388.
- 130 B. S. Ghanem, *et al.*, Energy-efficient hydrogen separation by AB-type ladder-polymer molecular sieves, *Adv. Mater.*, 2014, **26**(39), 6696–6700.
- 131 R. Swaidan, *et al.*, Physical aging, plasticization and their effects on gas permeation in "rigid" polymers of intrinsic microporosity, *Macromolecules*, 2015, **48**(18), 6553–6561.
- 132 Q. Song, *et al.*, Controlled thermal oxidative crosslinking of polymers of intrinsic microporosity towards tunable molecular sieve membranes, *Nat. Commun.*, 2014, **5**(1), 4813.
- 133 T. O. McDonald, *et al.*, Using intermolecular interactions to crosslink PIM-1 and modify its gas sorption properties, *J. Mater. Chem. A*, 2015, **3**(9), 4855–4864.
- 134 M. D. Guiver, *et al.*, Gas transport in a polymer of intrinsic microporosity (PIM-1) substituted with pseudo-ionic liquid tetrazole-type structures, *Macromolecules*, 2020, **53**(20), 8951–8959.
- 135 H. Dong, *et al.*, Significantly improved gas separation properties of sulfonated PIM-1 by direct sulfonation using SO<sub>3</sub> solution, *J. Membr. Sci.*, 2021, **635**, 119440.
- 136 D. Zhang, *et al.*, Effects of sulfonate incorporation and structural isomerism on physical and gas transport properties of soluble sulfonated polyimides, *Polymer*, 2020, **191**, 122263.
- 137 W. Xie, *et al.*, Highly selective benzimidazole-based polyimide/ionic polyimide membranes for pure-and mixed-gas CO<sub>2</sub>/CH<sub>4</sub> separation, *Sep. Purif. Technol.*, 2022, **282**, 120091.
- 138 T. Han, *et al.*, Ionic Microporous Polymer Membranes for Advanced Gas Separations, *Ind. Eng. Chem. Res.*, 2023, **62**(4), 1764–1775.
- 139 Y. Rong, *et al.*, Intrinsically porous polymer protects catalytic gold particles for enzymeless glucose oxidation, *Electroanalysis*, 2014, **26**(5), 904–909.
- 140 I. Kammakam, J. E. Bara and E. M. Jackson, Synthesis and characterization of imidazolium-mediated Tröger's base containing poly (amide)-ionenes and composites with ionic liquids for CO<sub>2</sub> separation membranes, *Polym. Chem.*, 2020, **11**(46), 7370–7381.
- 141 X. Xu, *et al.*, Ionic polyimide membranes containing Tröger's base: synthesis, microstructure and potential application in CO<sub>2</sub> separation, *J. Membr. Sci.*, 2020, **602**, 117967.
- 142 Z. Xu, *et al.*, Preparation and antifouling property improvement of Tröger's base polymer ultrafiltration membrane, *J. Membr. Sci.*, 2018, **561**, 59–68.
- 143 T. Huang, *et al.*, Improved permeability and antifouling performance of Tröger's base polymer-based ultrafiltration membrane via zwitterionization, *J. Membr. Sci.*, 2022, **646**, 120251.
- 144 L. Wu, *et al.*, Enhanced molecular selectivity and plasticization resistance in ring-opened Tröger's base polymer membranes, *J. Membr. Sci.*, 2021, **634**, 119399.
- 145 R. Swaidan, *et al.*, Fine-Tuned Intrinsically Ultramicroporous Polymers Redefine the Permeability/Selectivity Upper Bounds of Membrane-Based Air and Hydrogen Separations, *ACS Macro Lett.*, 2015, **4**(9), 947–951.
- 146 B. Comesaña-Gándara, *et al.*, Redefining the Robeson upper bounds for CO<sub>2</sub>/CH<sub>4</sub> and CO<sub>2</sub>/N<sub>2</sub> separations using a series of ultrapermeable benzotriptycene-based polymers of intrinsic microporosity, *Energy Environ. Sci.*, 2019, **12**(9), 2733–2740.
- 147 M. Rezakazemi, *et al.*, State-of-the-art membrane based CO<sub>2</sub> separation using mixed matrix membranes (MMMs): An

- overview on current status and future directions, *Prog. Polym. Sci.*, 2014, **39**(5), 817–861.
- 148 T.-S. Chung, *et al.*, Mixed matrix membranes (MMMs) comprising organic polymers with dispersed inorganic fillers for gas separation, *Prog. Polym. Sci.*, 2007, **32**(4), 483–507.
- 149 Q. Zhao, *et al.*, Architecting MOFs-based mixed matrix membrane for efficient CO<sub>2</sub> separation: Ameliorating strategies toward non-ideal interface, *Chem. Eng. J.*, 2022, **443**, 136290.
- 150 Z. Qin, *et al.*, Recent Progress in Ternary Mixed Matrix Membranes for CO<sub>2</sub> Separation, *Green Energy Environ.*, 2023, DOI: [10.1016/j.gee.2023.04.008](https://doi.org/10.1016/j.gee.2023.04.008).
- 151 S. H. Goh, *et al.*, Metal–Organic Frameworks (MOFs)-Based Mixed Matrix Membranes (MMMs) for Gas Separation: A Review on Advanced Materials in Harsh Environmental Applications, *Small*, 2022, **18**(20), 2107536.
- 152 M. M. Zagho, *et al.*, A review on recent advances in CO<sub>2</sub> separation using zeolite and zeolite-like materials as adsorbents and fillers in mixed matrix membranes (MMMs), *Chem. Eng. J. Adv.*, 2021, **6**, 100091.
- 153 A. S. Wiryoatmojo, *et al.*, Surface modification effect of carbon molecular sieve (CMS) on the morphology and separation performance of mixed matrix membranes, *Polym. Test.*, 2019, **80**, 106152.
- 154 A. F. Yazid, *et al.*, Incorporating Carbon Nanotubes in Nanocomposite Mixed-Matrix Membranes for Gas Separation: A Review, *Membranes*, 2022, **12**(6), 589.
- 155 F. Pazani, *et al.*, Engineered graphene-based mixed matrix membranes to boost CO<sub>2</sub> separation performance: Latest developments and future prospects, *Renewable Sustainable Energy Rev.*, 2022, **160**, 112294.
- 156 S. H. Goh, H. S. Lau and W. F. Yong, Metal-Organic Frameworks (MOFs)-Based Mixed Matrix Membranes (MMMs) for Gas Separation: A Review on Advanced Materials in Harsh Environmental Applications, *Small*, 2022, **18**(20), e2107536.
- 157 X. Feng, *et al.*, Mixed-matrix membranes based on novel hydroxamate metal–organic frameworks with two-dimensional layers for CO<sub>2</sub>/N<sub>2</sub> separation, *Sep. Purif. Technol.*, 2023, **305**, 122476.
- 158 Y. Liu, *et al.*, Multifunctional covalent organic framework (COF)-Based mixed matrix membranes for enhanced CO<sub>2</sub> separation, *J. Membr. Sci.*, 2021, **618**, 118693.
- 159 Z. Wang, *et al.*, Interfacial Design of Mixed Matrix Membranes for Improved Gas Separation Performance, *Adv. Mater.*, 2016, **28**(17), 3399–3405.
- 160 X. Wang, *et al.*, Sealing Tröger base/ZIF-8 mixed matrix membranes defects for improved gas separation performance, *J. Membr. Sci.*, 2021, **636**, 119582.
- 161 Y. Fan, *et al.*, Enhancement of H<sub>2</sub> Separation Performance in Ring-Opened Tröger's Base Incorporating Modified MOFs, *Ind. Eng. Chem. Res.*, 2022, **61**(50), 18537–18544.
- 162 J. Deng, Z. Dai and L. Deng, H<sub>2</sub>-selective Troger's base polymer based mixed matrix membranes enhanced by 2D MOFs, *J. Membr. Sci.*, 2020, **610**, 118262.
- 163 Z. Chen, *et al.*, Tröger's Base Polyimide Hybrid Membranes by Incorporating UiO-66-NH<sub>2</sub> Nanoparticles for Gas Separation, *Ind. Eng. Chem. Res.*, 2022, **61**(9), 3418–3427.
- 164 Y. Fan, *et al.*, Tröger's base mixed matrix membranes for gas separation incorporating NH<sub>2</sub>-MIL-53(Al) nanocrystals, *J. Membr. Sci.*, 2019, **573**, 359–369.
- 165 Q. Li, *et al.*, Unprecedented gas separation performance of ITTB/CNT nanocomposite membranes at low temperature by strong interfacial interaction enhanced rigidity, *J. Membr. Sci.*, 2021, **636**, 119590.
- 166 N. A. H. Md Nordin, *et al.*, Facile modification of ZIF-8 mixed matrix membrane for CO<sub>2</sub>/CH<sub>4</sub> separation: synthesis and preparation, *RSC Adv.*, 2015, **5**(54), 43110–43120.
- 167 M. Z. Ahmad, *et al.*, Investigation of a new co-polyimide, 6FDA-bisP and its ZIF-8 mixed matrix membranes for CO<sub>2</sub>/CH<sub>4</sub> separation, *Sep. Purif. Technol.*, 2018, **207**, 523–534.
- 168 Q. Wang, *et al.*, ZIF-8 hollow nanotubes based mixed matrix membranes with high-speed gas transmission channel to promote CO<sub>2</sub>/N<sub>2</sub> separation, *J. Membr. Sci.*, 2021, **630**, 119323.
- 169 M. Carta, *et al.*, An Efficient Polymer Molecular Sieve for Membrane Gas Separations, *Science*, 2013, **339**(6117), 303–307.
- 170 A. Ehsani and M. Pakizeh, Synthesis, characterization and gas permeation study of ZIF-11/Pebax @ 2533 mixed matrix membranes, *J. Taiwan Inst. Chem. Eng.*, 2016, **66**, 414–423.
- 171 M. Hou, *et al.*, Carbon molecular sieve membrane with tunable microstructure for CO<sub>2</sub> separation: Effect of multiscale structures of polyimide precursors, *J. Membr. Sci.*, 2021, **635**, 123883.
- 172 W. Qiu, *et al.*, Isomer-Tailored Carbon Molecular Sieve Membranes with High Gas Separation Performance, *ChemSusChem*, 2020, **13**(19), 5318–5328.
- 173 S. Bandehali, *et al.*, Polymers of intrinsic microporosity and thermally rearranged polymer membranes for highly efficient gas separation, *Sep. Purif. Technol.*, 2021, **278**, 119513.
- 174 S. H. Han, *et al.*, Tuning microcavities in thermally rearranged polymer membranes for CO<sub>2</sub> capture, *Phys. Chem. Chem. Phys.*, 2012, **14**(13), 4365–4373.
- 175 C. A. Scholes, *et al.*, Permeation and separation of SO<sub>2</sub>, H<sub>2</sub>S and CO<sub>2</sub> through thermally rearranged (TR) polymeric membranes, *Sep. Purif. Technol.*, 2017, **179**, 449–454.
- 176 Z. Wang, *et al.*, Carbon Molecular Sieve Membranes Derived from Troger's Base-Based Microporous Polyimide for Gas Separation, *ChemSusChem*, 2018, **11**(5), 916–923.
- 177 K. Hazazi, *et al.*, Catalytic arene-norbornene annulation (CANAL) ladder polymer derived carbon membranes with unparalleled hydrogen/carbon dioxide size-sieving capability, *J. Membr. Sci.*, 2022, **654**, 120548.
- 178 S. M. Meckler, *et al.*, Thermally Rearranged Polymer Membranes Containing Troger's Base Units Have Exceptional Performance for Air Separations, *Angew. Chem., Int. Ed. Engl.*, 2018, **57**(18), 4912–4916.

- 179 X. Hu, *et al.*, Thermally rearranged polybenzoxazole copolymers incorporating Tröger's base for high flux gas separation membranes, *J. Membr. Sci.*, 2020, **612**, 118437.
- 180 H. Guo, *et al.*, Carbon molecular sieve membranes fabricated at low carbonization temperatures with novel polymeric acid porogen for light gas separation, *Sep. Purif. Technol.*, 2023, **317**, 123883.
- 181 Z. Wang, *et al.*, Carbon molecular sieve membranes derived from Tröger's base-based microporous polyimide for gas separation, *ChemSusChem*, 2018, **11**(5), 916–923.
- 182 S. Kim, H. J. Jo and Y. M. Lee, Sorption and transport of small gas molecules in thermally rearranged (TR) polybenzoxazole membranes based on 2,2-bis(3-amino-4-hydroxyphenyl)-hexafluoropropane (bisAPAF) and 4,4'-hexafluoroisopropylidene diphthalic anhydride (6FDA), *J. Membr. Sci.*, 2013, **441**, 1–8.
- 183 S. Li, *et al.*, Mechanically robust thermally rearranged (TR) polymer membranes with spirobisindane for gas separation, *J. Membr. Sci.*, 2013, **434**, 137–147.
- 184 F. Alghunaimi, *et al.*, Synthesis and gas permeation properties of a novel thermally-rearranged polybenzoxazole made from an intrinsically microporous hydroxyl-functionalized triptycene-based polyimide precursor, *Polymer*, 2017, **121**, 9–16.
- 185 Y. Lee, *et al.*, Effective functionalization of porous polymer fillers to enhance CO<sub>2</sub>/N<sub>2</sub> separation performance of mixed-matrix membranes, *J. Membr. Sci.*, 2022, **647**, 120309.
- 186 J. Wang, *et al.*, Machine Learning in Gas Separation Membrane Developing: Ready for Prime Time, *Sep. Purif. Technol.*, 2023, **313**, 123493.
- 187 J. Guan, *et al.*, Design and prediction of metal organic framework-based mixed matrix membranes for CO<sub>2</sub> capture *via* machine learning, *Cell Rep. Phys. Sci.*, 2022, **3**(5), 100864.
- 188 H. Daglar and S. Keskin, Combining Machine Learning and Molecular Simulations to Unlock Gas Separation Potentials of MOF Membranes and MOF/Polymer MMMs, *ACS Appl. Mater. Interfaces*, 2022, **14**(28), 32134–32148.